MICROMACHINING USING AN EXCIMER (248 nm) LASER

By

CHOO, KOK LEONG

Bachelor of Science in Mechanical Engineering

Oklahoma State University

Stillwater, OK

1999

Submitted to the Faculty of the
Graduate College of the
Oklahoma State University
in partial fulfillments of
the requirement of
the Degree of
MASTER OF SCIENCE
May, 2004

MICROMACHINING USING AN EXCIMER (248 nm) LASER

Thesis Approved:

_____

Thesis Adviser

_____

_____

_____

Dean of Graduate College

ACKNOWLEDGEMENT

First, I would like to thank my adviser, Dr. Ranga Komanduri, for his guidance, input, and advice and for allowing me to perform research in the field of advanced manufacturing processes and nanotechnology. This project is funded by a grant from the National Science Foundation (EPS-9977830) through a subcontract from University of Arkansas. The principal investigator at the University of Arkansas on this project is Dr. Ajay Malshe. I would also like to thank Dr. H. B. Lu and Dr. L. M. Raff for serving as my committee. Thnks are due to Mr. Matt Lee, Mr. Sony Varghese, Mr. Yasufumi Ogawa and Mr. K. Ganesh for their ideas, advice, help and assistance in performing some of the experiments.

Special thanks go to my other half, Chan, Siu Mei, who is always encouraging and supporting me in everyway possible.

I am indebted to my parents, Mr. Choo Si Pei and Mrs. Ng Yoke Lan; my brother, Kok Keng, my sisters, Lai Kuan, Lai Yee and Lai Yen, who are always encouraging me in times of need, and without whose ever present support and sacrifices I would not have been able to study abroad.

Finally, I would like to thank one and all for helping me in completing this work.

TABLE OF CONTENTS

Chapter Page

Chapter Page

Chapter Page

Chapter Page

LIST OF TABLES

LIST OF FIGURES

Figure Page

Figure Page

CHAPTER 1

INTRODUCTION TO LASER

1.1 Introduction

Before undertaking a study on the laser machining process, it is necessary to understand the fundamentals of the laser system. In this chapter, we will briefly review the history, types of lasers, properties of laser, and laser safety.

1.2 History of Lasers

The word *LASER* is an acronym for the most significant feature of laser action, namely, *L*ight *A*mplification by *S*timulated *E*mission of *R*adiation. There are many different kinds of lasers, but they share a crucial element, namely, material capable of amplifying radiation. This material is called the gain medium, because radiation gains energy passing through it.

Stimulated Emission

The physical principle responsible for the amplification is called simulated emission. This concept was originated from Albert Einstein's 1916 paper [1] or the sources of quantum mechanics. If an electron is in an excited state, when a photon previously emitted, and having the proper energy collides, the electron would drop to a lower energy

state, and emit another proton of the same energy that would move in the same direction, resulting in two identical photons traveling together in the same direction and in phase.

Maser

However, the concept of stimulated emission remained primarily of academic interest until 1950s, when Charles H. Townes together with a postdoctoral assistant and a graduate student built the first *MASER*, which is an acronym for *M*icrowave *A*mplification by the *S*timulated *E*mission of *R*adiation [2].

The Birth of Laser Theory

Townes and Schawlow were the first to publish a detailed account on the construction of an "optical maser." Their famous paper "Infrared and Optical Maser," was published in the December, 1958 issue of the Physical Review [2]. This paper along with the US Patent No. 2,929,922 had a profound impact on American laser research.

The Great Laser Race

Publication of the Schawlow-Townes paper stimulated many researches to build optical masers. Meanwhile, Theodore Maiman at Hughes Research Laboratories in Malibu, California was attempting to apply his knowledge of ruby masers to fabricate a laser. Despite warning from Schawlow and others that ruby is unsuitable for laser, on May 16, 1960, Maiman succeeded in making the ruby laser work for the first time [3].

The First Commercial Lasers

It didn't take long for laboratories around the world to duplicate Maiman's ruby laser, but not all laboratories wanted to build their own. The first commercial lasers began appearing about 1961 – large ruby type designed to deliver high-power pulses. One of the firsts in the market was TRION in Michigan.

1.3 Types of Laser

There are seven major types of laser as shown in Figure 1.1. Excimer laser used on this investigation falls in the gas lasers category.

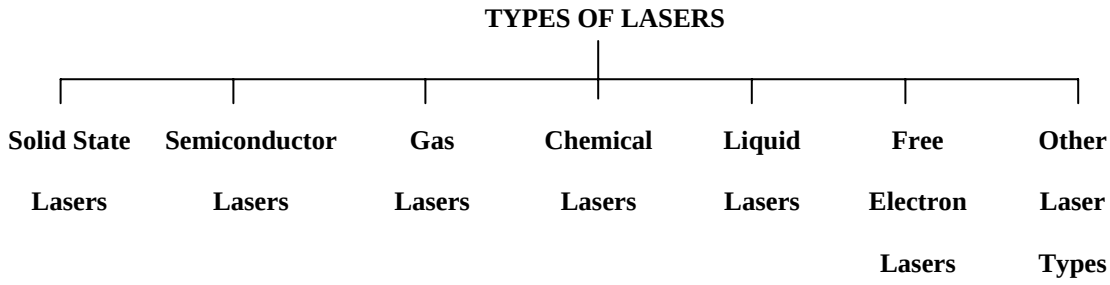

Figure 1.1 Seven major families of laser.

1.4 Excimer Laser

Excimer lasers are a family of lasers in which light is emitted by a short-lived molecule made up of one rare gas atom (e.g., argon, krypton, or xenon) and one halogen atom (e.g., fluorine, chlorine, or bromine). Most commonly used excimer lasers are listed in Table 1.1.

From 1975 to 1979 many researchers worked on the initial development of a family of gas lasers, known as the "Excimer" laser. They include Charles Chase (Tachisto),

Terry Mckee (Lumonics), Richard Basting (Lambda Physik), J.J. Ewing, Ralph Burnham, Robert Sze, Richard Slater (Avco), Charles Rhodes, Paul Christensen, and others from U.S. national laboratories. They contributed significantly toward the early development of this technology.

TABLE 1.1

MAJOR EXCIMER LASERS

Type	Wavelength
F_2*	157 nm
ArF	193 nm
KrCl	222 nm
KrF	248 nm
XeCl	308 nm
XeF	350 nm

*Not a rare-gas halide, but usually grouped with excimers.

The name "Excimer' is a contraction of "Excited Dimer," a description of a diatomic molecule in which the component atoms are bound in the excited state but not in the ground state. The important gas molecules are rare gas halides including argon fluoride (ArF), krypton fluoride (KrF) and xenon chloride (XeCl). These diatomic molecules have very short lifetimes and dissociate releasing the excitation energy through UV photons.

Although Excimer lasers are of the gas type, special attention is given to them because they can also be considered as chemical laser, essentially consisting of a mixture of rare gas and a halogen in a cavity into which energy is deposited by an electron beam or an electrical discharge to cause an electrically excited molecule which can only exist in this excited state. In the present investigation an excimer with krypton fluoride (KrF) is

used. This gas under lasing conditions returns to its constituent atoms emitting photons (either spontaneously or by simulated emission) to produce a laser beam at 248 nm in the ultraviolet region (namely in the 100 – 400 nm) of the spectrum.

Since excimer lasers are gas and chemical type and the wavelength is shorter than the other popular types like CO_2 or Nd:YAG lasers, it is of interest for many applications.

1.4.1 Physical Fundamentals

Rare-gas halides are peculiar molecules that emit laser light on an unusual type of electronic transition. The two atoms are bound only when the molecule is in an excited state. When the molecule drops to the ground state, which is the lower laser level, the molecule falls apart. That produces a population inversion in a rather unusual way – there can't be any molecules in the lower laser level because they are not bound together.

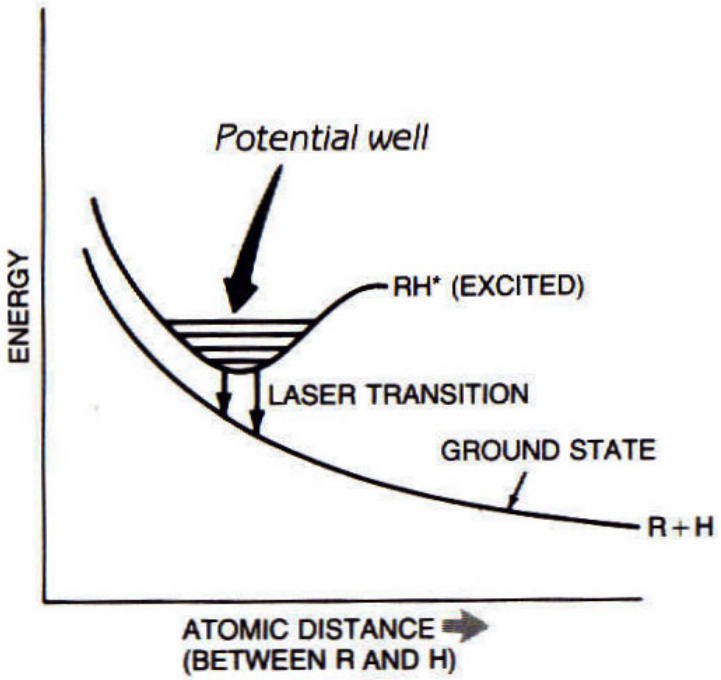

Figure 1.2 Internal energy of a rare-gas halide molecule in excited and ground states [3].

Figure 1.2 shows the energy levels of a typical rare-gas halide as a function of the spacing between the two atoms in the molecule. *R* represents the rare gas and *H* the halide. The dip in the excited-state curve shows where the molecules are metastable. The absence of a dip in the ground-state curve indicates that the molecules fall apart. When the molecule is excited, the energy is at a minimum when the two atoms are at a certain distance apart, trapped in a potential well. When they are in that potential well, they can occupy several vibration levels as well (shown as horizontal lines in the potential well). However, in the "ground-state," with the lowest possible energy, there is no bonding energy to hold the two atoms together and the molecule fall apart, as shown in the lower curve. This reflects something we know from elementary chemistry, namely, rare gases do not like to form compounds, even with elements as highly reactive as halogens.

Excimer lasers are excited by passing a short, intense electrical pulse through a mixture of gases containing the desired rare gas and halogen. Normally, 90% or more of the mixture is a buffer rare gas (typical helium or neon) that does not take part in the reaction. The mixture also contains a small percentage of the rare gas (argon, krypton, or xenon) that becomes part of the excimer molecule, and a smaller fraction of the molecules that supply the needed halogen atoms. The halogen atoms may come from halogen molecules, such as F_2, Cl_2, or Br_2, or from molecules that contain halogens, such as nitrogen trifluoride (NF_3). The advantage of avoiding pure halogens is that they are very reactive. Fluorine, in particular, is so treacherous to handle that the developers of one high-energy laser that used fluorine spoke of "the fire of the week."

Electrons in the discharge transfer energy to the laser gas, breaking up halogen molecules and causing formation of electronically excited molecules like xenon fluoride

(XeF*, the * means excited). The reactions involved are very complex and depend on the type of gases. The molecules remain excited for about 10 nanoseconds, then drop to the ground state and dissociate. The molecular kinetics (as well as the duration of the driving electrical pulses) limit the laser operation to pulses lasting tens or hundreds of nanoseconds. The energies involved are large, and the output is at ultraviolet wavelengths.

Excimer-laser repetition rates are more dependent on the power supply than on the gas. The principal limitation is the speed of high-voltage switches. The highest repetition rates are around 1000 Hz, but more typical values are tens to few hundreds of hertz. Pulse energies range from about 10 mJ to a few joules, and differ somewhat among gases, with KrF and XeCl is generally being more energetic. Average power – the product of the pulse energy times the repetition rate – can reach a couple of hundred watts, although lower values are more common. Note that in general the pulse energy tends to decrease with repetition rate.

1.4.2 Structure of Excimer Laser

Excimer lasers have such high gain that they almost don't need cavity mirrors. In practice, excimer lasers have fully reflective rear mirrors and uncoated output windows that reflect a few percent of the beam back into the cavity and transmit the rest.

As in other high-gain pulsed lasers, the discharge in an excimer laser is perpendicular to the length of the tube. The excimer laser tubes must resist attack by the highly corrosive halogens in the laser gas. Excimer laser tubes are filled with the laser gas mixture then sealed and operates for a certain number of shots until the gas needed to be

replaced. The tube's total volume is much larger (typically 100 to 1000 times) than the volume where the discharge excites laser action. Often, the gas is passed through a recycling system that helps regenerate the proper gas mixture and extend the life of the gas fill. The laser's pulse energy drops with time, until the spent gas must be pumped out of the chamber and replaced. The number of shots depend on the gas, and can be many millions of shots for gases, such as xenon chloride.

Although that number of shots may sound impressive, a little multiplication will show that at high repetition rates it doesn't amount to very much time. A 200-hertz laser generates 720,000 pulses an hour. Thus, gas supply is part and parcel of any excimer laser set-up.

1.4.3 Practical Excimer Lasers

Excimer lasers are the best available pulsed ultraviolet lasers with wall-plug efficiency of only a couple of percent. Most of the lasers are used in research, but they are finding increasing applications in medicine and high technology industrial systems, including refractive surgery on the eye and in the manufacture of semiconductor electronic devices. These commercial applications have pushed manufacturers to make more reliable excimer lasers, although the use of halogens still remains a concern.

Laboratory excimer lasers have long been designed to handle several gas mixtures. This reflects the need for a research laboratory, which one-day may be working with the 308-nm xenon-chloride line, and the next day 193-nm argon-fluoride wavelength. However, the researchers have to pump out the old gas mixture, passivate the tube to remove contaminants, then pump out the mixture and replace it with a new laser gas

mixture. This is acomplex, time consuming operation. Industrial excimer lasers are typically made for a specific gas mixture.

Excimer lasers remain complex systems and expensive. The initial investment for a 50 to 250 W laser is from $100,000 to $250,000. Complete turnkey multi-axis machine tools with the laser integrated can be procured for $500,000 to $1 million per machine, depending on the machine volume and laser choice. An estimate for a complete laser drilling machine is approximately $150,000 per machine axis. Several vendors offer lower-cost systems that may not be sufficiently robust for two- or three-shift operation.

Filters, oil traps and de-ionizing cartridges are relative low-cost items which required periodic replacement is part of maintenance. Providing the planned downtime, one half to one day each month or quarter, for maintenance is a primary stumbling block in industry. Lenses can cost from around $100 to $1,000 each. A high quality lens is generally preferred, utilizing a high quality antireflection multicoating. Flash lamps are typically replaced every few million pulses with the replacement rate highly dependent on the laser parameters. Lamps may be replaced as frequently as once a month and cost $100 to $300 per a pair.

1.5 Laser's Properties

Lasers take many different shapes. Other characteristics, such as output wavelength and power level, also differ among lasers. Different types of lasers also share some common properties, such as the concentration of their output energy into a narrow beam. Some of the characteristics are interrelated. Major laser properties that influence

materials processing are wavelength, output power, duration of emission (pulse or continuous), beam divergence and size, coherence, efficiency, and power requirements.

1.5.1 Wavelength

Wavelength is the fundamental characteristic of visible light and other forms of electromagnetic radiation. Each type of laser emits a characteristic wavelength or range of wavelengths. The wavelengths depend on the type of material that emits the laser light, the laser's optical system, and the way the laser is energized. Laser action can produce infrared, visible, and ultraviolet light. Table 1.2 lists some important laser types and their wavelengths in nanometers (1 nm = 10^{-9} meter) [5].

TABLE 1.2

IMPORTANT LASER TYPES AND THEIR WAVELENGTH [5].

Type	Wavelength (nm)
Krypton-Fluoride Excimer	248
Xenon-Chloride Excimer	308
Nitrogen Gas (N2)	337
Organic Dye (in solution)	300-1000 (tunable)
Kripton Ion	335-800
Argon Ion	450-530 (488 and 514.5 strongest)
Helium Neon	543, 632.8, 1150
Semiconductor (GalnP family)	670-680
Ruby	694
Semiconductor (GaAlAs Family)	750-900
Neodymium:YAG	1064
Semiconductor (InGaAsP Family)	1300-1600
Hydrogen-Fluoride Chemical	2600-3000
Carbon Dioxide	9000-11000 (main line 10,600)

Most lasers are ‘monochromatic’, which means they emit only one wavelength. Actually, they emit a range of wavelengths, but the range is so narrow that for most practical purposes it can be taken as a single wavelength. Some of these lasers emit light at different wavelengths under different conditions. For example, the helium-neon laser is best known for its red output at 632.8 nm. However, the same gas mixture can be used with different optics to emit green light at 543 nm, or to emit infrared. Some lasers can emit two or more wavelengths simultaneous. This is called multi-line operation. In some cases, the wavelengths are close together.

1.5.2 Output Power

Output power measures the strength of a laser beam, which differs widely among different lasers. Strictly speaking, power is the flow of light energy from the laser in the form of a laser beam; it is measured in watts and defined by

$$\text{Power} = \frac{\text{d(energy)}}{\text{d(time)}}$$

Laser output power covers a wide range. Some lasers produce beams containing less than a thousandth of a watt (a milliwatt) and others produce thousands of watts (kilowatts). Some lasers can be adjusted over a limited power range, but others are designed to emit a stable power level. Some types of lasers cannot be scaled to high power levels. For example, the helium-neon laser cannot produce more than a few dozen milliwatts. Only a few types, notably, carbon dioxide, Nd:YAG and chemical lasers, can produce thousands of watts in steady beam.

1.5.3 Duration of Emission

Laser emission duration can be divided into pulses and continuous. Pulses come in various durations and repetition rates. The length or duration of a pulse can range from millisecond (10^{-3}s) to femtoseconds (10^{-15}s). The pulses may be repeated once a minute, or may appear thousands or even millions of times in a second.

There are important and fundamental relationships among pulse length, energy, repetition rate, and power. A laser may have extremely high peak power during a short pulse, but due to the fact that pulse is short, it doesn't contain much energy. To make a simple approximation:

$$\text{Pulse Energy} = \text{Peak Power} \times \text{Pulse Length}$$

or

$$\text{Energy} = \int \text{Power} \cdot \text{d(time)}$$

The average power in a pulsed laser beam is different from the peak power; it is a measure of the average energy flow per second and given by:

$$\text{Average Power} = \frac{\text{Number of Pulses} \times \text{Pulse Energy}}{\text{Time}}$$

If the number of pulses per unit time is a measure of repetition rate, and the time is normalized to one second, then the average power becomes:

$$\text{Average Power} = \text{Repetition Rate} \times \text{Pulse Energy}$$

Both peak and average power can be important quantities depending on the laser application. Both are measured in watts, but as would be expected, peak power is higher. Pulse energy is measured in joules. The conversion between the two units is watt = joules/sec.

1.5.4 Beam Divergence and Size

If a laser beam can be seen shining through dusty air, it looks like a thin string. However, if you look carefully, it has a certain diameter, the farther the beam travels the larger is the diameter. This spreading is called divergence. The divergence of a laser beam allows it to propagate over significant distance without changing significantly in diameter. This factor also allows it to be collected and focused easily.

Figure 1.3 shows the beam divergence of a laser spot. Beam divergence is measured in milliradians and given by

$$\text{Radius} = \text{Distance} \times \sin(\text{beam divergence})$$

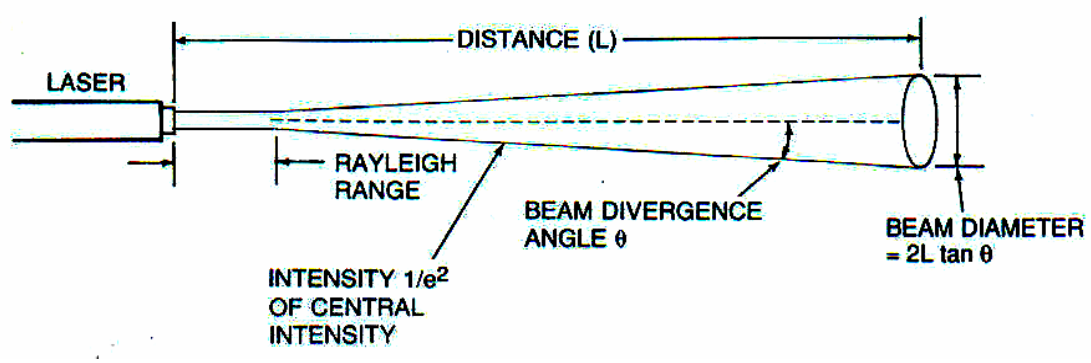

Figure 1.3 Calculating the size of a laser spot from a beam divergence [5].

1.5.5 Coherence

Light waves are said to be coherent if they are all in phase with one another. Figure 1.4 shows the difference between coherent and incoherent light waves. For coherent light waves, peaks and valleys are all lined up with each other. However, for incoherent light waves, the peaks and valleys do not line up. Laser light is coherent; ordinary light (white light) from the sun, a fluorescent tube, is incoherent.

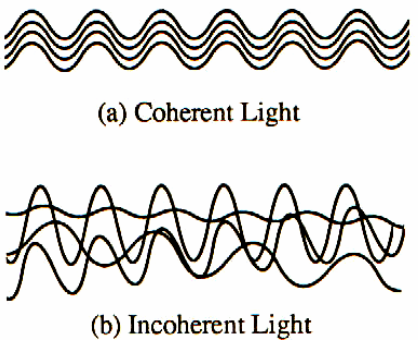

Figure 1.4 Coherent and Incoherent light.

The more monochromatic a laser is, the more coherent it is. Monochromatic light needs not to be coherent, but light that is not monochromatic cannot remain coherent over a long distance.

1.5.6 Efficiency and Power Requirement

A laser's wavelength, output power, coherence, and pulse characteristics all are important in selecting a laser. Two other factors also enter the picture, namely, the efficiency and power requirements. Lasers differ widely in how efficiently they convert input energy into light energy. Like other light sources, they are not very efficient in generating light, with the best converting up to about 20% of input energy into light. Many types convert as a little as 0.01% or even 0.001% of the input energy into light.

Efficiency becomes a more important consideration at higher output powers. It's not a big problem if a 1-milliwatt laser produces a watt waste heat because it is easy to dissipate. However, it would be very difficult to dissipate the million watts of waste heat produced if a one-kilowatt laser operated at the same efficiency.

1.6 Laser Safety

There are two main potential hazards associated with lasers, namely, the laser beam and the power supply. Even low-power laser beams can pose some dangers to the eye while high-power laser beams can burn the skin. The power supply, like any source of high voltage – or even wall current – can kill.

A laser beam is made up of parallel light rays. The concentration of parallel light rays in a small beam makes laser power as low as a milliwatt range to be a potential hazard to eyes. The reason is that the eye focuses those rays, concentrating their optical power in a small enough area that they can burn the retina. The hazard of a few milliwatts visible laser beam is comparable to that from looking directly at the sun. An accidental glance past sun may dazzle your eyes, but staring directly at the sun can cause permanent eye damage. This is same for laser. The first safest rule is never look directly into any laser beam.

Higher laser powers pose more serious eye hazards. As continuous-wave power levels increase, it takes less time for the light to do lasting damage to the eye. If the power is concentrated in short high-power pulses, even a single shot can do lasting damage. It can leave a blind spot that impairs vision.

Both visible and invisible laser light poses hazards to your eyes. Invisible (near infrared and near ultraviolet) light can enter your eye, and near infrared light can reach your retina without you ever realizing it. Hazards become less at the wavelengths longer than about 1.55 μm because the light cannot reach your retina, but you nonetheless should exercise care when working with any laser. Some near infrared laser can be very

deceptive because they seem to be emitting extremely weak red beams, but are actually emitting significant powers at wavelengths which your eyes sense very inefficiently.

Laser safety goggles are made to block the wavelengths emitted by specific lasers and transmit other light. Good goggles should block light from reaching your eye via any side paths, such as accidental reflections from the side. Remember that it is vital to use goggles made for the type of laser you are using, for example goggles made for red helium-neon wavelength do not block light from an argon laser.

In the history of laser industry, nobody has been killed by a laser beam. However, several people have been killed when they touched high-voltage source within the laser. Beware, even when the power is off, components such as capacitors in high-voltage power supplies can retain a lethal dose of electricity for a long time.

CHAPTER 2

FUNDAMENTALS OF LASER –MATERIAL INTERACTIONS

2.1 Introduction

This chapter briefly describes the physical processes that occur during the interaction of laser radiation with materials. Knowledge of these processes is important for understanding the capabilities and limitations of laser-based materials processing. These interactions are the basis for laser applications in material processing.

In general, when a laser beam meets the workpiece, as shows in Figure 2.1, several effects arise, including, reflection, absorption and transmission of the light.

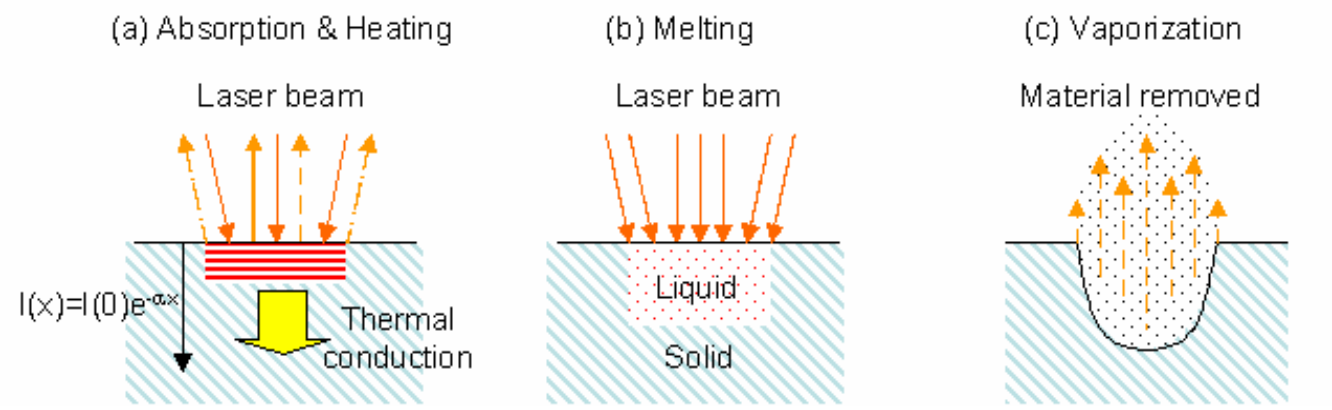

Figure 2.1 Interaction of laser beam with workpiece.

2.2 Reflectivity, Absorptivity and Transmisivity

When a laser impinges on the surface of a workpiece, a fraction of the energy is reflected at the surface, and a part penetrates into the workpiece. A surface cannot absorb or emit photon. Attenuation takes place inside the solid, as does the emission of irradiative energy. In practical systems, the thickness of the surface layer over which absorption of irradiation from a laser beam occurs is very small compared to the overall dimensions of the workpiece.

Consider laser radiation impinging on a medium of finite thickness, as shown in Figure 2.2. In general, some of the irradiation will be reflected away from the medium, a fraction will be absorbed inside the layer, and the rest will be transmitted through the slab.

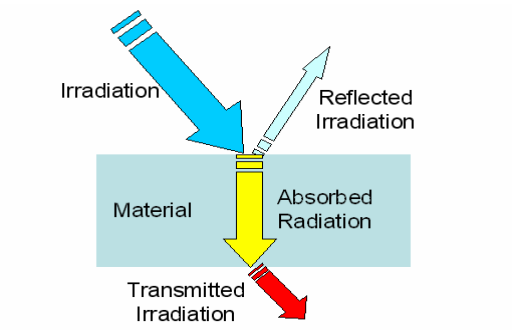

Figure 2.2 Reflection, absorption and transmission by a slab [11].

Three fundamental irradiative properties are defined as followed:

$$\textit{Reflectivity, } \rho = \frac{\text{reflected part of the incoming radiation}}{\text{total incoming radiation}}$$

$$\textit{Absorptivity, } \alpha = \frac{\text{absorbed part of the incoming radiation}}{\text{total incoming radiation}}$$

$$\textit{Transmisivity, } \tau = \frac{\text{transmitted part of the incoming radiation}}{\text{total incoming radiation}}$$

Since all radiation must be either reflected, absorbed, or transmitted, it follows that

$$\alpha + \beta + \tau = 1 \qquad (2.1)$$

For opaque medium, then $\tau = 0$, then

$$\alpha + \beta = 1 \qquad (2.2)$$

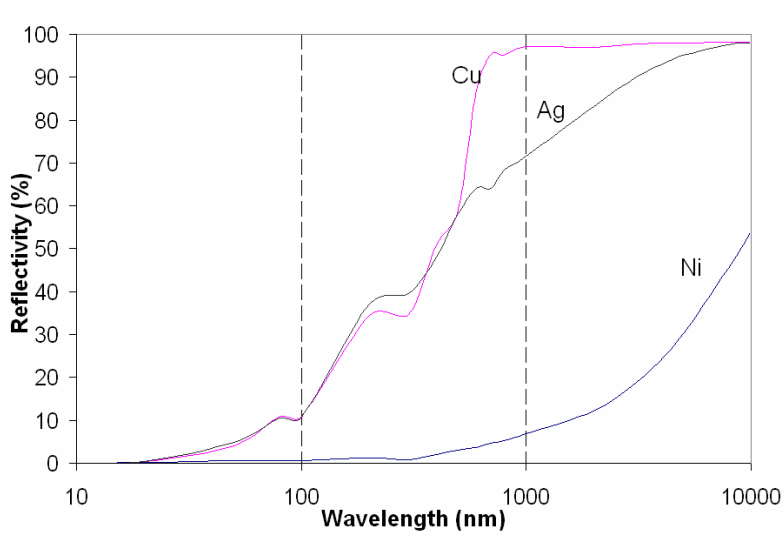

Figure 2.3 Reflectivity of silver, copper and nickel at different wavelengths [11]

The amount by which the beam is reflected depends on the wavelength of the laser radiation, the condition and properties of the material, such as its surface finish, the amount to which it is oxidized, and its temperature. In particular, the high reflectivity of many materials at certain laser wavelengths renders them unsuitable for machining. In general, the longer the wavelength of the laser beam, the higher the reflectivity of metals becomes. This observation is confirmed by the results shown in Figure 2.3 for some metals.

Modification of the surface layers and oxide films could change the reflectivity for the workpiece. For example, the reflectivity of copper at a wavelength of 694.3 nm has been reported to be reduced from 95% to less than 20% by oxidizing the surface. Surface

roughness also influences the reflectivity of the workpiece. Through geometric optical explanation, for rough surfaces, laser beam hitting the surface may undergo two or more reflections off the local peaks and valleys (resulting in increased absorption), after which it leaves the surface into an off-specular direction.

Nonetheless a reduction in reflectivity leads to an increase in absorption of the laser energy by the surface, with subsequent increase in the material removal. This absorption is examined in the following.

The absorption of light in metals takes place by an internal photoelectric effect which raises the electrons to higher energy states in the conduction band of the metal. Now the mean free time between collisions for electrons in a conductor is on the order of 10^{-14} to 10^{-13} s. Thus in 1 nanosecond, the electrons will have made 10^{14} to 10^{15} collisions among themselves. Since this is a very short period compared to even the shortest laser pulse, the energy absorbed by the electrons from the laser beam is rapidly passed to the lattice.

The depth over which the absorption takes place may be approximated from the mean free path of the valence electrons, according to the relation

$$I(x) = I(0) \cdot e^{-\alpha x} \qquad (2.3)$$

where

I(x) is the light intensity, W, at depth x of the penetration into the material

I(0) is the incident intensity

α is an absorption coefficient, m^{-1}

For a non-scattering material (without defects, inclusions, bubbles) the absorption coefficient, α is related to the absorptive index *k* by

$$\alpha = \frac{4\pi k}{\lambda} \qquad (2.4)$$

Most of the energy is found to be absorbed in a 'skin depth' S given by

$$S = \alpha^{-1} \tag{2.5}$$

Typically, the energy is absorbed to a depth of about 0.1 μm (for visible and infrared wavelength). For most organic compounds, absorption is found to take place in less than 1 μm (for CO_2 and infrared radiation).

In summary, the laser energy may be regarded as a surface effect, with the energy penetrating further into the material by thermal conduction.

2.3 Heat Conduction

Conduction is the dominant heat transport mode at low laser power density application. The conduction of heat from the laser into the workpiece material is an extremely complex effect. As a result, no satisfactory theory of heat conduction has yet been applied to laser machining. Nonetheless, useful information relevant to laser machining can be derived from a simple approach.

Firstly, since the workpiece is assumed to be composed of an isotropic material, the heat flow through it can be described by the diffusion equation

$$\frac{\partial T}{\partial t} = \kappa \nabla^2 T \tag{2.6}$$

where

T is absolute temperature, K

t is time, s

κ is diffusivity , m^2s^{-1}

And, the diffusivity is given by

$$\kappa = \frac{k}{\rho \cdot c} \tag{2.7}$$

where

k is coefficient of thermal conductivity, $Wm^{-1}K^{-1}$

ρ is density, kgm^{-3}

c is specific heat, $Jkg^{-1}K^{-1}$

Useful information about the way heat from the laser is spread through the workpiece can be deduced from the solution to the diffusion equation (2.6) on the assumptions that the distribution of the temperature occurs is one-dimensional and that the workpiece is considered as semi-infinite.

For conditions of zero initial temperature throughout the material, and with the surface x = 0 maintained at T_0 for time t, where t > 0, the solution from Carslaw and Jaeger [10] is givenly

$$T(x,t) = T_0 \cdot erfc\left(\frac{x}{2\sqrt{\kappa \cdot t}}\right) \tag{2.8}$$

where the error function ‘erfc’ is given by

$$erfc(z) \equiv 1 - erf(z)$$
$$= \frac{2}{\sqrt{\pi}} \cdot \int_0^{\infty} e^{-\xi^2} \cdot d\xi$$

$$erf(z) = \frac{2}{\sqrt{\pi}} \cdot \int_0^{x} e^{-\xi^2} \cdot d\xi \tag{2.9}$$

2.4 Melting of Surface

On sufficient heating by the laser the workpiece begins to melt. Again the results from Carslaw and Jaeger [10] are useful. The temperature rise due to a heat flux incident

upon the surface (x = 0) of the workpiece, still assumed to be a semi-infinite medium, can be calculated as

$$T(x,t)\,|_{x=0} = \left[\frac{2F_0}{k}\right] \cdot \left(\frac{\kappa \cdot t}{\pi}\right)^{\frac{1}{2}} \tag{2.10}$$

where

F_0 is constant heat flux, $Js^{-1}cm^{-2}$

2.5 Convection

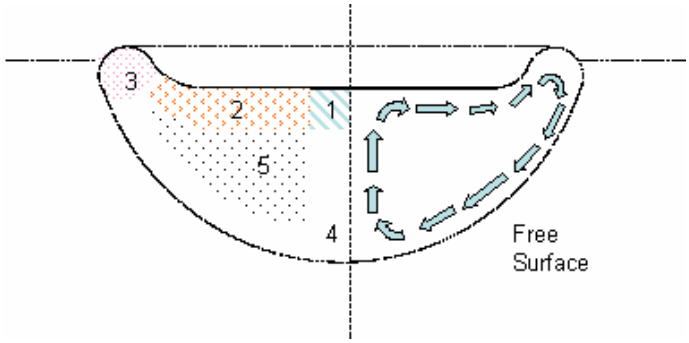

1. Stagnation Flow Region
2. Free Surface Boundary Layer Region
3. Cooled Corner Region
4. Solid-Liquid Interface Boundary Layer Region
5. Isothermal Inviscid Core

Figure 2.4 General features of convection in a molten pool [11].

Convection becomes the dominant heat transport mechanism when a molten pool is created. Surface tension variations arise due to temperature gradients along the interface, and shear stresses acting on the interface induce fluid motion. Convection in molten pool affects a large number of laser processes, such as melt quenching, alloying, and welding.

Convection is primarily responsible for mixing in the melt pool and therefore controls the composition during surface alloying. Figure 2.4 shows the general features of convection in a molten pool [11].

2.6 Vaporization

Very rapidly after melting by the laser, vaporization of the workpiece surface commences. The rate of vaporization may be related to the incident flux, F, of the laser by the expression

$$F = \frac{dx}{dt} \cdot C \tag{2.7}$$

where

(dx/dt) is the rate of recession of the workpiece surface

C is the energy needed to vaporize unit volume of workpiece.

2.7 Plasma Shielding

Plasma shielding normally refers to the fact that once the laser beam breaks down the atmosphere, the light is absorbed in the ensuing plasma, and does not reach the work piece or other intended target of the beam. This absorption of laser energy not only shields the workpiece from the laser beam, but also produces some effects, such as shock wave.

When a laser beam with sufficient energy is brought to a tight focus in matter (solid, liquid, or gas), it will cause the breakdown of the medium and the evaluation of highly

ionized plasma. The breakdown threshold is a strong function of the purity of the medium.

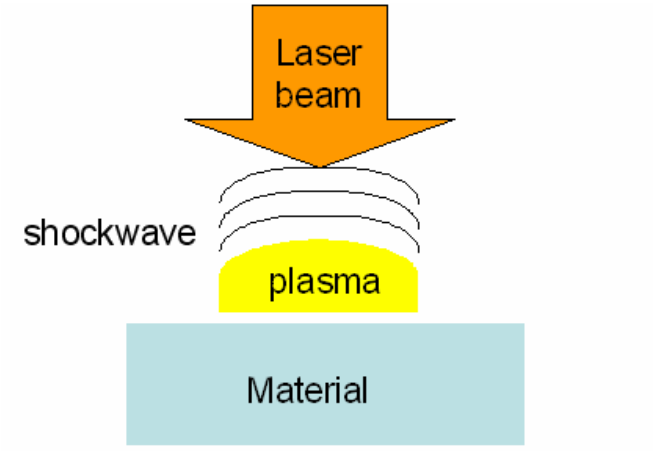

Figure 2.5 Schematic illustrations of the principal features of a laser-supported absorption wave in ambient air [11].

The hot, high-pressure plasma strongly absorbs the laser energy as it expands, forming a propagating absorption wave. Salient features of laser-induced absorption wave propagation away from the surface of a material are shown in Figure 2.5. This laser absorption wave propagates back along the laser beam as long as the beam has sufficient irradiance to sustain the process. The expansion front at higher irradiances propagates at shock velocities as a detonation wave. The plasma and the shockwave combine and move at the same velocity. These shock velocities are greater than the speed of sound, and the fluid dynamics of shock propagation controls the evolution of these waves. The plasma shields the work material at the early stage in the pulse, and the plasma temperature in the expansion fans is too low to effectively transmit thermal energy to the material, thus effectively shielding off the target material.

The presence of the plasma created by the laser beam has significant consequences for the application of lasers. Plasma at low irradiances can result in higher thermal coupling to a workpiece than optical absorption, whereas at higher irradiances the plasma prevents thermal coupling. The pressures in the plasma can produce a mechanical effect on the workpiece, particularly at higher irradiance. In general, the propagation of the absorption waves increases, the laser energy carried by the beam away from the intended point of application, and reduces the desired effect of the beam on the workpiece.

CHAPTER 3

LITERATURE REVIEW

3.1 Introduction

Excimer laser ablation – the direct etching of material with a pulsed UV light – has been the subject of sustained research activity since the early 1980s, when the technique was first demonstrated by Srinivasan and Mayne-Banton [16]. They named the process "ablative photodecomposition" (APD). The ablation process is characterized by pulse-by-pulse removal of small amounts of material, typically in the range of a few hundred Å to a few μm, with minimal damage to the surrounding area.

Considerable research effort has been devoted towards an understanding of the fundamental physical and chemical processes involved in laser ablation. Most of the laser energy is absorbed by a thin layer, typically in the range of 0.1 to 0.5 μm. Numerous models have been proposed to explain the observed etching behavior of various polymeric materials. These models invariably assume the ablation process to be either (1) photochemical, with the absorbed photons leading directly to bond breaking in the material, or (2) photothermal, with the deposited energy being converted to heat, and subsequently leading to thermal decomposition [17]. It is generally accepted that in reality ablation proceeds by some combination of these two routes. Experimental work by Srinivasan and Garison [17] shows that photochemistry plays less of a role for

wavelengths greater than 193 nm. The main mechanism for ablation seems to be thermal in origin with some photochemical bond-breaking.

3.2 Polymer

A photon of short-wavelength laser has energy ranging from 4 to 10 eV, which covers the bond energy of most polymeric materials. A photon of a 248 nm KrF excimer laser has energy of 5.2 eV, which is strong enough to break most covalent bonds. Table 3.1 gives the bonding energies of different types of covalent bonds. As a result, photochemical action dominates the polymer ablation by a short-wavelength laser.

TABLE 3.1

BONDING ENERGY FOR DIFFERENT TYPES OF COVALENT BOND.

Type of Covalent Bond	Bonding energy (eV)
C—C	3.60
O — O	1.47
O == O	5.16
H — H	4.51
O — H	4.81
C — H	4.29
C — N	3.16
H — N	4.03
N — N	1.69
N == N	4.33

Srinivasan and Leigh [18] exposed an un-focusing 193 UV laser (τ=12 ns, f=1 Hz) with fluence in the range of 10-180 mJ/cm^2 on polyethylene terephalate or PET workpiece of 75 μm thickness. They found that single pulse radiation caused etching of

the surface of PET and resulted in numerous gaseous products, such as CO, CO_2 and hydrogen. They considered 30 compounds which ranged from C_2 to C_{12}, benzene, toluene, benzaldehyde and ethylbenzene. They also pointed out the possibility of the excess energy of the photon pulses to be carried away by those fragment and cause no significant rise in the temperature on the photo-etched film. They named this process as "ablation".

Srinivasan *et al.* [19] also showed photographs of ablation and etching of the surface of PMMA by 248 nm laser radiation. They reported that modification of the surface structure of the PMMA to be visible initially at 12ns and completed in about 60 ns. Emerging solid material, preceded by shock wave first became visible at 60 ns, reaching a maximum in intensity at 6 μs and continued until 20 μs. Solid materials or debris from the ablated zone did not leave the surface until the UV pulse is over ~1 ms.

Morphological changes and chemical modifications of materials treated with an excimer laser have been report by Lauren and coworkers [20]. They performed surface treatment on polyether-etherketone (PEEK) with ArF (λ=193 nm, τ=20 ns, f=20 Hz) and KrF (λ=248 nm, τ=30 ns, f=20 Hz) and their results indicate that laser wavelength strongly affects the nature and properties of the treated materials. At 193 nm, bonds breaking (ether) induced under photon irradiation led to the formation of polar oxidized groups (carboxyls and hydroxyls) that gives hydrophilic and acidic properties to the surface. These new surface properties are responsible for an increase in the adhesion properties until massive oxidation degrades the mechanical properties of the surface and decreases the bonding properties. For 248 nm, surface degradation does not allow a significant improvement of the adhesive properties despite the formation of polar groups

and assume that this could be related to either thermal effect or photon induced chain scissions (degradation).

Feng *et al.* [21] presented results of ablation of polypropylene (PP) using a 248 nm KrF excimer laser (τ=30 ns, f =10 Hz) with a fluence in the range of 0.4–2 J/cm^2. They showed both experimentally and theoretically that thermal and photochemical mechanisms are to be operative simultaneously during the irradiation process. They also showed existence of thermal affected zone (TAZ) together with ablative zone (AZ) and unaffected zone (UAZ) in the ablated crater. Increase in both fluence and the number of pulses led to more striking thermal effect as demonstrated by the spatial expansion of the rim for polypropylene.

Chen *et al.* [22] performed multi-pulse drilling on polyimide (0.050 mm in thickness) and PETP using 248 nm excimer laser. Increase in etch rate with increase in fluence was reported. Clean and smooth edges were reported at fluence below 2.7 J/cm^2, while high fluences led to the formation of some structures (or debris) at the top surfaces of the edges. At high fluence, the process no longer remained purely photochemical in nature and significant thermal degradation was reported. They also pointed out that wall angle decreases with an increase of energy fluence (taper of the holes) due to diffraction effects at the edge of the mask that produces lower fluences and lower etch rates in the region. Optimal energy densities for polyimide and PETP ablation were reported to be 1.7 J/cm^2 and 0.36 J/cm^2, respectively.

Dyer and Karnakis [23] reported incubation of UV absorbing chromophores by photoinduced modification appears to play a major role in controlling abaltion of low density polyethylene (LDPE) under irradiation of ArF (193 nm). They also found that

long term, low fluence permits high quality etching compared to higher fluence which give poorer quality involving high density of small blow-holes suggestive of the release of gaseous products. At low fluence, little or no redepositted debris appeared. They also pointed out a small increase in laser energy transmission for LDPE during the first few pulses and steady decrease as the number of pulses increase. They assumed that the first few pulses would remove the contaminants on the surface.

Braun *et al.* [24] spin coated polyimide (Pyralin PI 2560, DuPont, thickness 12 μm) and ablated it with KrF (τ= 20 ns) in atmosphere from 25˚C to 200˚C. They showed the ablation rates to drop with increase in temperature for laser fluences between 60 and 2750 mJ/cm^2. By using Beer's Law of absorption, they fitted an empirical linear correction term, which decreases with increase in substrate and ambient temperatures. Only small differences in index of refraction (1.75 @ 25˚C and 1.78 @ 220˚C) have been observed and that can not explain the decreasing ablation rate vs. increasing substrate temperature. As to date, no satisfactory physical nor chemical explanation could be found for this behavior.

Srinivasan *et al.* [25] etched PMMA with 248 nm which has a FWHM of 40-100 ns. They found the etch depth to depend on the pulse width. They also found that solid products that are generated from the leading edge of the laser pulse shielding off the latter portion of the incoming pulse in polyimide.

Dijkkamp *et al.* [26] reported results of experiments designed to study the role of thermal processes in pulse laser induced ablation of polymers. They observed rapid decomposition caused by the thermal processes.

Dyer *et al.* [27] measured the thermal coupling and etch rate for Polyethylene terephthalate (PET) and polyimide films irradiated with 193, 248 and 308 nm. They reported thermal energy balance up to threshold fluence and remains constant there after, the excess energy being carried away by the ablated material and limit surface temperature rise. The temperature of ablated material was calculated to be $>10^3$K.

Gorodetsky *et al.* [28] reported calorimetric and acoustic studies of the ablation process in Kapton^{TM} using 193, 248 and 308 nm. Above threshold fluence as much as 80-90 % of the laser energy was used to break chemical bonds. Absorption energy density is independent on the wavelength. Ablation energy is used for bond breaking and ejection of the fragments. They concluded that both photochemical and photothermal effect are important to the ablation process.

Danielzik *et al.* [29] found that 193 nm will directly scission the chemical bonds of PMMA into MMA monomer. Infrared temperature measurements of MMA monomer which has been ejected was conducted and found that temperature increased with increase in fluence.

Srinivasan *et al.* [30] using high fluence (>1 J/cm^2) of 193 and 248 nm ablated Polyimide, PMMA and TNS2 (an IBM proprietary material) photoresist. From their model, they predicted high fluence has a substantial thermal contribution in the fluence range of 2-18 J/cm^2 per pulse.

Brannon *et al.* [31] used infrared spectroscopy and coupled gas chromatography/mass spectroscopy to identify several gases evolved during etching polyimide with 248, 308 and 351 nm in air and vacuum. CO_2, CO and H_2O, gases such as HCN, traces of benzene, and perhaps other high-molecular weight hydrocarbon are formed during the ablation.

Small amounts of brownish, incompletely combusted, condensed material remained near the etch site. O_2 was shown to take no direct role in the etch rate.

Brandon *et al.* [31] and Srinivasan *et al.* [32] reported the formation of black solid "soot" when polyimide was ablated. This black solid was made up of elemental carbon.

Dyer *et al.* [33] reported stress waves generated by ablation and sub-threshold thermoelastic mechanism in irradiated polymer. At high fluence, ablation was reported to commence within 4-6 ns of the start of the laser pulse and generate short acoustic impulses (~20 ns) with a peak stress of $>10^7$ Pa.

Dyer *et al.* [34] reported incubated absorption and ablation in polypropylene irradiated with 193 nm. Ablation occurs after a significant number of pulses as a result of photoinduced modification of the polymer which induces new chromophores, raising the absorption coefficient. The quality of the ablated surface is reported to be superior under this condition as any thermal loading is lower and radiation penetration is confined to a much shallower level.

Dyer *et al.* [35] reported that the scale of the embryonic surface non-uniformity plays an important role to determining the final features produced. They also showed that re-deposition of ablated material extends to a distance of 0.5 mm at the edges of the ablation site.

Changes in the surface of a film of polyethylene terepthalate (PET) and polyimide (Kapton^{TM}) with 248 nm (FWHM 20 ns) in air have been measured by Srinivasan and *et al.* [36] by probing the surfaces with visible laser pulses of <1 ns at delay times of 10-10000 ns. They reported an intense and rapid darkening of the surface at <60 ns which may be due to scattering of the beam by gas bubbles. In 100-1000 ns, a large blast wave

was reported to be visible. At the end, the polymer surface was not darkened but an etch pit was apparent.

Sutcliffe *et al.* [37] defined the term "incubation pulses" as pulses of ultraviolet laser irradiation which are directed initially at a polymer surface and which etch less depth per pulse than subsequent pulses which remove identical depths of material at each pulse. A model based on a time-dependent treatment of the ablation of organic polymer surfaces by UV laser radiation was proposed.

Srinivasan *et al.* [38] reported incubation phenomena in PMMA at 193 and 248 nm (<1 ns). They observed elevation of surface of PMMA the first 3 pulses before ablation took place. The elevated material is soluble and can be washed away by solvent resulting in a net hole. This build up was reported by Kuper and Stuke [39] as the formation of photoproducts such as methyl formate.

Davis *et al.* [40] studied the transmission of PMMA during laser ablative photodecomposition. When threshold fluence is used, a discrete change of the transmittance after the first pulse was observed due to a combination of the deposited debris. When several times of the threshold fluence was used, a rapid decrease in transmission occurred during the first pulse due to scattering and absorption of the laser light by the ejecting material during the initial part of the pulse. The increased scattering by the plume, during the first pulse, caused the intensity transmitted to the resist to drop and the rate of removal of material to fall.

Srinivasan *et al.* [41] found that with 193 nm, 18 % of the ablated PMMA wais MMA, whereas at 248 nm less than 1 % appeared as MMA. Their results suggest that ablative photodecomposition involve both a one-photon process, which gives rise to

MMA and low molecular weight polymeric fragments and a multi-photon process, which gives rise to products such as C_2 with high translation energy. At longer wavelengths, a high temperature rise within the ablated volume may be necessary to increase the quantum yield for breaking. Estler and *et al.* [42] also performed similar experiment with 266 nm, the major products were dominated by CO_2, CO and methymethacrylate (MMA).

Dyer *et al.* [43] studied the ablation process on Uniplex polyimide (PI) and low density polyethylene (LDPE) at 193nm using high speed shadow photography (HSSP), probe beam deflection (PBD) and time resolved interferometry (TRI). They found the ablation products to travel at supersonic velocities and form shock front with HSSP. 'Mushroom cloud' of large fragment products was captured by HSSP. Threshold fluence for the PI and LDPE was found to be 20 and 200 mJ/cm^2, respectively. They also found that the laser 'incubation' pulses for the LDPE was 60 pulses.

3.2 Silicon

The literature on laser ablation of materials, in general, is quite extensive. An attempt will be made to include representative works that closely cover the subject area under investigation, namely, short pulse laser ablation of silicon with a 248 nm excimer laser in air and under water. This way the scope can be limited and consequently, the material to be covered under the literature review. Kruusing [46, 47] recently published an extensive review of both underwater and water-assisted laser processing of materials in two parts. Each part covers some 120 references and should be consulted for more details on research work conducted by other researchers.

Kruusing [46] considered the presence of water in laser ablation in the following three categories: (1) the presence of water in the form of moisture or humidity in air, (2) water as a working environment in some underwater processing applications, and (3) addition of water for special purposes, such as to avoid redeposition of the debris generated on to the finished surface, or to cool the workmaterial, or act as a chemical agent, or to increase plasma pressure, or to conduct light. All water-assisted laser processing techniques rely on the basic physical phenomena involving transmission (or absorption) of light by water; water vaporization; plasma formation, expansion, and quenching; bubble formation, growth, and collapse; and finally shock wave formation and propagation.

Some of the advantages of water-assisted laser processing include the following: light transmission, development of higher plasma pressure due to confinement, water carrying away the debris, more effective cooling, useful chemical reactions, reduced pollution by waste gases and aerosols, reduced noise level, higher optical breakdown threshold than in air, and smaller focal spot size.

Some of the disadvantages of laser ablation under water include the following: some light is absorbed by water; light may be scattered by the water surface, suspensions, and bubbles; power loss due to water cooling; water photolysis; water vapor hazardous to electronics; and possible corrosion of materials.

Krussing [47] reported the laser ablation rate under water to be higher than in air for some materials (or experimental conditions), while for other materials, it is just the opposite. For example, the etching rate of silicon was reported to be two times higher in

water than in air at laser fluences of up to 5 J/cm^2. In contrast, in the case of various metals, Krussing [47] reported that the etching rate is about half of that in air.

Davis *et al*. [48] showed high resolution direct etching of GaAs (thickness of 420 μm) using excimer laser with wavelength of 193 nm (ArF), 248 nm (KrF) and 351 nm (XeF). They pointed out that threshold fluence (23, 33, 80 J/cm^2 respectively) for etching in air increases at longer excimer wavelengths. The morphology of the etched region depends on the wavelength. They also found that when irradiating the GaAs at all wavelengths with low incident fluences ($\leq$ 180 mJ/cm^2) in either vacuum (10^{-2} Torr) or N_2 (1 atm) environments, the etch depth per pulse is less than a quarter of that observed when exposure takes place in air. Some etching of GaAs occurs as a result of photochemically induced reaction with atmospheric oxygen. According to Herzberg [84], wavelengths longer than ~ 244 nm cannot photodissociate O_2 directly by single photon process. Davis *et al*. [48] proposed that the reaction may be induced by the hot substrate interacting with oxygen to form an oxide layer on the surface that changes the absorption characteristics of GaAs.

Dupont *et al*. [49] conducted an experimental wavelength to characterize and enhance the ablation of materials using common industrial laser sources from UV (248 and 308 nm), to visible (532 nm), to infrared (1064 nm) using a stainless workmaterial. They investigated the effect of plasma confinement on material ablation. A flowing water film was introduced to trap the plasma created upstream of the sample thereby stopping the expansion of the plasma and increasing in the mechanical impulses (shock waves) communicated to the workmaterial. They reported an increase in efficiency of ablation by a factor of 2 to 15 for a given incident power density. Dupont *et al*. [49] also found this to

be the case with alumina and silica glass. This observation runs counter to the results of the review presented by Krussing [47].

Park *et al*. [50] investigated the transient pressure generated by the interaction of short-pulsed laser light with the liquid-solid interface using a photoacoustic probe beam deflection method and a broadband piezoelectric transducer. They postulated that when a short pulse (nanoseconds) KrF excimer laser beam irradiates water on a solid surface, it induces rapid thermal expansion and explosive vaporization. They reported compressional pressure wave with peak intensity on the order of 1 MPa at laser fluences up to ~100 mJ/cm^2. By monitoring the bubble growth kinetics, Park *et al*. [50] observed that pressure generation is enhanced by the bubble expansion in the superheated water for laser fluences exceeding the bubble nucleation thresholds.

Sano *et al*. [51] found an improvement in residual stresses from tensile to compressive by underwater laser irradiation due to impulsive pressure of the laser induced plasma generated by the interaction of the intense laser pulse with the workmaterial. The plasma was generated by the irradiation of the second harmonic of a Q-switched Nd:YAG laser (λ= 532 nm) on a SUS 304 stainless steel workpiece. The spot size was 0.75 mm and the pulse duration was 5 ns. They reported the formation of a high-pressure plasma on the surface of the workmaterial by irradiation of an intense laser pulse and this pressure is significantly enhanced by the presence of water. They estimated that the pressure of the water-confined plasma to exceed 2 GPa. They also deduced that some 20% of the plasma internal energy would represent the thermal energy.

Kim and Grigoropoulos [52] and Kim *et al.* [53] investigated the mechanisms of pulse laser-induced ablation of strongly absorbing liquids and the generation of acoustic

transients. They used aqueous solutions of K_2CrO_4 and pure water and irradiated with KrF excimer laser and CO_2 laser, respectively. They observed the ablation process, including the vapor cavity formation and the acoustic wave propagation, using laser flash photography. When the absorbing liquid surface is irradiated by a laser pulse and the energy exceeds a certain threshold, ablation is initiated by thermal (effected by temperature rise) or mechanical (caused by local pressure drop) mechanisms depending on the evolution of temperature and pressure fields. If the heating rate is gradual, the ablation is induced by thermal evaporation due to temperature rise under ambient pressure without significant pressure variation during the process. However, the ablation threshold is determined by the local pressure drop in the case of 'rapid' heating by a short pulsed laser.

Kim and Grigoropoulos [52] also reported no significant surface deformation or ablation plume ejection during the laser pulse irradiation despite the high surface temperature rise above the superheat limit. A noticeable surface deformation occurs after the laser pulse. The upward vapor plume ejection and the shock-wave propagation in air indicate that surface depression is caused by the recoil momentum applied by the ablation plume. In this stage, intense hydrodynamic motion of the bulk liquid is activated, generating upward flow and bulk-liquid ejection. This suggests that significant enhancement of mass ejection can be achieved by the action of cavitational bubble dynamics after the laser pulse irradiation.

Ho *et al*. [54] conducted a computational heat transfer and gas dynamics study in pulse laser evaporation of metals. They showed that the ejected high-pressure vapor generates shock waves against the ambient background pressure.

Gieger *et al* [55] conducted excimer laser ablation tests under a thin water film to modify the microstructure of materials, mainly, ceramics. They used a KrF excimer laser with an energy density of 9 J/cm^2 and a pulse frequency of 10 Hz. They compared dry machining with underwater machining and found that in underwater machining, the redeposition of ablated material was completely avoided resulting in better quality of finished surface and the need to remove the debris generated subsequently. They also found that melting of the irradiated material is reduced by applying a thin film of water. They reported that for some ceramic materials(e.g. alumina), the ablation rate is increased significantly (~15 times) while for many other materials, for example, SiC, Si_3N_4, ZrO_2, AlN, glass, steel, polyamide, the ablation rates were much lower (1/3 to 1/2) compared to the machining in air.

Andreic *et al*. [56] investigated droplet formation during laser sputtering of high-purity single-crystal silicon with a nitrogen laser radiation wavelength of 337 nm, pulse duration of 6 ns, a maximum energy density of 1.1 J/cm^2, and non-uniform target-energy distribution. They observed many micrometer-sized droplets ejected out of it and splashed onto surrounding target area. They proposed that droplets are produced with a single laser pulse as a result of hydrodynamic instability of the molten surface layer. They attribute the intense splashing as a consequence of the large plume pressure generated by the most intense parts of the laser beam.

Feng *et al*. [57] investigated the co-occurrence of photochemical and thermal effects during laser polymer ablation using a 248 nm excimer laser with a fluence in the range of 0.4 to 2 J/cm^2 and at a repetition rate of 10 Hz. They showed that depending on the photon energy relative to the bond breaking energy, photochemical and/or thermal

mechanisms can be predominant. It appears that in the case of ablation of silicon by short pulse lasers, the thermal mechanism may be more predominant.

Jeong *et al*. [58] investigated various material removal mechanisms involved in single-pulse laser ablation on a single-crystal silicon by high irradiance (10^9 to 10^{11} W/cm^2). They pointed out that an understanding of the material removal mechanisms requires the identification of the dominant energy transport mechanism. According to them, the material removal can occur by both thermal and athermal mechanisms. The incident laser radiation on silicon creates a large population of highly excited non-equilibrium electrons near the sample surface. This can lead to bond breaking, an athermal mechanism. Alternately, the excited electrons transfer energy to phonons during electron-phonon relaxation. The energy is redistributed through lattice vibrations and consequently heat is conducted into the sample. This heat may melt or vaporize the sample. Material removal in the form of large micrometer sized droplets can also result from hydrodynamic instability of the molten liquid layer.

Yoo *et al*. [59] used a Nd:YAG laser emitting a beam at 266 nm by quadrupling the fundamental frequency. The silicon sample was ablated using a laser beam size of 50 μm. They found a sudden increase in the slope of the crater volume to laser irradiance at ~2.2 x 10^{10} W/cm^2. This is accompanied by large size droplets leaving the silicon surface with a time delay of ~300 ns. They proposed that explosive boiling (phase explosion) may be the dominant mechanism for material removal for laser irradiance greater than ~2 x 10^{10} W/cm^2.

Zhu *et al*. [60] conducted laser ablation of silicon using a KrF excimer laser of wavelength 248 nm and pulse duration of 23 ns. They reported that laser ablation rate is

highly enhanced by the water film. They assumed that plasma generated in the water confinement region induces a much higher pressure. Once generated, the plasma expands adiabatically at a supersonic velocity, creating a shock wave in front. The high pressure, high temperature plasma results in much higher ablation rate. They reported the laser fluence threshold for silicon to be ~1.5 J/cm^2, which is close to the value found in the present investigation, namely, 1.4 to 1.7 J/cm^2.

Jaschke *et al*. [61] conducted ultrafast (20 and 500 fs) laser ablation of silicon using MD simulations and experiments using a Ti:Sapphire laser. They determined ablation thresholds for pulse durations of 25 and 400 fs. A similar study in the nanosecond region would be extremely useful for experimental studies involving short pulse laser ablation of silicon.

Craciun *et al*. [62] investigated the surface morphology of single crystal (100) silicon irradiated by 266 and 1064 nm laser pulses emitted by Nd:YAG laser. The found the morphology at the bottom of the crater with 266 nm wavelength, which is well absorbed by silicon, (optical absorption coefficient, a = 10 cm^{-1}) remained flat and featureless. The rims of the craters shown signs of radial liquid flow but the vaporization is confined to the surface region.

Amer *et al*. [63] investigated induced stresses and structural changes in silicon wafers as a result of laser micromachining using μ-Raman spectroscopy. They used a KrF excimer laser (248 nm wavelength) with energy of 30 μJ per pulse and a pulse frequency of 100 Hz. They found high tensile stresses (~0.8 to 1GPa) and formation of amorphous silicon (up to 14%) by laser irradiation.

3.3 Borosilicate Glass

Kawaguchi *et al*. [64] exposed polished silica glass to pulsed KrF radiation. Somewhat below the threshold for surface optical damage, transient localized luminescence due to micro-plume formation is observed. Surface optical breakdown itself is accompanied by localized luminescence due to excited neutral Si atoms region. These craters reflect the localized heating and vaporization that give rise to the Si luminescence. The morphology of surfaces damaged by cumulative exposure at fluences below the damage threshold and by single pulses at fluences above the threshold is similar, suggesting that damage under cumulative exposure involves the damage centers responsible for single pulse damage.

Ihlemann [65] based on his comparative study of different wavelengths, pulse durations, and surface qualities concluded that different ablation mechanisms are involved: The first seems to be based on volume absorption, bond breaking and material expansion, and the second appears to be controlled mainly by damage in relation to the singularity conditions at the surface.

Omori and Inoue [66] observed thermal effect in the excimer laser ablation of inorganic materials. In the case of femtosecond laser, two different absorption mechanisms were observed. The first occurs during the initial laser pulses with fluences above the ablation threshold and determines the incubation range. There, multi-photon absorption results in moderate energy volume densities. The second mechanism is determined by a much higher absorption at defects created irreversibly during each additional pulse. It results in gasification without major participation of the melt. If only multi-photon and instant color centre generation prevail, crater diameters should be

independent of the number of pulses since each single 300 fs pulse would generate its own absorptivity which reversibly would vanish afterwards. However, the irreversible laser-induced defects have to be generated for efficient ablation. The rate depends on the local defect generation which is a direct function of the local intensity decaying towards the edges of the laser spot profile. Therefore, fluence increases resulting in greater hole diameters.

Sokolowski *et al*. [68] observed hydrodynamic expansion of a hot, possibly supercritical fluid, in the case of femtosecond laser-induced ablation for semiconductor and metal surfaces. They found that during the ablation process, material undergoes a transition from an initial metallic state into a highly refractive, insulating phase.

Buerhop *et al*. [69] conducted laser ablation and surface modification of glasses using CO_2 laser and XeCl excimer laser. They reported float glass fractures after irradiated for 40 s at 60 W/cm^2 with CO_2 and, vitreous silica withstands higher intensities and material removal occurs by evaporation. For XeCl laser, experiment was conducted between 9 and 20 J/cm^2. When the threshold fluence was exceeded, noise emission, plasma generation and ablation of front surface were observed. Glasses with higher absorption coefficient have lower ablation rates. Glass contenting 8% iron gave a constant ablation rate (0.7 μm/pulse) regardless with increases of fluence. Float glass gave 2 μm/pulse and with slight increase in ablation rate with increase of fluence. However, borosilicate and vitreous glass showed a decrease in ablation rate with increase of fluence. However, the reason for this is unknown.

Buerhop *et al.* [70] used CW CO_2 laser (8.6 μm), pulsed Nd:YAG laser (1064 nm) and pulsed XeCl excimer laser (308 nm) to treat fused silica and soda-lime silicate glass

using power densities of 10^6 W/cm^2. They investigated melting, softening and ablation effects for all the glasses. Evaporation of material produced 0.3 mm diameter holes in fused silica under CW CO_2 laser. And, no obvious surface reaction by Nd:YAG laser, somehow XeCl gave high ablation rate of 10 μm/pulse but rough surface finish. They also reported tangential crack around the hole during the cooling process for CO_2 and Nd:YAG laser heat treatment of soda-lime-glass. For XeCl excimer laser, with threshold fluence of 3 J/cm^2, cracks were observed only in the solidified thin molten layer.

Jackson *et al.* [71] performed excimer laser ablation of neodium (Nd) doped glass and Nd doped yttrium aluminum garnet (YAG) using ArF (193 nm) and KrF (248 nm). They found the threshold fluence in the range of 0.5-1.6 J/cm^2.

Dyer *et al.* [72] found the ablation threshold fleunce for soda lime glass to be 1.0 J/cm^2 for 248 nm. Fluence above this value produced microcracking on the surface. Also, the fracture extended well beyond the margin of the irradiated zone. No significant incubation effect was observed below the ablation threshold even after 10^3 pulses.

Keiper *et al.* [73] performed drilling on borosilicate glass (Pyrex®) with 248 nm and 193 nm. Wall angle of 3.5˚ and 1.6˚ were reported with respect to 100 and 30 μm beam diameter. Break off of material were reduced by applying a thin layer of alcohol between a second wafer underneath the drilling wafer.

Konovalov *et al.* [74] reported 157 nm laser ablation of fused silicate generates localized tensile stress in a thin surface layer (~275 nm) that is independent of fluence (1.9-4.7 J/cm2) and ablation depth (150-1000 nm).

Allcock *et al.* [75] observed and analyzed CO_2 laser-induced microcracking of glass. They concluded that residual stresses caused by thermal cycling caused microcracking.

According Zhang *et al* [76], when a workpiece is irradiated by an intense (>1 GW/cm^2) laser pulse, the surface layer instantaneously vaporizes into a high temperature and high pressure (1~10 GPa) plasma. This plasma induces shock waves during expansion from the irradiated surface, and mechanical impulses are transferred to the target. If the plasma is not confined (in open air), the pressure can only reach several tenth of one GPa. If the plasma is confined by water or other media, the shock pressure can be magnified by factor of 5 or more compared to the open air condition [83]. The shock pressure lasts 2 to 3 times longer than the laser pulse duration. When shock wave is acting on the substrate, material beneath the shock undergoes both plastic and elastic deformations. Shock pressure is attenuated as it propagates downwards and outwards. When the shock wave reaches the bottom, it is bounced back. Peyre *et al* [77, 78, 79] and Jeong *et al* [80] studied laser-driven shockwave in stainless steel and aluminum.

CHAPTER 4

PROBLEM STATEMENT

In order to understand the interactions between the laser beam and the work material, a systematic multi pulses laser micromachining studies were conducted. Results from analytical studies of multi pulses laser drilling process would help us develop and optimize the process.

The first objective of this work was the installation of excimer laser with associate optics for laser micromachining. It may be noted that excimer laser micromachining facility is being established for the first time at Oklahoma State University.

The second objective is to align the laser and use it under safe, operating conditions.

The third objective is to provide means for computer numerical control (CNC) of the X, Y, Z and U (rotation)-axis motions of the workpiece and the excimer laser generator and to link them to a computer in which the micromachining process is being controlled.

The fourth objective is to conduct laser micromachining experiments on silicon wafer and borosilicate glass. The objective is to determine the response of these materials with the excimer laser beam under several operating conditions, such as pulse width, number of pulses, and pulse energy density. The surface quality of the holes drilled is analyzed using an optical microscope, MicroXAM laser interference microscope, scanning electron microscope (SEM), and environmental scan electron microscope (ESEM)

The fifth objective is to optimize the process parameters to obtain best finish and uniform geometry with minimum surface damage.

The sixth objective is to analyze the effect of a presence of a layer of liquid (water) on the surface of workpiece during laser micromachining.

CHAPTER 5

DISCRIPTION OF EXCIMER LASER MICROMACHINING SYSTEM AND OPERATING PROCEDURE

5.1 Introduction

The excimer laser micromachining system used in this investigation can be divided into three main components: (1) Excimer laser generator system, (2) Stage and motion controller, and (3) Optical or laser beam delivery system. A computer station is used to interface the excimer laser generator system with the stage and motion controller.

5.2 Excimer Laser Generator System

The excimer laser beam is generated by a medium power (25W) COMPex 205i laser manufactured by Lambda Physik. Figure 5.1 and 5.2 show a schematic and a photograph of the COMPex 205i. It can be used from a range of microprocessing operations, such as microdrilling, microcutting, micromarking, and surface treatment. In this investigation the laser system utilizes a krypton fluoride (KrF) gas as the lasing medium (248 nm give wavelength).

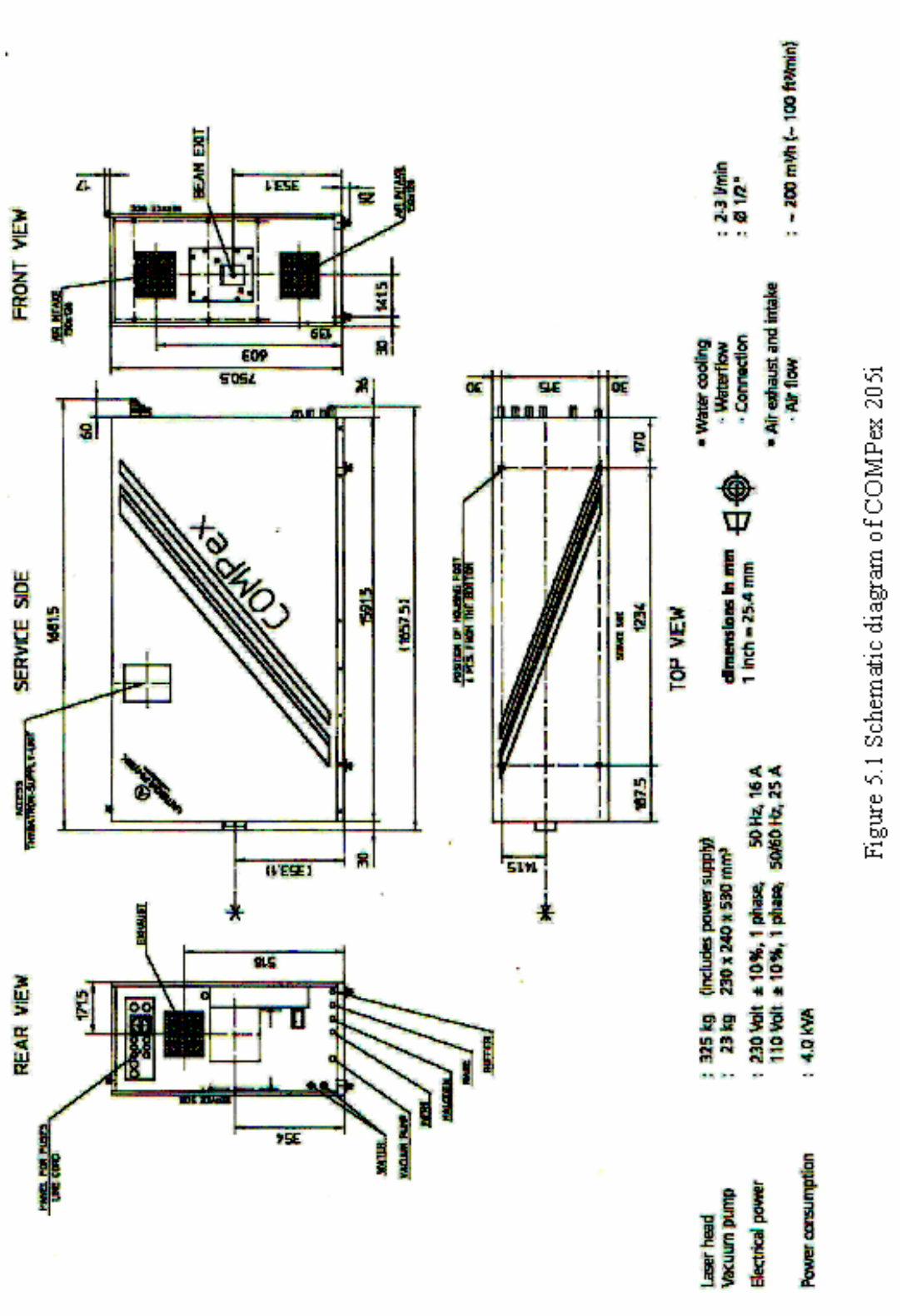

Figure 5.1 Schematic diagram of COMPex 205i

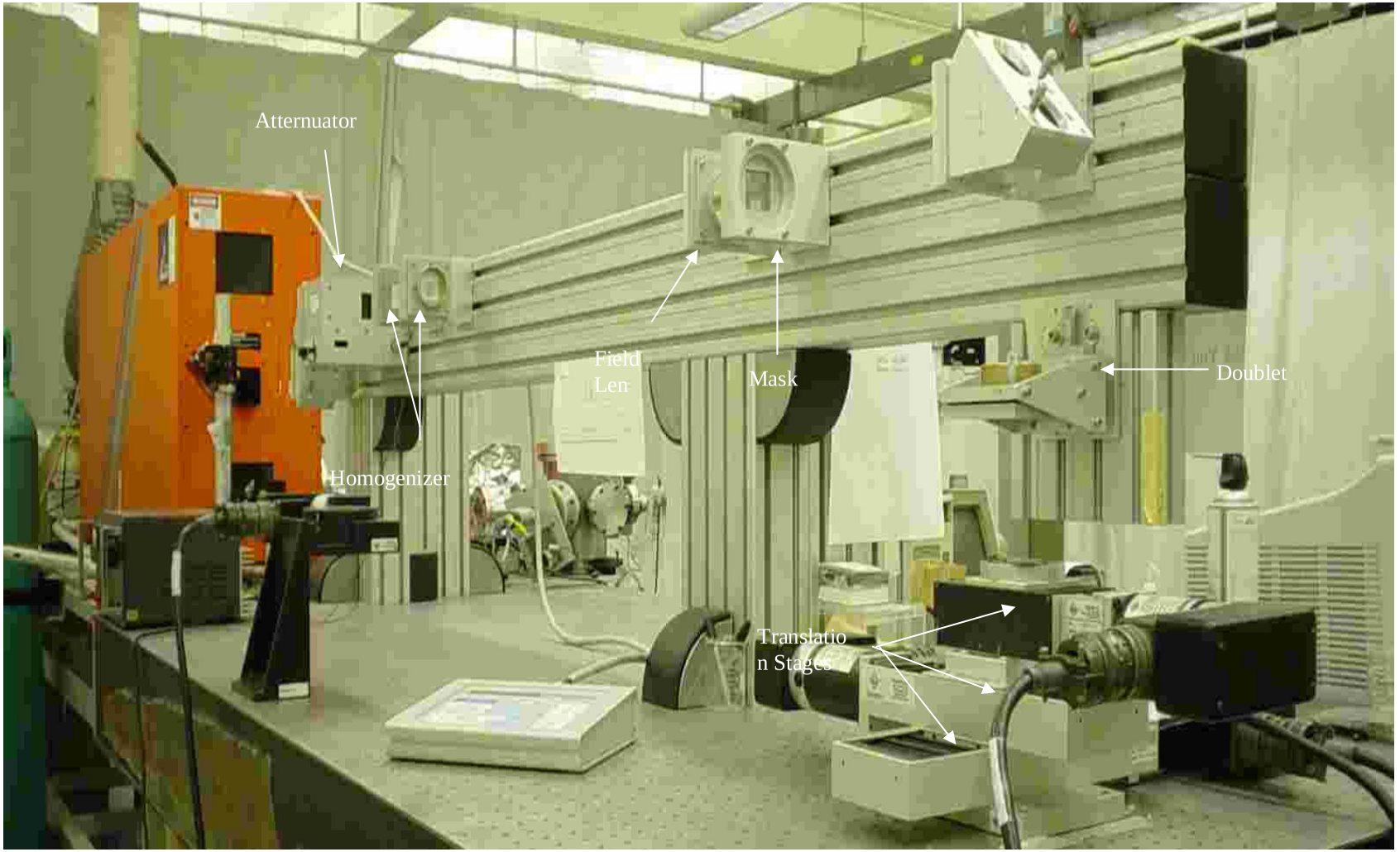

Figure A.2 Photograph of the experiment setup for excimer laser micromachining.

COMPex 205i Excimer Laser Specification

COMPex 205i Excimer Laser is equipped with Lambda Physik's NovaTube technology which provides stable laser performance, reduced maintenance, and lowest possible operating costs. Typical gas lifetime of COMPex 205i is on the order of 10^6 laser pulses. It should be installed in a dry and clean area and the ambient temperature should not exceed 25 °C. Table 5.1 gives the specification of COMPex 205i excimer laser with KrF (248 nm).

TABLE 5.1

SPECIFICATION OF LAMBDA PHYSIK COMPEX 205i EXCIMER LASER

COMPex 205i Excimer Laser	F_2	ArF	KrF	XeF
Wavelength (nm)	157	193	248	351
Pulse Energy *[1] (mJ)	16	400	600	300
Max. Average Power *[2] (W)	0.7	15	25	15
Maximum repetition rate (Hz)	40	50	50	50
Pulse Duration (nominal, ns)	n.m.	20	25	20
Pulse-to-Pulse Stability [*3] (± %)	n.m.	4	4	4
Beam Dimensions *[4] (mm^2)	$24x6^{-12}$	$24x6^{-12}$	$24x6^{-12}$	$24x6^{-12}$
Beam Divergence *[4] (mrad)	3x1	3x1	3x1	3x1
Time Jitter [*5] (± ns)	2	2	2	2

All specifications are measured with an energy monitor and optimized gas mixture.
*[1] Pulse energy is measured at low repetition rate.
*[2] Maximum average power is measured at maximum repetition rate.
*[3] Based on 90% of all pulses.
*[4] Typical value, FWHM.
*[5] Typical value, 1 Sigma.

Power Supply

The COMPex 205i is connected to a 115 V (10%) 25A power supply.

Gas System

Table 5.2 gives the specification of the gases using in the system. All gas cylinders have a ¼" (or 6 mm) Gyrolock pressure regulator. Gases are injected and stored in the lasing tube. Laser energy drops with time, until then the spent gases must be pumped out and replaced. All gas inlets are closed all the time and the valves are opened only during the refill process.

TABLE 5.2

SPECIFICATION OF GASES USED TO GENERATE 248NM EXCIMER LASER FOR COIMPEX 205i.

	Buffer	Rare	Halogen	Inert
Type of Gas	Ne	Kr	5% F^2/ 95% He	He
Purity	99.995%	99.99%	99.995%	99.995%

Fluorine and hydrogen chloride are used in small concentrations. They are corrosive and toxic when used over a long period of time. A vacuum pump is connected to the evacuation outlet for purging all gases out from the COMPex 205i and headed to a suitable exhaust.

Cooling System

Air and water-cooling systems are used to cool down the laser tube in the COMPex 205i. The air is constantly sucked in with a throughput of 300 m^3/h.

When the temperature of the laser tube reaches about 35 °C, a temperature controlled valve inside the COMPex 205i will be on and allow the cooling water (2-3 l/min, 15-20

°C) to flow in. The hose line is limited to ½" diameter and the maximum water pressure is 4 bars.

Laser Controller

The laser generator system is controlled by the following triggers:-

(1) Internal Trigger: Figure 5.3 shows the control terminal which is connected to the trigger. The control panel is used to purge gases, control the power and the pulse energy. It also can control the pulse repetition rate and firing of the laser.

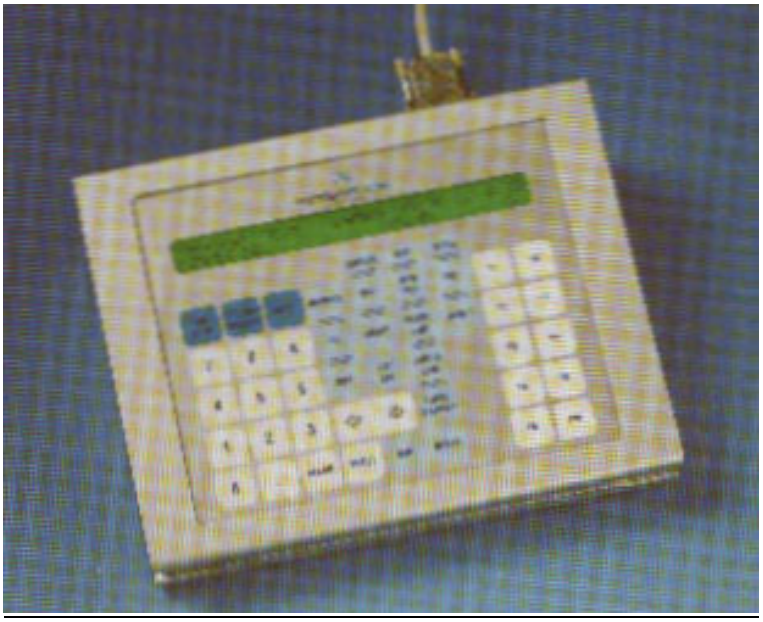

Figure 5.3 Control terminal of the COMPex 205i excimer laser

(2) External Trigger: The external trigger is connected to the computer station to which the stages and the motion control are interfaced. Pulse rate, pulse width and commands to firing of the laser are sent through a cable connected to this trigger.

5.3 Stages and Motion Control System

Figure 5.4 shows a schematic of UNIDEX 500 control system. It is a combination of the U500 PC bus-based motion control card and windows-based MMI interface software. The U500 system integrates with amplifiers and positioning stages to form a complete, programmable, customized control system that is suitable for a wide range of motion control applications.

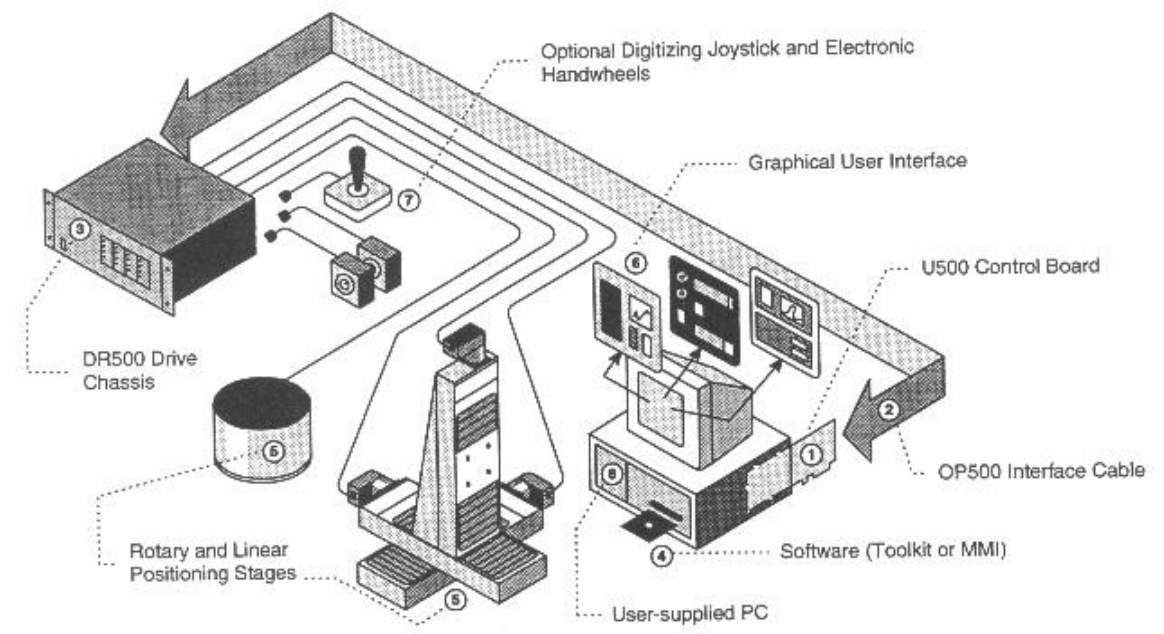

Figure 5.4 UNIDEX 500 system diagram [13].

The stages used are Aerotech's ATS100-150 (X-axis), ATS100-100 (Y-axis), AVS105 (Z-axis) and ART310 (rotation). Figure 5.5 shows a cutaway view of a single positioning stage. X and Y-axes stages are linear positioning devices that use a ball screw to drive a stage table back and forth along a single axis of motion. Each stage features an extremely low profile and ideal balance of accuracy, resolution, and load bearing

characteristics. Their advanced performance is the result of combining a one-piece base with a 2 mm-lead, precision-ground, preloaded ball screw and a linear motion guide (LMG) bearing system.

The one-piece base, machined from extruded aluminum, adds stiffness and stability. Other design features include high quality, preloaded duplex screw bearings to reduce axial play, integral bellows way covers to keep contamination out of the internal mechanism. Optical limit switches and mechanical end stops are used to protect the stage table from over travel. All of these stages are manufactured to exacting tolerances for straightness and flatness. Table 5.3 gives the specifications for the stages.

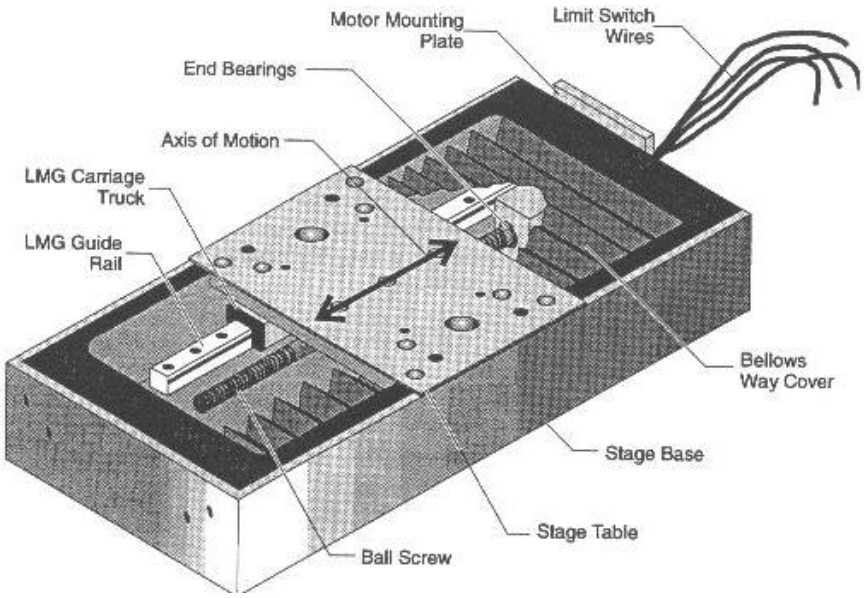

Figure 5.5 Cutaway view for Aerotech's ATS100-200 stage [14].

TABLE 5.3

SPECIFICATION OF AEROTECH'S POSITIONING STAGE

	X Axis	Y Axis	Z Axis	U Axis
Stage	ATS100-150	ATS100-100	AVS105	ART310
Motor	1035LT	1035LT	1035LT	1035LT
Encoder step/rev	2000x4	1000x4	1000x4	1000x4
Lead/gear ratio	2 mm	2mm	2 mm lead with 5:1 wedge	54:1
Machine Resolution	0.00025mm	0.00025 mm	0.0001 mm	0.0016666º
Program Resolution	0.001 mm	0.001 mm	0.001 mm	0.001º
Maximum Speed	4500 mm/min	4500 mm/min	300 mm/min	4000º/min

5.4 Optic Delivery System

The optical delivery system consists of five main parts: (1) Attenuator module, (2) Homogenizer, (3) Field lens, (4) Mask, and (5) Doublet. Figure 5.6 shows a schematic of the optical delivery system.

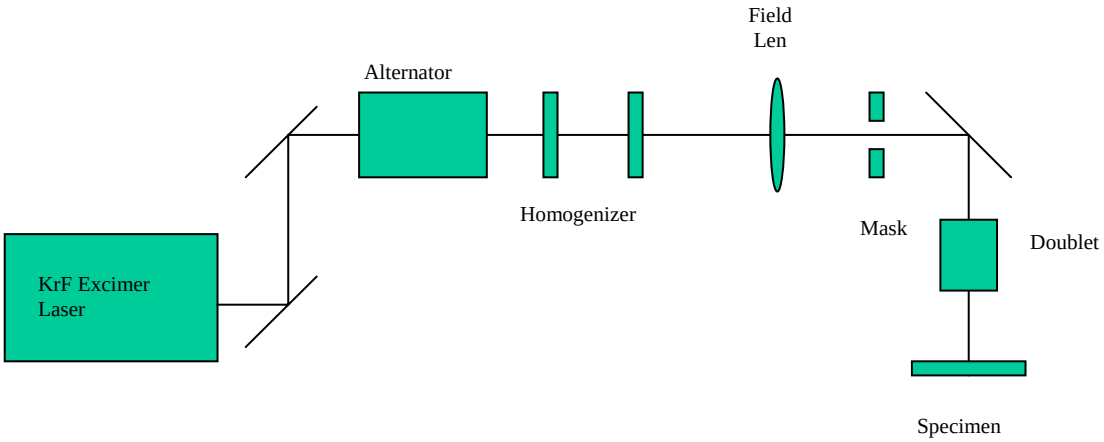

Figure 5.6 Schematic of the optical delivery system for 248nm excimer laser.

Attenuator Module

The optical attenuator uses a specially coated attenuating element and a counter rotating compensator plate, which compensates the laser beam displacement. The angle of the elements can be varied using a hand-driven dial on the front panel of the attenuator housing. The optical transmission could be changed from 10 to 90% by changing the angle. In another words, the attenuator module is used to control the intensity of the laser.

Homogenizer

The homogenizer consists of two arrays of cylindrical lenses and condenser lenses. The main function of the homogenizer is to cut the raw excimer laser beam (non-homogeneous intensity profile) into segments and overlay the segments at the object plane to create a homogeneous intensity profile. Figure 5.7 shows the operational principle of a single axis homogenizer. It may be noted that in this investigation a dual axis homogenizer is used.

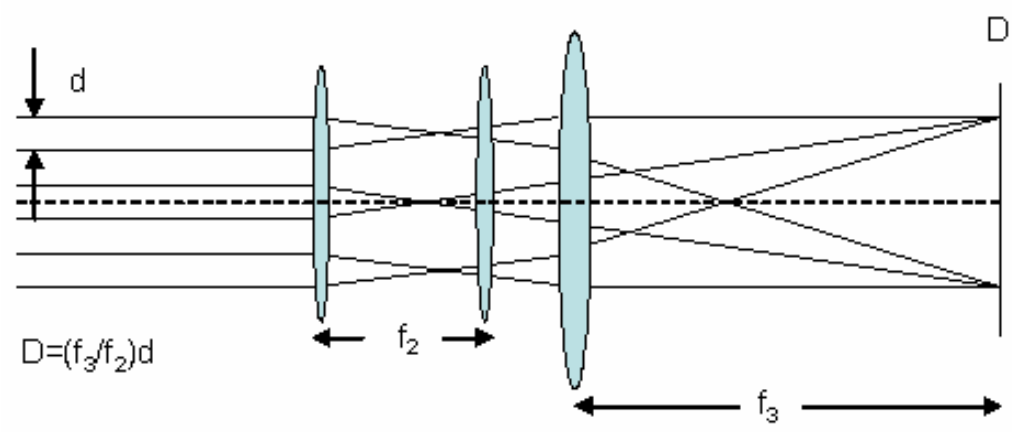

Figure 5.7 Operation principle of the homogenizer (only one axis shown)

The laser beam is segmented. Each partial beam of width d is distributed onto the full width D of the illumination field which is located at a distance of f_3 behind the curved surface of the condenser lens.

All lenses are plano-convex. The focal length, *f* of the lenses is given by

$$f = \frac{r}{(n-1)}$$

where

r = radius curvature

n = index of refraction of the material (for e.g. fused silica 1.508)

Field Lens

The function of the field lens is to gather laser light and converge it into a doublet. Without the light gathering qualities of the field lens, the image would not be clear and uniformly illuminated. Instead, it would be dark and shadowed along the edges.

Mask

A mask is used to control the shape of the structures produced. There are three common types of masks: 1) Free standing metal mask, 2) metal film on quartz substrate, and 3) Dielectric mask. These will be briefly discussed in the following.

Free Standing Metal Mask

These masks can withstand high irradiation energies but due to their high absorptivity in the UV range they are damaged at high repetition rate. Furthermore, their structure

geometry is restricted, and due to their thickness of 10 to 100 mm they cannot be used for high-resolution patterning.

Metal Film on Quartz Substrate

These masks are better suited for high resolution but their damage threshold is rather low even for single pulses.

Dielectric Mask

These masks have a high damage threshold due to their high reflectivity and can be used for high-resolution patterning and for effective use of the laser energy. Due to high cost, a free standing metal mask is used.

Doublet

The imaging doublet is composed of 2 spherical lenses, each with a radius of curvature of r =50 mm. These lenses are mounted with a separation of about 7 mm of the curved surfaces. The doublet is mounted with the curved sides of the lenses both pointing towards the object (mask). The main function of the imaging doublet is to demagnifying the object or mask. Table 5.4 gives the distances from the mask plane to the center of the doublet and from the center of the doublet to the image plane.

TABLE 5.4

DOUBLET SPECIFICATION

Demagnification	5X
Objective Distance	306 mm
Image Distance	61.2 mm
Track Length	367 mm

5.5 Alignment of the Excimer Laser Optical System

To obtain maximum output power from the laser system, it is necessary to align the optical rail assembly components. The resonator is aligned with a laser pilot. The alignment procedure is given in “Lambda Physic Instruction Manual.”

As mentioned in Section 5.4, the optical deliver system consists of 5 parts. All the optical elements have to be set in the positions as given in Table 5.4. The procedures are given in “MicroLAS Excimer Laser Based Micromachining System.”

5.6 System Operational Instructions

The system operational instructions are given in Appendix A and may be referred to for details.

CHAPTER 6

METHODOLOGY

6.1 Introduction

Following are the standard test procedures used for the laser micromachining tests. It involves (1) sample preparation, (2) determination of pulsed laser fluence, (3) determination of focus point, (4) pulsed laser microdrilling, (5) pulsed laser micromachining, (6) pulsed laser machining in different media, (7) optical microscopy, (8) MicroXAM laser interference microscopy, and (9) Scanning electron microscopy.

6.2 Sample Preparation

Laser micromachining is very sensitive. Hence, thin layer of dirt or oil on the surface of the sample can influence the absorption of the UV light. A clean surface is necessary to eliminate detrimental side effects. The following cleaning procedure will remove most common surface contaminants.

1. Place the sample in a beaker with a detergent solution and the beaker in an ultrasonic bath for 120 sec.
2. Rinse with distilled water.
3. Place sample in a beaker filled with distilled water and the beaker in an ultrasonic bath for 120 sec.

4. Rinse with methanol.
5. Place sample in a beaker with methanol and the beaker in an ultrasonic bath for 120 sec.
6. Use compressed air to dry up the sample.

(NOTE: Wear Latex powder-free gloves to prevent oil or dirt contamination)

6.3 Determination of Pulsed Laser Fluence

Pulse energy reduces with gas life time, i.e. after a large number of pulses, pulse energy will decrease. It is therefore, important to determine the fluence or energy per unit area each time before the experiment. A Melectron M400 energy detector is used to measure the laser energy. Laser energy for 50 pulses is measured before every experiment. The fluence is calculated using the following equation:

$$f = \frac{E_{avg}}{\pi \cdot (\frac{D}{10})^2} \qquad (5.1)$$

where

E_{avg} = the average of the single pulse laser energy

D = diameter of the hole of mask

6.4 Determination of Focus Point

Imaging plane has to be obtained by performing ablation test. Sample of Plexiglass® or PMMA is used for this purpose. Machining program (PC-PSOP and G code) is written to command the firing of excimer laser and the movement of the X-, Y-, Z-table. After

machining, samples are analyzed as described in Sections 6.5 to 6.9. Experimental and results are given in Chapter 7.

6.5 Pulsed Laser Micro Drilling

Different number of pulses are used to irradiate different materials. Optimal fluence for micromachining is found for different materials. Experimental results are discussed in Chapters 8 and Chapter 9.

6.6 Pulsed Laser Micro Machining

Pulsed laser with 25 ns FWHM is used to machine different materials. The experimental results are discussed in Chapter 10.

6.7 Pulsed Laser Machining in Different Media

A liquid medium is using to reduce thermal damage to the laser irradiated area. Different media are used and the experiments results given in Chapters 8 to 10.

6.8 Optical Microscope Observation

Using an optical microscope, the surface profiles of the pulsed laser micromachining are observed. Diameter and width of the irradiated area are measured. The thermal damage areas are observed and compared for different micromachining conditions.

6.9 MicroXAM Laser Interference Microscopy Observation

As diameter and width of the holes generated by micromachining is in micrometers, it is difficult to cut the sample into half to observe the cross section without damaging the original profile of the irradiated area. Laser interference microscope (MicroXAM) is used for examining the surfaces. MicroXAM uses different wavelengths of light to scan through the irradiated area and gives a 3-dimensional profile of the area. The height and depth for the holes can be obtained using this technique.

6.10 SEM Observation

An ABET-32 scanning electron microscope (SEM) was used to observe the laser micromachining samples for detailed examination of the thermal damage, cracking, HAZ, re-deposition, etc. The sample has to be thoroughly cleaned to eliminate any foreign particles, before placing it in the SEM. The following cleaning procedure has to be followed. Steps 1 to 6 are the same as mentioned in Section 6.2. Steps 6 and 7 are additional

7. A thin electrical-conducting coating has to be applied to non-electrical conducting materials.
8. Place the samples in the SEM chamber and follow the instructions to obtain the image of the sample. Photographs are taken to compare the finish surfaces.

CHAPTER 7

INFLUENCE OF LASER FOCUS POINT

7.1 Introduction

Prior to conducting excimer laser micromachining, it is important to know the effect of laser focal point on the quality of the hole drilled. Materials with low ablation fluence such as polymers are the best candidate for these studies. On this investigation polymethyl methacrylate (PMMA) was chosen because it is cleanly depolymerized at elevated temperatures to gaseous product and has lithographic application.

7.2 Properties of PMMA

A 2.5 mm thick PMMA (Plexiglass®) was used in these studies. Figure 7.1 shows the chemical structure for PMMA and Figure 7.2 shows the absorption coefficient, ablation threshold and energy per unit volume at ADP threshold of PMMA at different wavelengths. Table 7.1 gives the physical, thermal, and optical, properties of PMMA.

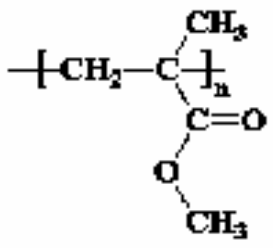

Figure 7.1 Chemical structure of PMMA

TABLE 7.1

PHYSICAL, THERMAL, OPTICAL AND PROCESSING PROPERTIES OF PMMA.

Physical Properties	
Density	1.15 - 1.19 g/cc
Moisture Absorption	0.3 - 0.33 %
Melt Flow	0.9 - 27 g/10min
Mechanical Properties	
Hardness, Rockwell M	63 - 97
Tensile Strength, Ultimate	47 - 79 MPa
Tensile Strength, Yield	55 - 85 MPa
Tensile Modulus	2.2 - 3.8 GPa
Flexural Modulus	3 - 3.5 GPa
Flexural Yield Strength	81 - 138 MPa
Compressive Yield Strength	100 - 117 MPa
Shear Modulus	1.4 GPa
Izod Impact, Notched	0.12 - 0.2 J/cm
Izod Impact, Unnotched	2.7 J/cm
Charpy Impact, Unnotched	1.9 - 6 J/cm²
Charpy Impact, Notched	0.2 - 0.4 J/cm²
Gardner Impact	0.23 - 1.4 J
Tensile Creep Modulus, 1 hour	1800 - 2700 MPa
Tensile Creep Modulus, 1000 hours	1200 - 1800 MPa
Thermal Properties	
CTE, linear 20°C	60 - 130 µm/m°C
Heat Capacity	1.46 - 1.47 J/g°C
Thermal Conductivity	0.19 - 0.24 W/m-K
Melting Point	130 °C
Maximum Service Temperature, Air	41 - 103 °C
Deflection Temperature at 0.46 MPa (66 psi)	80 - 103 °C
Deflection Temperature at 1.8 MPa (264 psi)	41 - 100 °C
Vicat Softening Point	47 - 117 °C
Glass Temperature	100 - 105 °C
Flammability, UL94	HB
Oxygen Index	18 %
Optical Properties	
Refractive Index	1.49 - 1.498
Haze	1 - 96 %
Transmission, Visible	80 - 93 %
Processing Properties	
Processing Temperature	243 - 250 °C

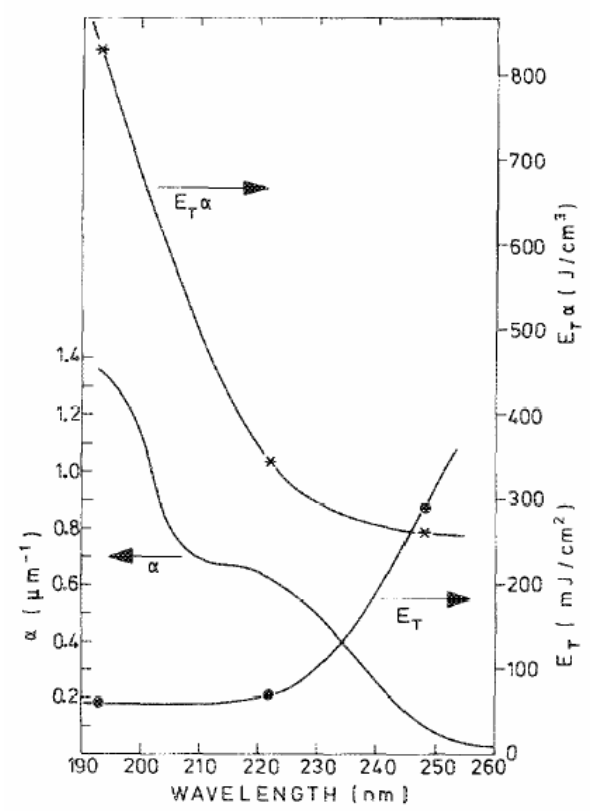

Figure 7.2 Absorption coefficient (α), ablation threshold fluence (E_T) and energy per unit volume at ADP threshold ($E_T\,\alpha$) of PMMA with different wavelength [40].

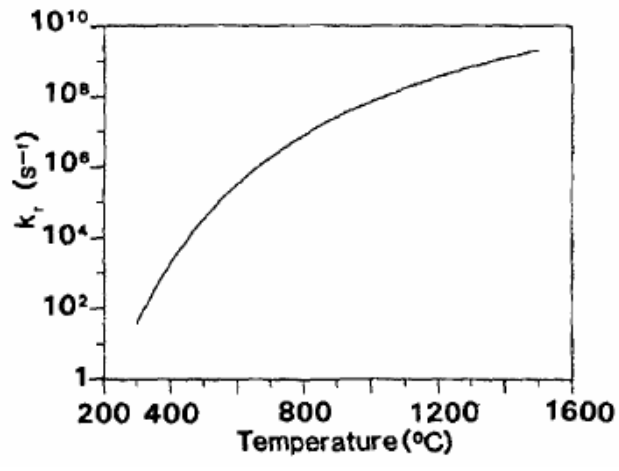

Figure 7.3 Variation of rate constant (k_r) for thermal degradation of PMMA with temperature [30].

7.3 Experiment

Excimer laser pulse with a wavelength of 248 nm and pulse duration of 25 ns was generated with a Lambda Physik COMPex 205i Excimer Laser. The repetition rate was fixed at 10Hz with fluence of 0.535 J/cm^2 per pulse. The experimental setup is as described in Chapter 5. A mask with a 2 mm diameter of hole is used. As the laser beam passed through the doublet (5X), the final beam diameter obtained is 400 μm. The PMMA substrate was mounted on the translation stage. The PMMA substrates were exposed to different number of pulses (1, 2, 5, 10, 20, 50, 100, 200, 500 and 1000). The area around the finished surface was examined by optical microscopy. The ablation depth is obtained by cutting the substrate into half, in which cross section is obtained.

7.4 Results and Discussion

7.4.1 Diameter

Initially, the diameter of the holes increased with the number of pulses, after which it remained constant from 50 to 200 pulses at or close to the focal point. It may be noted that positive value means the focus point falls above the substrate. Figure 7.4 shows the variation of the diameter of the holes with the number of pulses, at different focal points.

When the focal point falls above the substrate, an oval hole was observed as show in Figures 7.5 (e) to (g). This is due to non-focusing image, where energy of the beam has been broken down into small rectangular energy boxes.

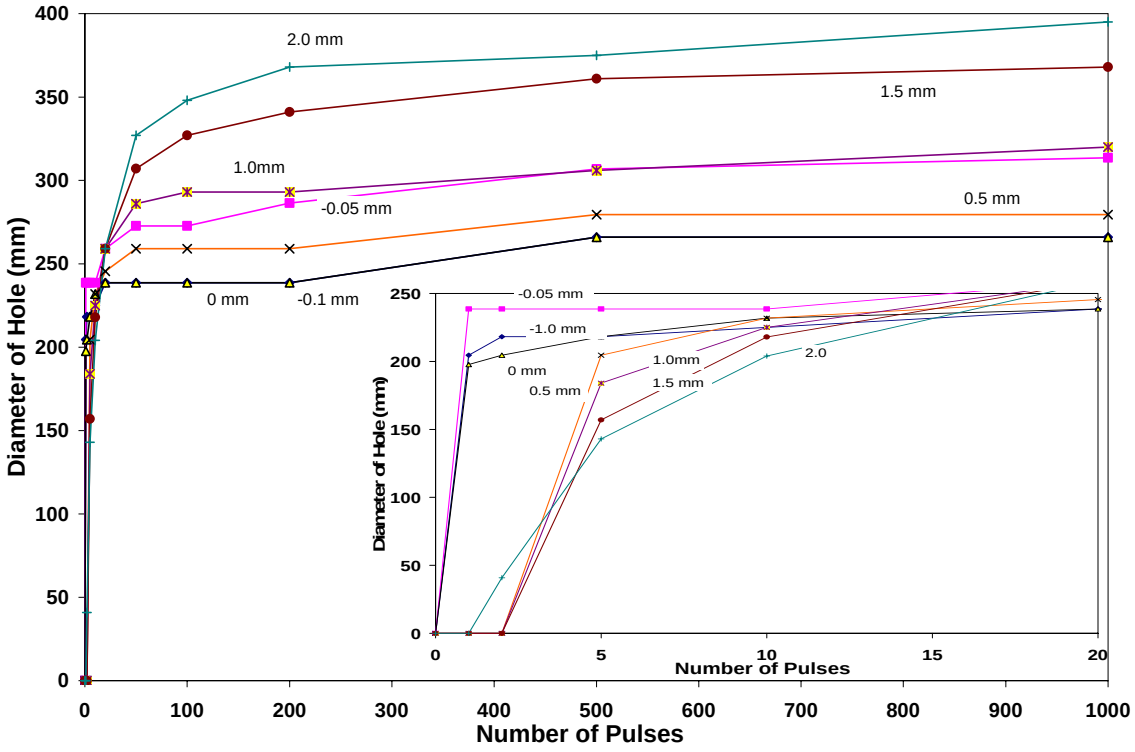

Figure 7.4 Variation of the diameter of holes vs. the number of pulses at different focal points.

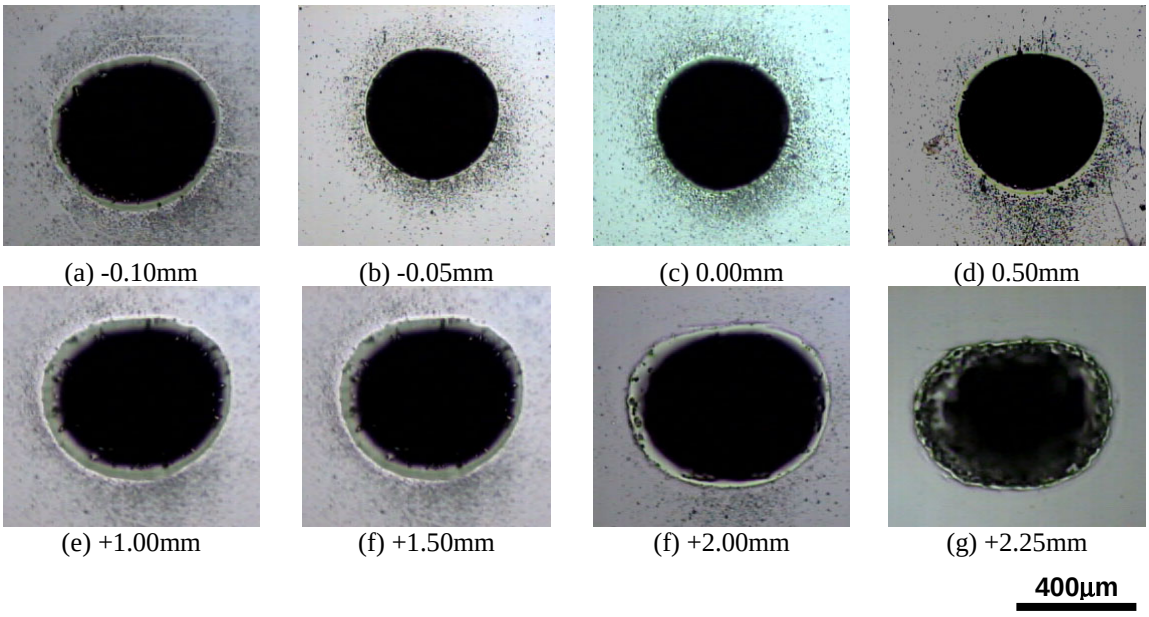

Figure 7.5 Optical micrographs of holes on PMMA irradiated with 200 pulses of excimer laser at different focal points.

7.4.2 Ablation Depth

Figure 7.6 shows the cross sectional profiles for the holes ablated after 200 pulses. It can be seen that the profiles are far different depending upon the distance from the focal point to the surface.

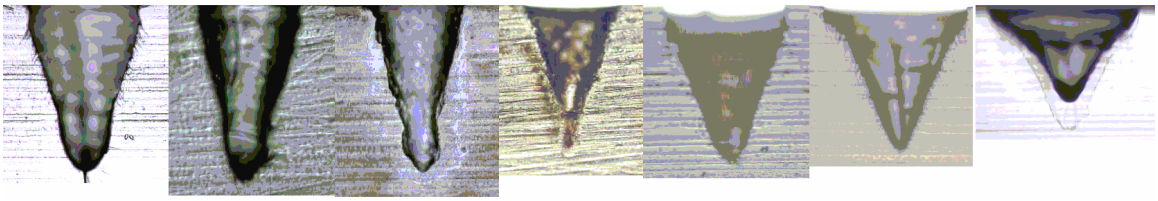

(a) -0.10mm (b) -0.05mm (c) 0mm (d) 0.5mm (e) 1.0mm (f) 1.5mm (g) 2.0mm

400µm

Figure 7.6 Cross section profiles for holes exposed to 200 pulses at different focal point relative to the surface of the substrate.

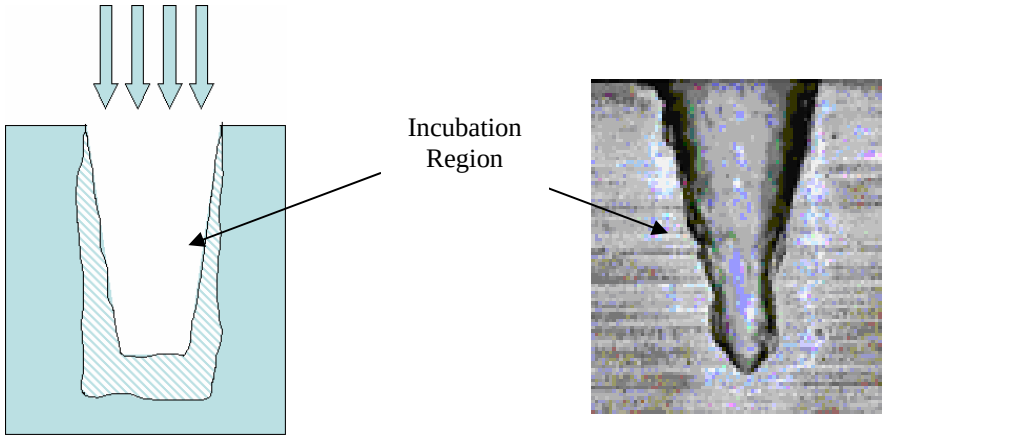

Figure 7.7 Cross section profiles for hole showing incubation region

A secondary affected region can be seen for some samples. As mentioned by Dyer and *et al.* [23], this region is called the incubation region, at which photoinduced modification of the material takes place. Figure 7.7 shows the cross section of a hole

showing the incubation region. This incubation region can be removed by subsequent ultrasonic agitation in an isopropyl alcohol bath. This is an evidence that the structure of the material has been modified.

Figure 7.8 shows the variation of ablation depth with the number of pulses for different focal points. From the results obtained, ablation depth decreases rapidly when the focal point falls far above the surface of the material (2.0 mm). It can be seen from the data, the initial ablation rate is between 3 to 4 μm per pulse until 100 pulses and subsequently decreases to 1μm per pulse.

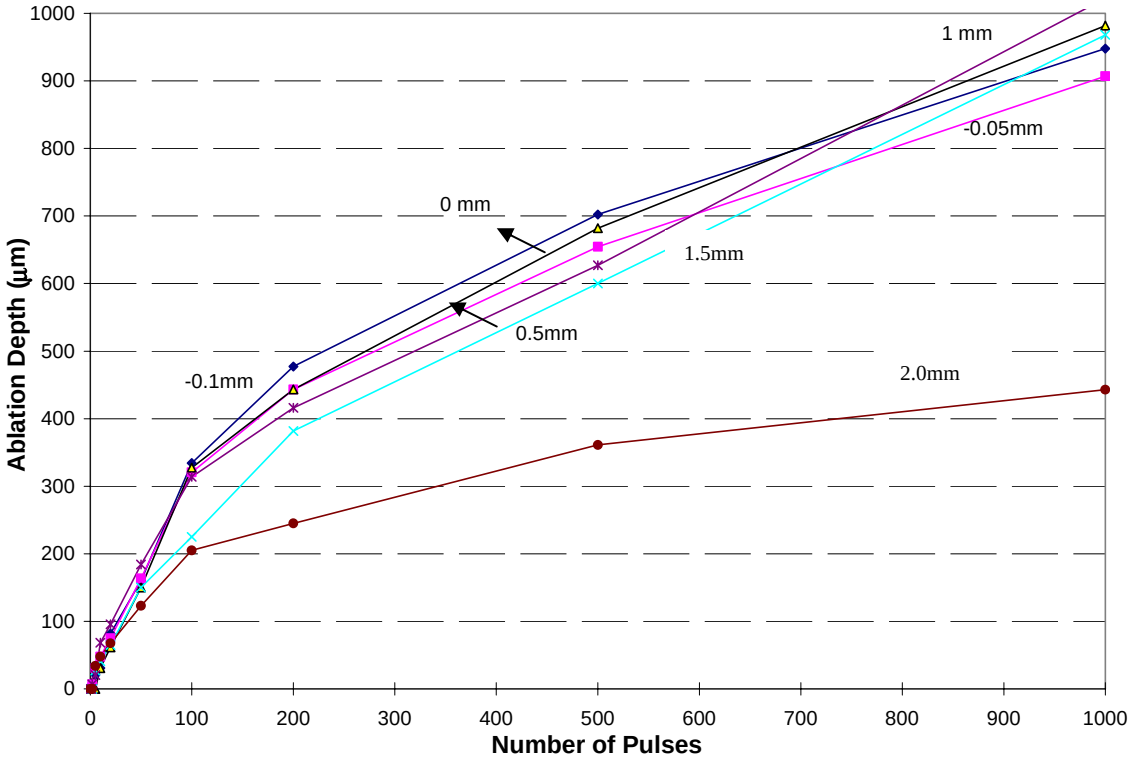

Figure 7.8 Variation of ablation depths vs. the number of pulses at different focal points.

7.4.3 Taper Effect

Figures 7.9 (a) to (g) show cross sections of the holes for PMMA irradiated with different number of pulses at various focal points. Taper effect can be observed for all cases. This is caused by the debris deposited at the sides of the wall which cause energy lose due to reflection, called the wall effect.

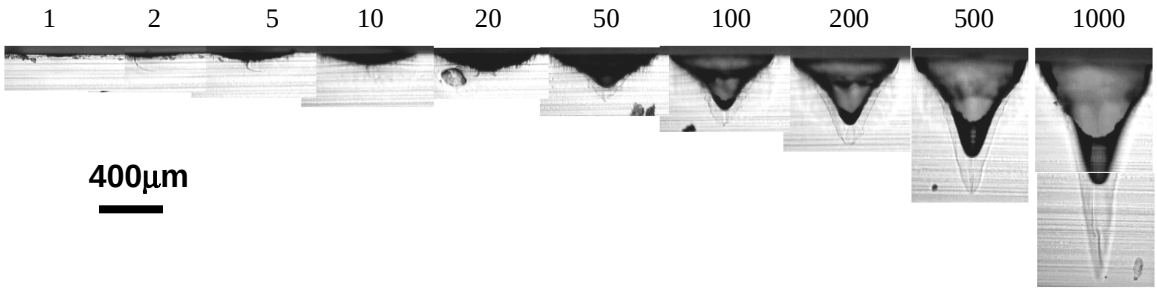

(a) f = +2.0 mm

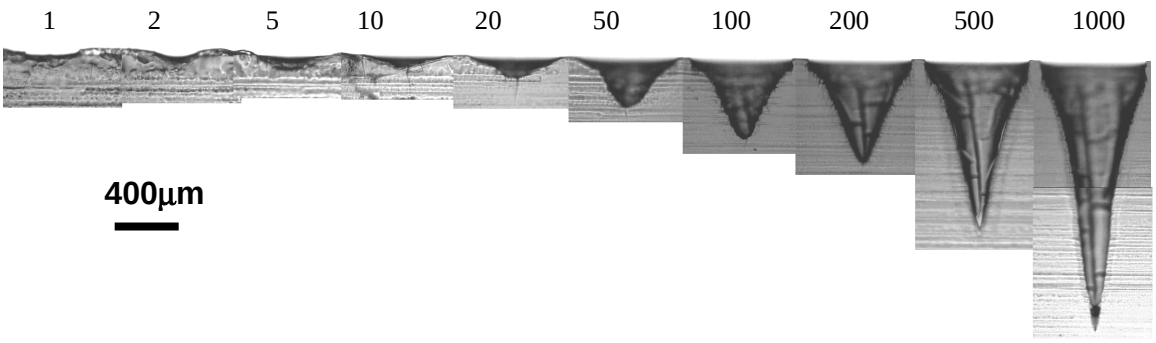

(b) f = +1.5 mm

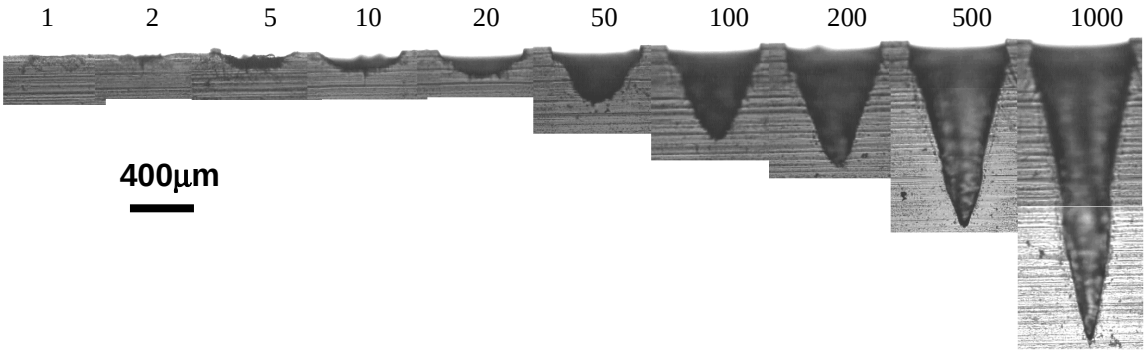

(c) f = +1.0 mm

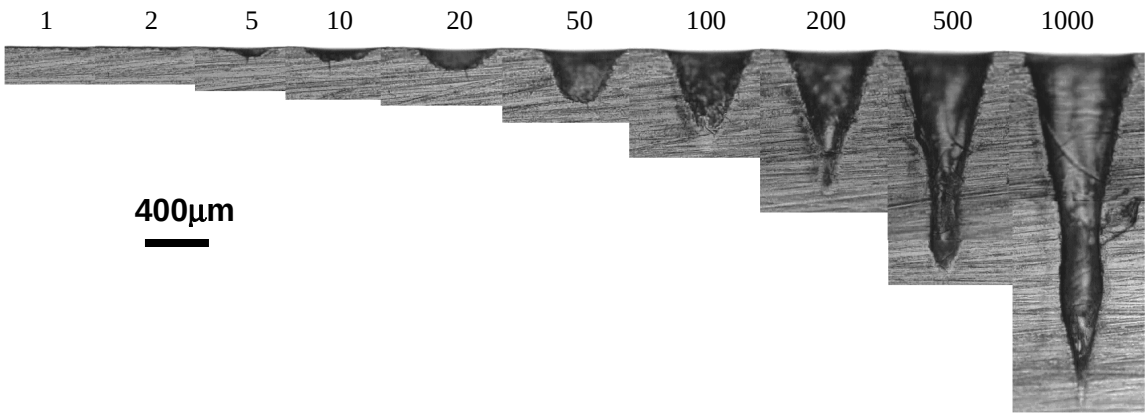

(d) f = +0.5 mm

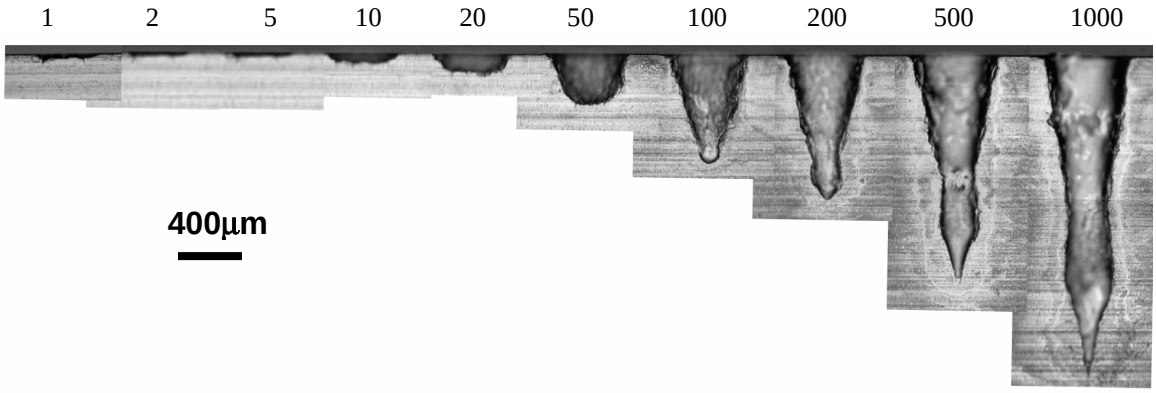

(e) f = 0 mm

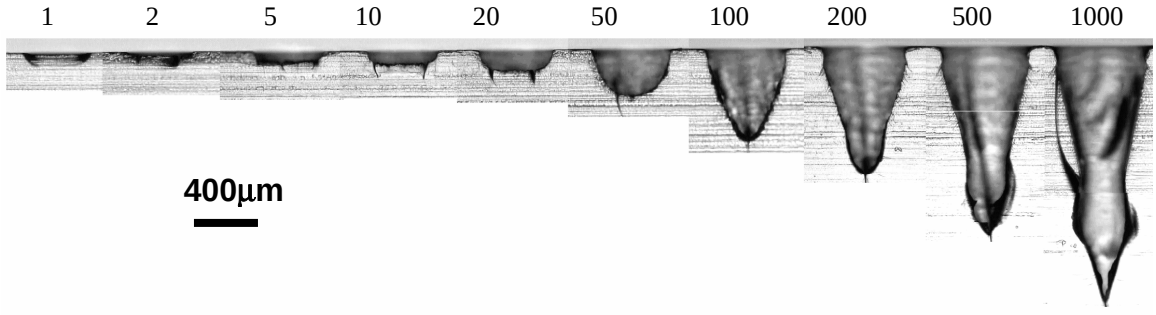

(f) f = -0.5 mm

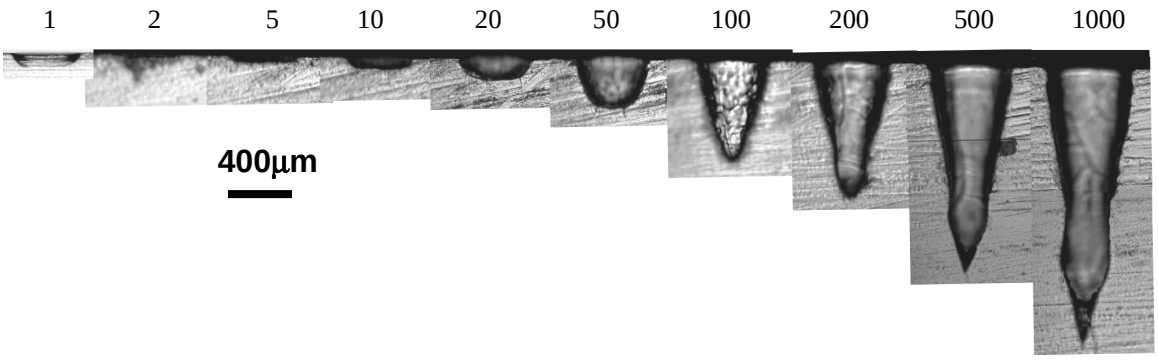

(g) f = - 1.0 mm

Figures 7.9 Cross sectional view for the holes ablated from 1 pulse to 1000 pulses (left (a) to (g) to right) at different focal points, f.

7.4.4 Droplet Formation

Starting from 5 pulses, splash droplets were found surrounding the ablated holes. The quantity of splash droplets increased with the number of pulses. These droplets can be removed by placing it in an ultrasonic isopropyl alcohol bath. Figure 7.10 shows the splash droplets that surrounds the ablated hole.

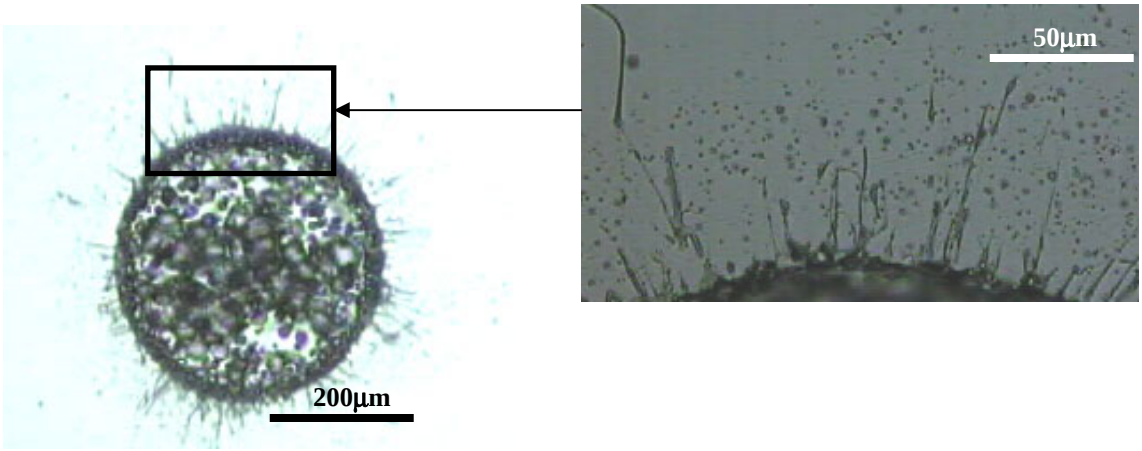

Figure 7.10 Optical micrograph showing significant splash droplets surrounding an ablated hole.

Kelly and Rothenberg [44] analyzed the possibility of droplet ejection during laser sputtering of various metals and semiconductors. In their opinion, convex surface irregularities somehow form on the target surface first. They are then accelerated from the liquid surface during laser ablation due to volume change on melting followed by thermal expansion of the liquid. In this way, the condition for droplet ejection implies the pretextured surface will be formed after a significant number of pulses.

Ang *et al.* [11] proposed another possible mechanism, namely, the instability of capillary wave in a molten surface layer. This is a single pulse mechanism in which large scale surface structures (LSS) with a characteristic spacing of 20-30 μm are formed on the target surface as a result of surface melt instability that is generated by the plume pressure. This results in break away of liquid at peaks of a periodically unstable capillary wave and the ejection of the droplets. All this happens during a single laser pulse. The expanding plume pressure then splashes droplets back onto the target surface (recondensation).

CHAPTER 8

PULSED LASER MICROMACHINING OF SILICON WAFER

8.1 Introduction

The material covered in this chapter is a joint work and reference [82] give details. Excimer lasers are high-pressure gas lasers which emit short pulse (a few nanoseconds) radiation in the ultraviolet range of the electromagnetic spectrum [45]. Since the absorption length of the UV light is very short for semiconductor materials, the intense energy is concentrated only at or near the surface. The high-pulse energy (2 J/cm^2) and extremely short duration (ns) leads to rapid melting, vaporization, and plasma formation of the irradiated material. The transfer of heat into the bulk is relatively small since a large fraction of laser energy is removed immediately with the ablated material. Consequently, the subsurface damage can be very small. Hence, micromachining with an excimer laser can be highly suitable for materials that are very sensitive to both thermal and mechanical stresses, such as glasses, ceramics, and semiconductor materials.

Laser machining from near infrared to ultraviolet, therefore, can be used for precision machining of materials in the micrometer range. The type of interaction between the laser beam and the material being ablated depends not only on the thermo-optical properties of the workmaterial for a given laser (wavelength) irradiation but also by the appropriate choice of the laser parameters used (wavelength, pulse energy, pulse duration, energy

density). Because of high photon energy per pulse, short-wavelength excimer laser radiation is used for ablation of practically all materials and especially materials that are thermally sensitive. Excimer laser ablation of semiconductor materials has proven to a promising and a very powerful tool for micromachining applications, such as the fabrication of microelectro-mechanical systems (MEMS), and in the semiconductor IC, medical, and biomedical fields.

There is great deal of interest in utilizing excimer lasers not only for micro-machining of semiconductor materials but also in the production of nanomaterials, nanocoatings, etc. An important requirement in the micromachining of semiconductor materials is the production of high-quality machined surfaces. In the case of laser ablation, the surface of the ablated material is usually surrounded by redeposition of molten material or debris that has to be removed subsequently by other methods. An alternative would be to remove it during the laser ablation process itself. This can be accomplished by laser machining under water. There are other advantages of laser ablation under water, as will be discussed in the following, especially when machining materials which are highly sensitive under thermal and mechanical stresses and where the subsurface damage has to be minimal. The main objective of this chapter is to perform short pulse (25 ns) laser ablation of silicon using a KrF (λ = 248 nm) excimer laser in air and under water at various laser fluences and number of pulses and compare the results.

8.2 Experiment

The excimer laser micromachining system used in this investigation was described in Chapter 5. A highly polished, as-received single-crystal silicon was used as the

workmaterial. The surface of the silicon was irradiated with 1 – 5000 short laser pulses at a frequency of up to 10 Hz and under different fluences ranging from 1- 2.23 J/cm^2 in order to ablate a hole in silicon wafer. In the case of underwater machining, the silicon wafer was completely immersed in water with the water level ~2 mm above the surface of the silicon and then the surface was irradiated with the excimer laser beam. Figure 8.1 is a schematic of the set-up used for underwater laser ablation micromachining of silicon workmaterial. The ablated hole was subsequently examined using conventional optical and scanning electron microscopes and MicroXAM laser interference microscope for surface mapping as well as to determine the ablation depth and the crater height. The results of machining under water and in air are then compared.

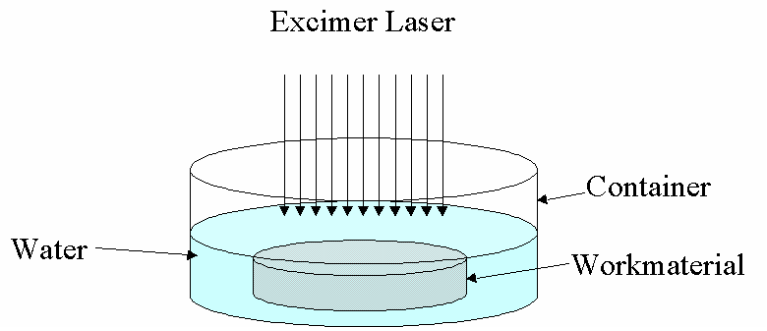

Figure 8.1 Schematic of the setup used for laser ablated micromachining of silicon under water.

8.3 Results and Discussion

Figure 8.2 (a) and (b) show optical macrographs of the top views of silicon workpieces ablated at a pulse energy of 0.8 mJ and at different number of pulses from 10 to 5000 in air and under water, respectively. Figure 8.3 (a) and (b) show details of the same samples at higher magnification. Two important differences between machining in air and under water can be clearly seen. The first one is the absence of thermal damage in

the case of underwater machining from 10 pulses to all the way up to 5000 pulses while significant thermal damage in the case of machining in air. This thermal damage increases with the number of pulses in the case of machining in air. It is for this very reason that underwater machining is preferred. The second one is the nature of the material removal in the two cases. While the ablated surface is smooth in the case of machining in air, it is somewhat rough in the case of underwater machining. The surface of the silicon ablated under water shows the result of molten silicon rapidly solidified with a dendritic structure.

(a) In air (b) Under water

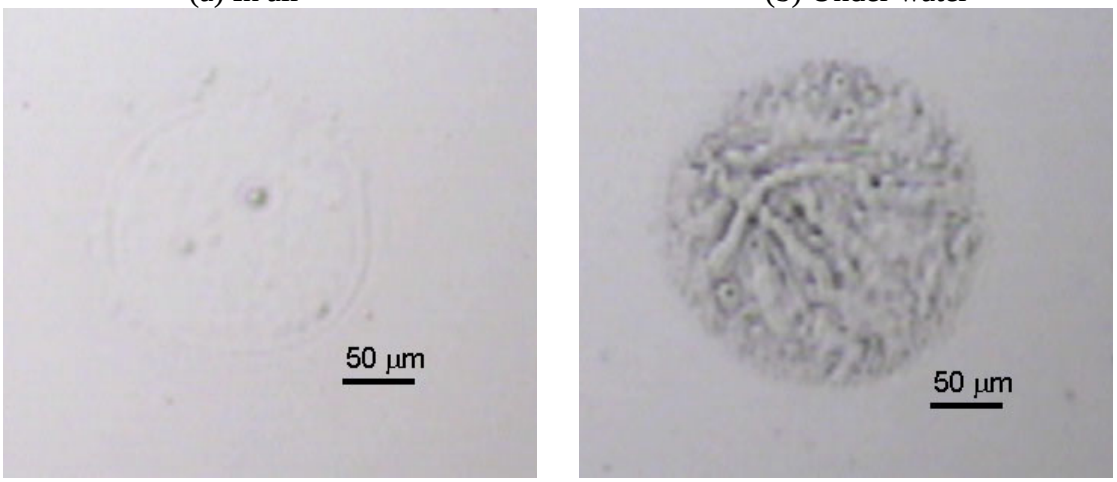

10 pulses

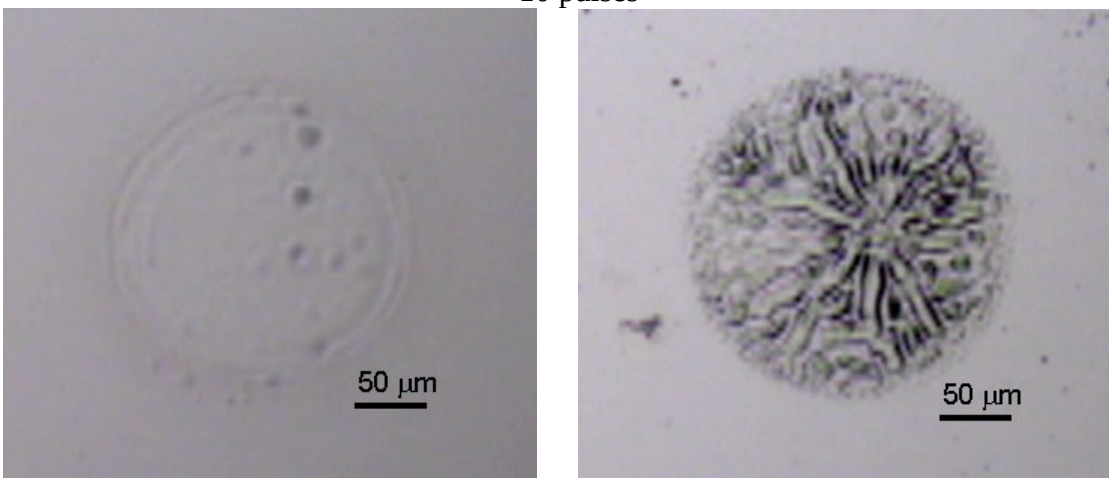

20 pulses

(a) In air (b) Under water

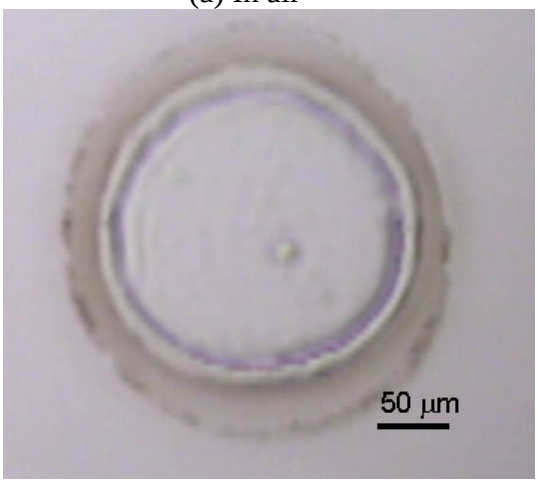

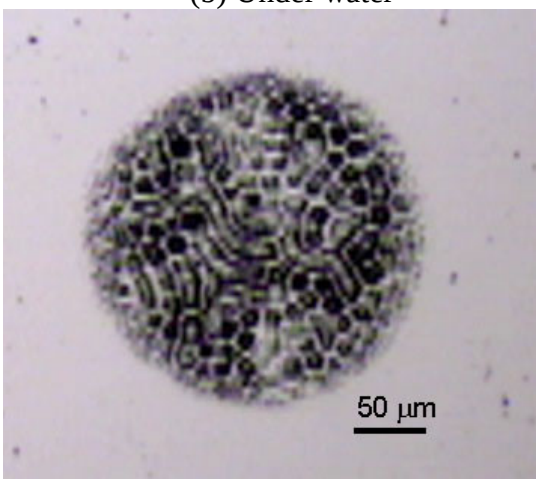

50 pulses

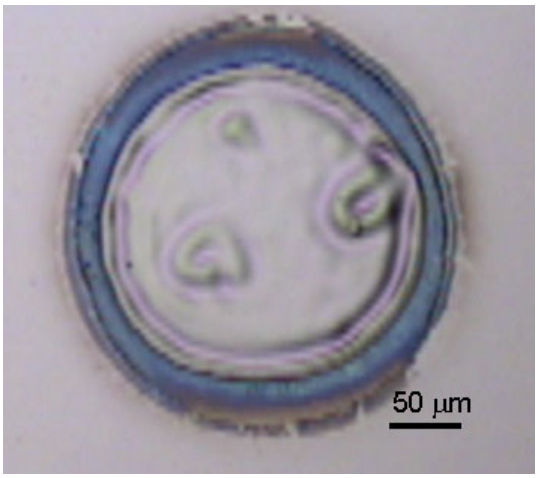

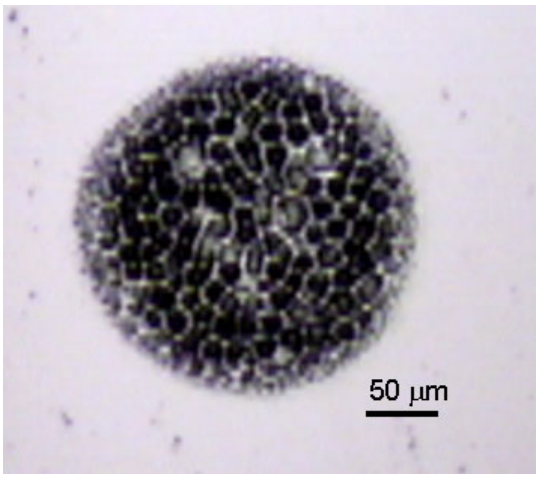

100 pulses

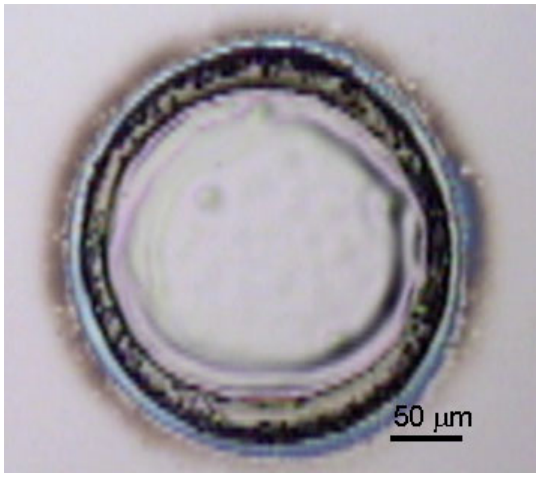

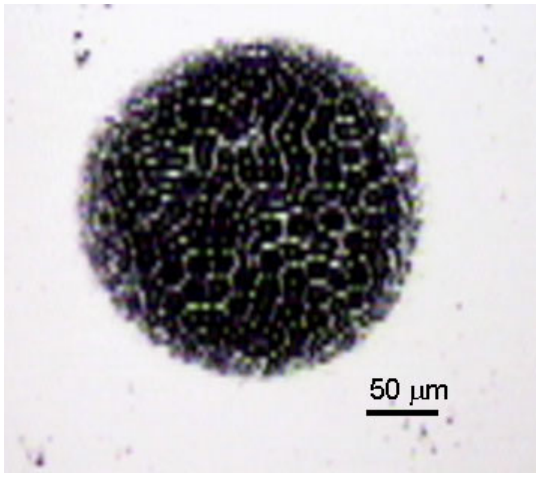

200 pulses

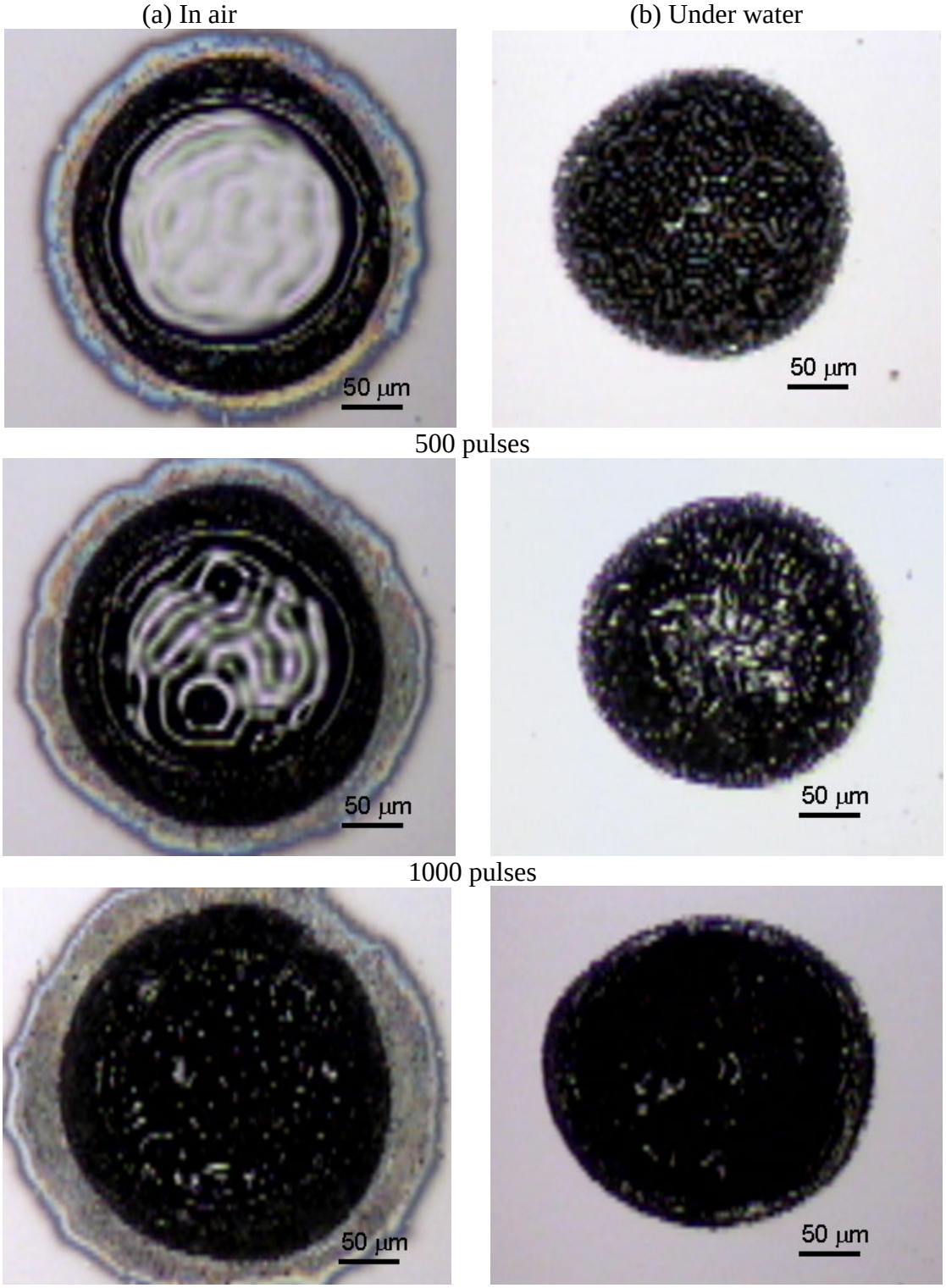

Figure 8.2 Optical macrographs of the top views of silicon workpieces ablated at a pulse energy of 0.8 mJ and at different number of pulses from 10 to 5000 in (a) air and (b) under water, respectively.

(a) In air (b) Under water

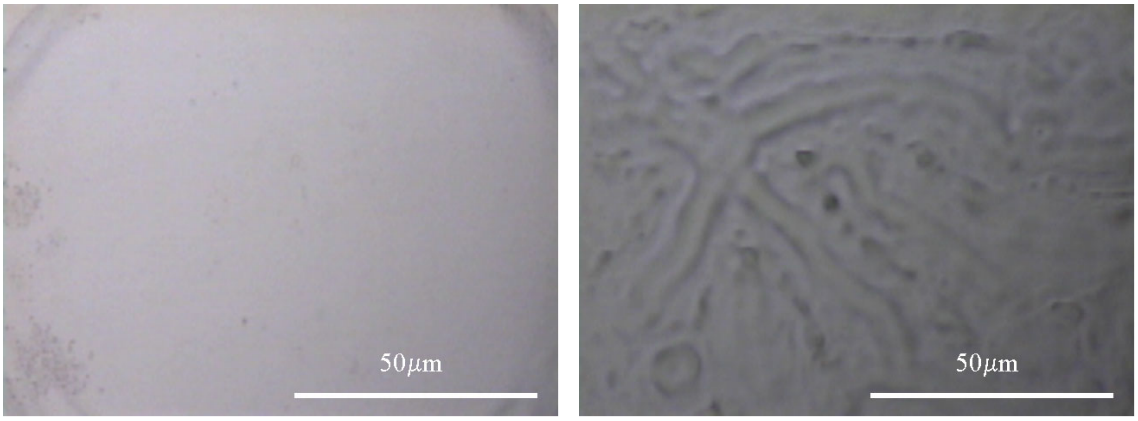

10 pulses

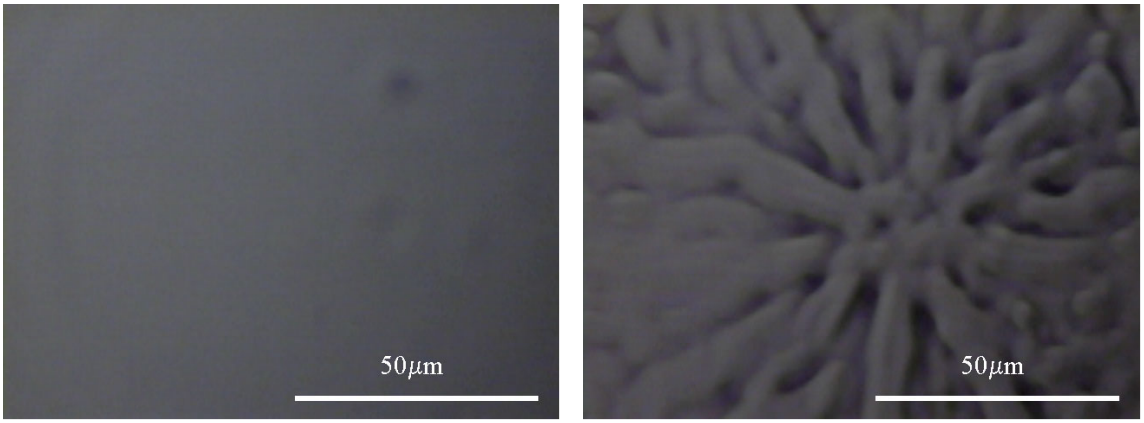

20 pulses

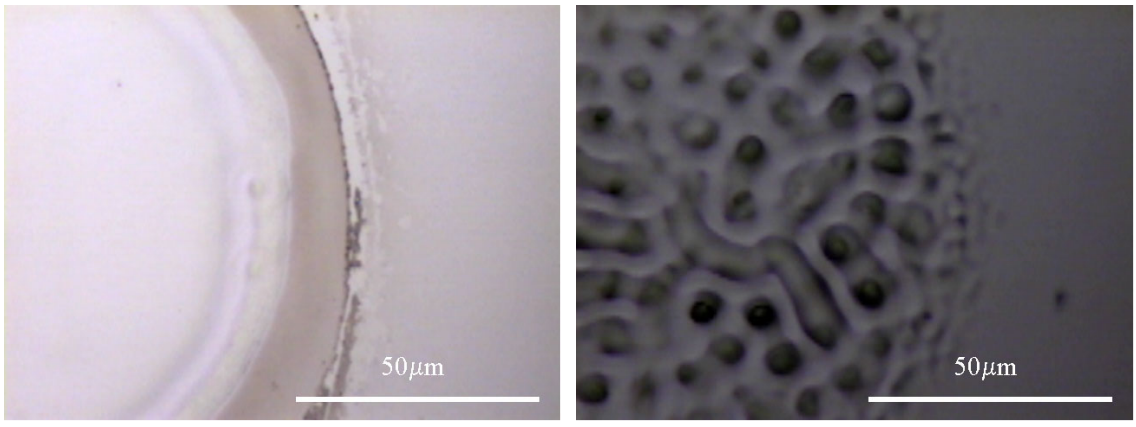

50 pulses

(a) In air (b) Under water

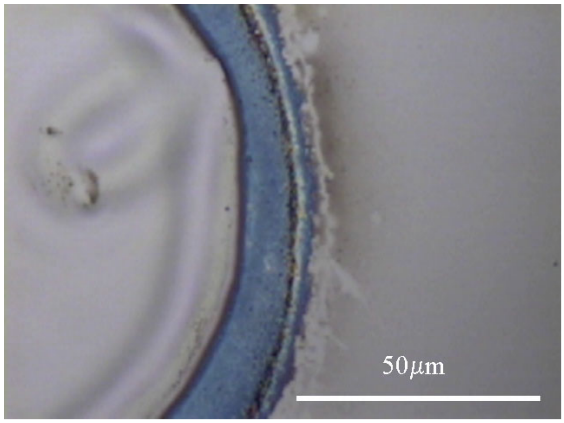

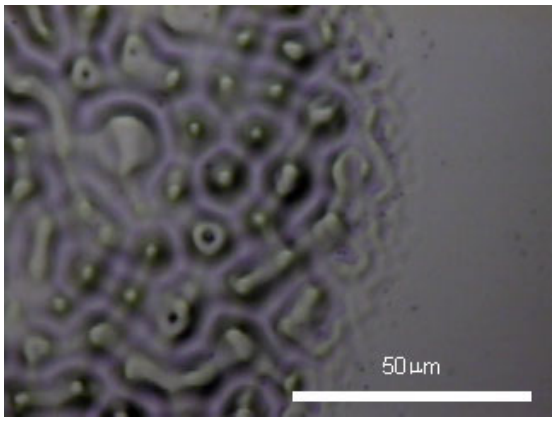

100 pulses

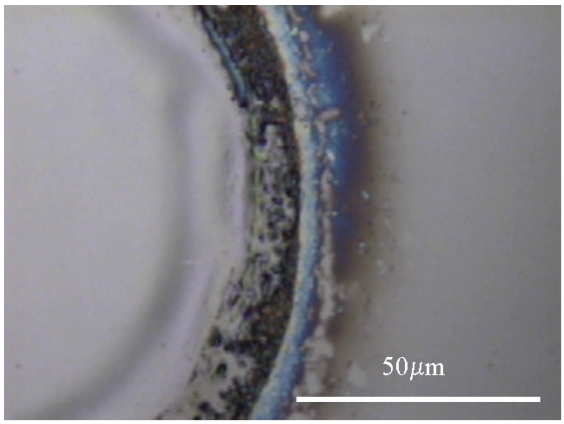

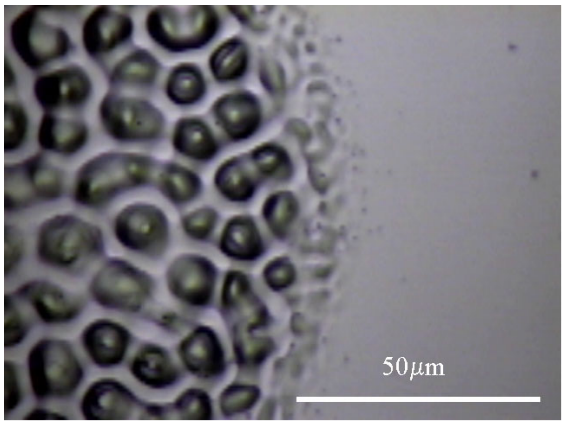

200 pulses

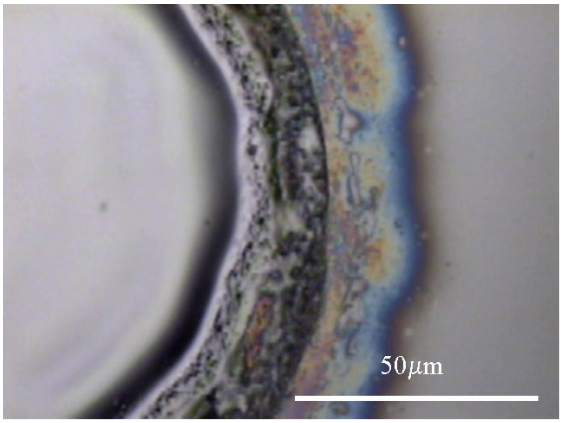

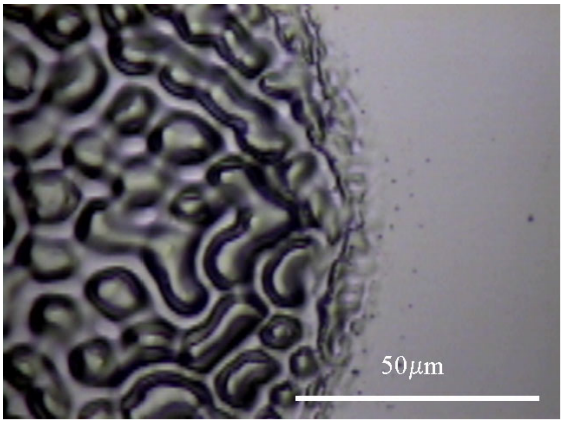

500 pulses

(a) In air (b) Under water

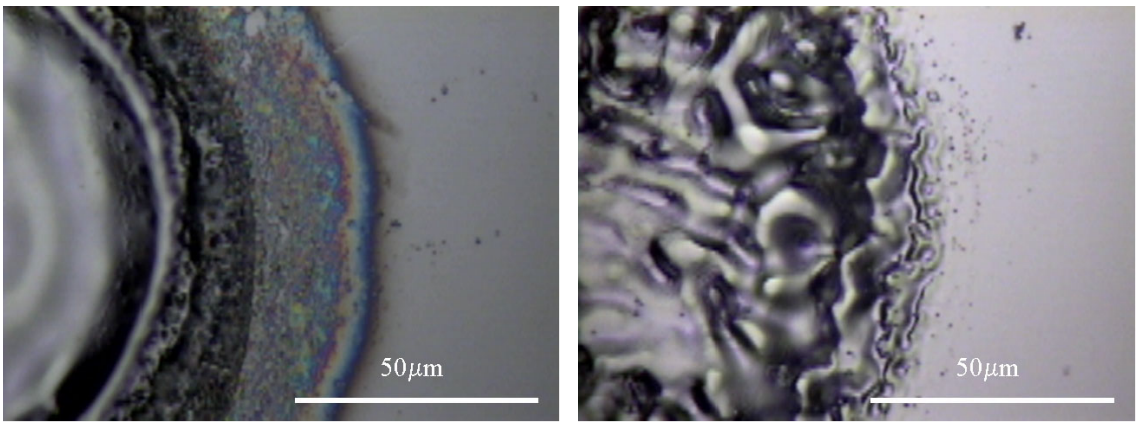

1000 pulses

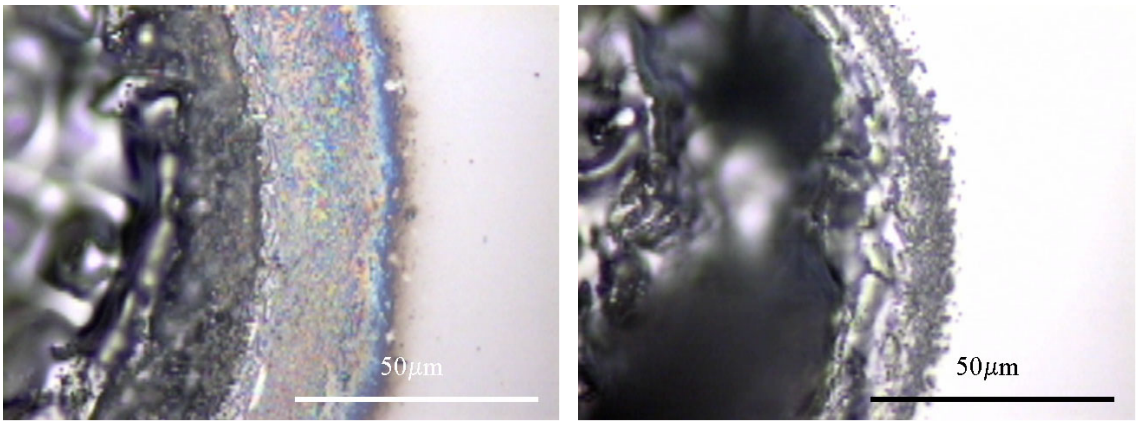

5000 pulses

Figure 8.3 Optical macrographs of the top views of silicon workpieces machined showing details at higher magnification.

Figure 8.4 (a) and (b) show MicroXAM 3D mapping of the ablated surfaces in silicon at a pulse energy of 0.8 mJ and at various number of pulses in air and under water, respectively. Even at 10 pulses, there is significant ablation in both cases that is not quite apparent from the optical micrographs. There are also some differences in the nature of ablation. For example, maximum ablation occurs in the center in air, while under water, it is more uniformly distributed.

(a) In air (b) Under water

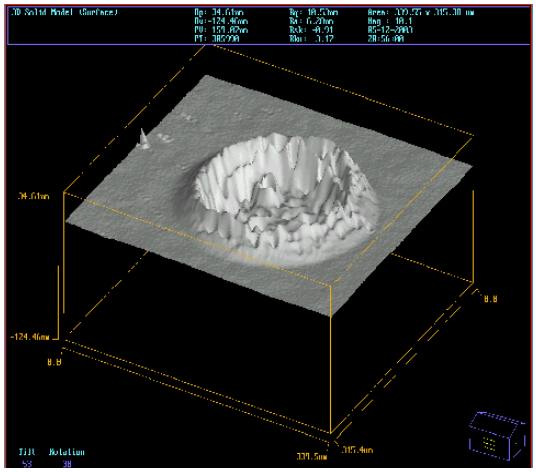

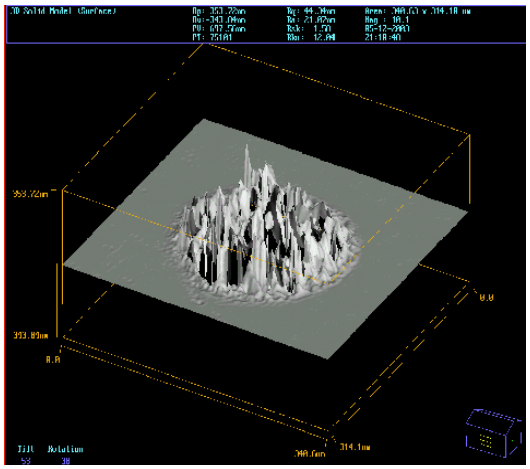

10 pulses

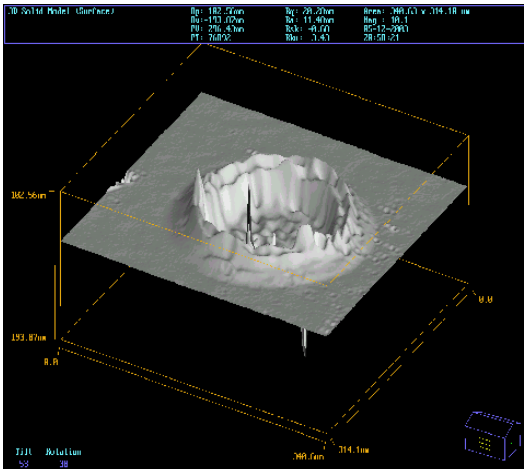

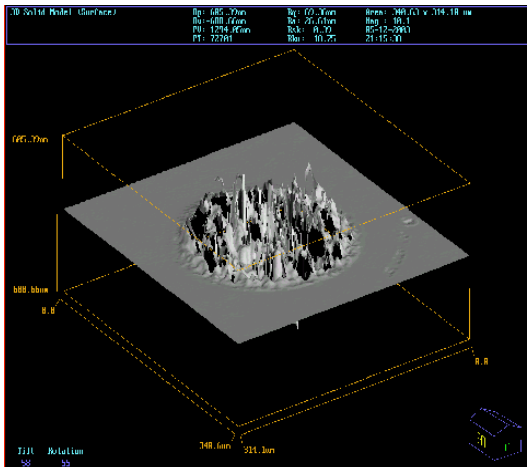

20 pulses

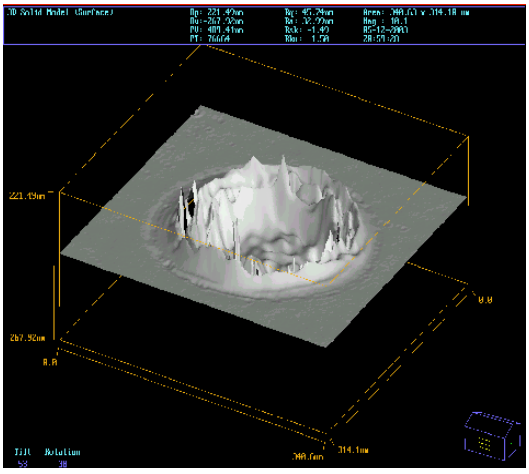

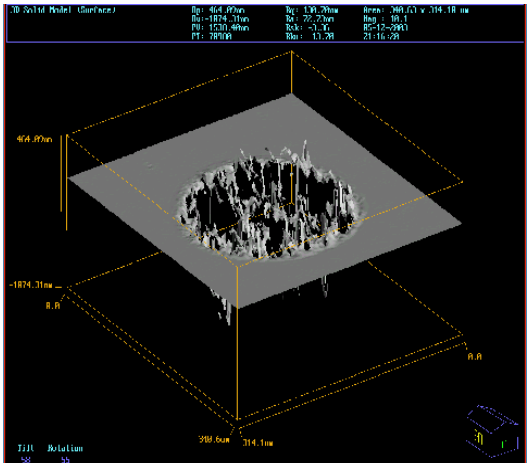

50 pulses

(a) In air (b) Under water

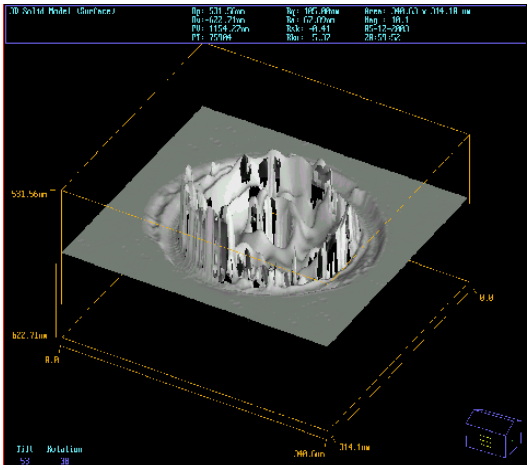

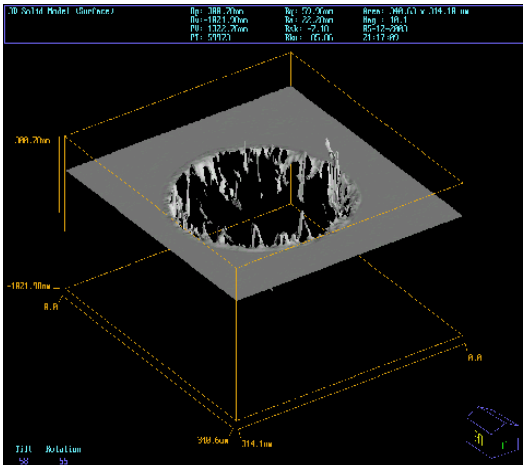

100 pulses

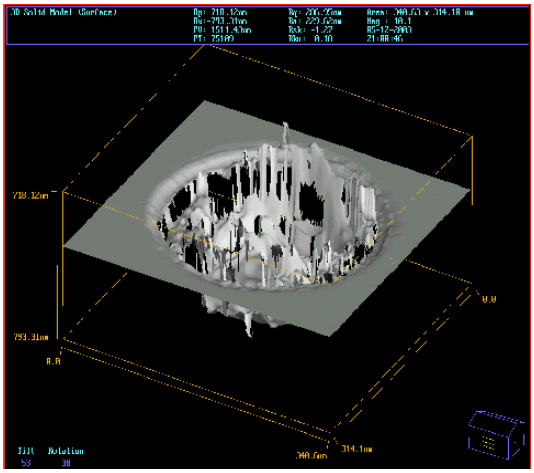

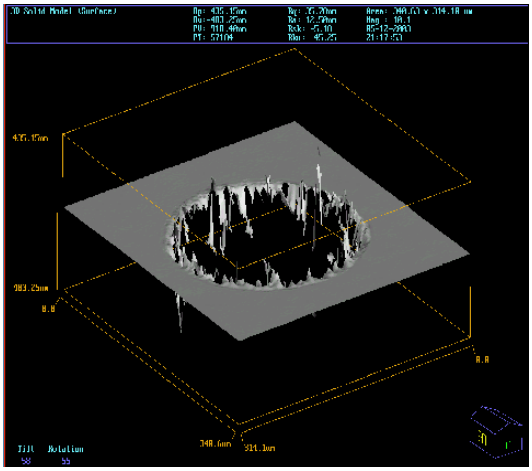

200 pulses

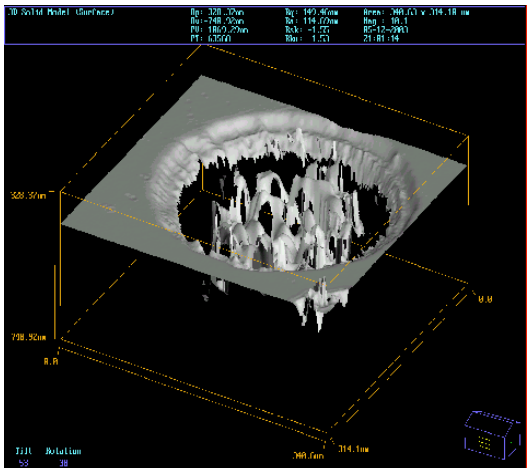

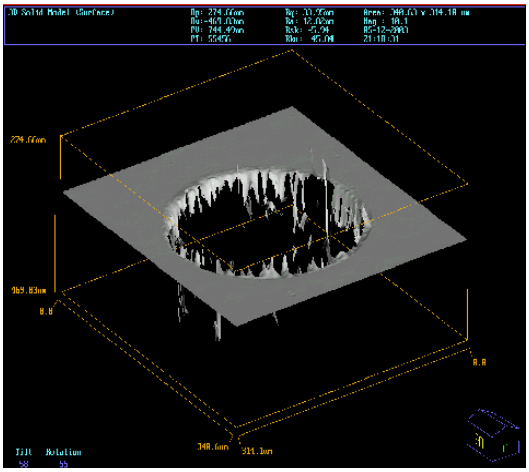

500 pulses

(a) In air (b) Under water

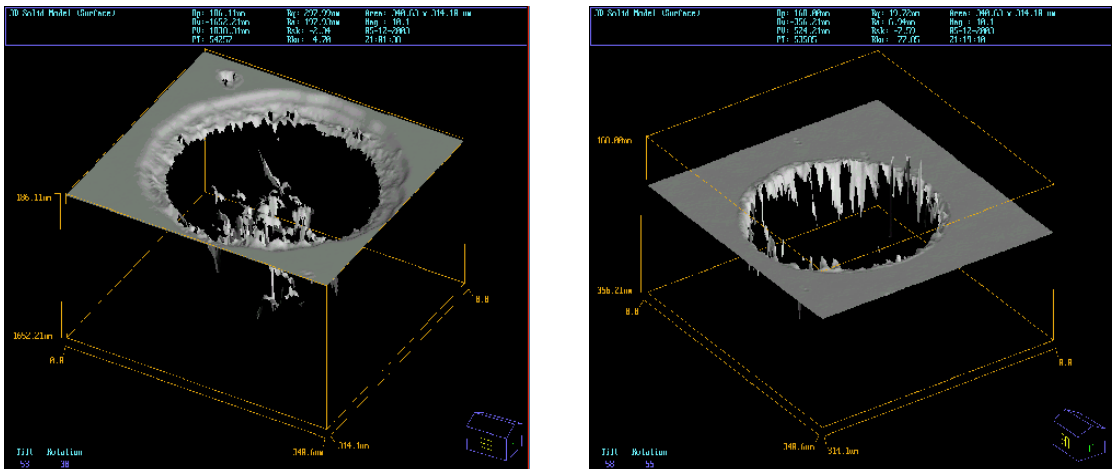

1000 pulses

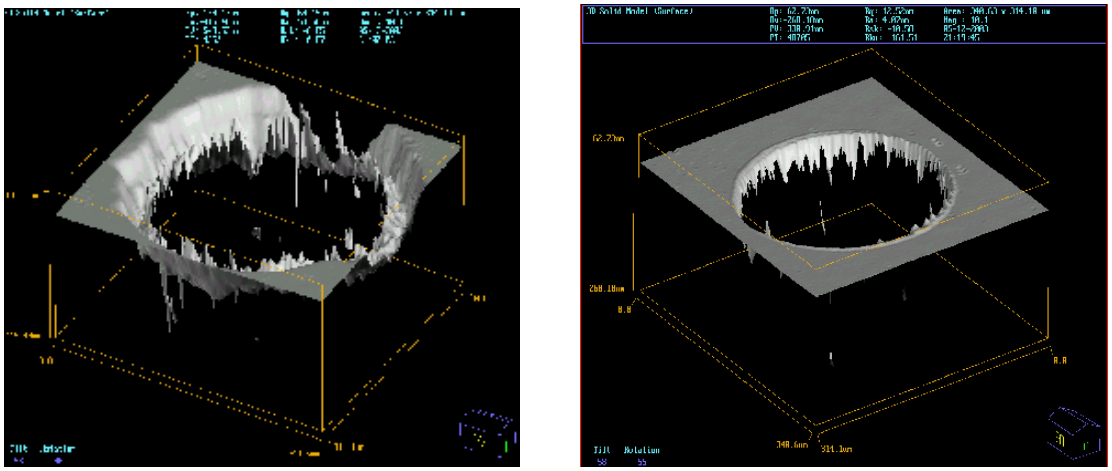

5000 pulses

Figure 8.4 MicroXam 3D mapping of the ablated surfaces in silicon at pulse energy of 0.8 mJ and at various number of pulses (a) in air and (b) under water, respectively.

As Kim and Grigoropoulos [52, 53] suggested, the surface depression in silicon in air may have been caused by the recoil momentum applied by the upward vapor plume ejection and the shock-wave propagation. This also results in the formation of a shoulder on the periphery of the ablated hole. In contrast, under water, the removal is more uniform with the absence of a shoulder on the periphery of the hole.

Figure 8.5 (a) and (b) give the cross-sectional profiles obtained using MicroXam laser interference microscope. These are obtained by measuring the cross section profiles at a given line on the diameter of the hole. The raised portion on the periphery and depression in the center corresponding to the hole formation in air is clearly evident. In contract, there are projections as well as depressions in the case of ablation under water. When the hole depth exceeds the limit of the instrument, it is possible to obtain the average depth by choosing an area on the hole rather than a line profile. The data given in the following Figures (Figure 8.7 and 8.8) of the variation of ablation depth with number of pulses or laser fluence is obtained by this method.

Figure 8.6 (a) and (b) show the SEM micrographs for ablated surfaces in silicon at a pulse energy of 0.8 mJ with 1000 pulses in air and under water, respectively. By comparing the figures in air and under water at a magnification of 250X, an additional ring is clearly seen in the case of in air ablation. The ring extended about 60 μm from the edge of the beam diameter (~200 μm). The ring is created by the redeposition material (compare the SEM micrographs at 1000X and 2000X). By carefully observing the SEM micrograph, it can be seen that the size or diameter of the redeposited materials getting smaller towards the outer diameter of the ring. The redeposited material is ejected out in the ablation process. It is obvious that, the small chromospheres have less weight and can travel longer distances. However, no redeposited material could be seen at the center of the ablated hole. No redeposited material is seen in the case of under water ablation. Water would rapidly solidify the evaporated material and the redeposited material will not stick on to the surface. At a magnification of 2000X, formation of a shoulder on the periphery of the ablated hole can be seen. This phenomenon which causes the recoil

momentum applied by the upward vapor plume ejection and the shockwave propagation [52, 53] has been nearly eliminated in underwater ablation. Inside the edge of the periphery, convection of the melt pool which has been mentioned in Section 2.5 is clearly seen in the case of ablation in air. The convection did not happen in the case of under water ablation because thin film water absorbed the heat uniformly at the surface. By comparing the center of the ablated hole, fine structure (ripple form) is observed in both cases. The ripple form is uniformly distributed. However, it appears to be denser in the case of under water. This ripple or dendritic structure is a result by rapid solidification of the molten pool.

Figure 8.7 (a) and (b) show the variation of ablation depth with laser fluence for different number of pulses in air and under water, respectively. It can be seen that there is a threshold value of laser fluence below which material removal by ablation does not take place. For example, it is ~1.7 J/cm^2 in the case of underwater machining and 1.4 to 1.7 J/cm^2 in the case of machining in air. The laser fluence threshold value for silicon is close to the value reported by Zhu et al. (1999), namely, ~1.5 J/cm^2. The threshold value is determined by the onset of crater formation on the silicon workmaterial by laser ablation. This value is found to increase with decrease in the number of pulses. In underwater machining, when the laser fluence is above the critical value, the ablation depth appears to be independent of the number of pulses above 2000, while in air it seems to be dependent on the number of pulses throughout the range investigated. Also, the maximum critical value of laser fluence seems to be lesser in air (1.7 J/cm^2) than under water (2 J/cm^2). At higher laser fluences (>2.2 J/cm^2), the ablation depth increases so rapidly that it would be out of range for the MicroXam microscope.

(a) In air (b) Under water

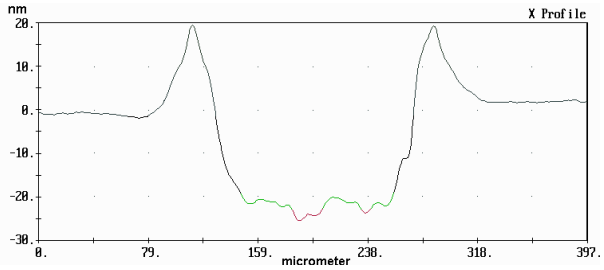

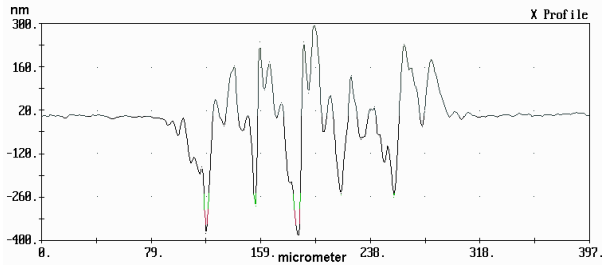

10 pulses

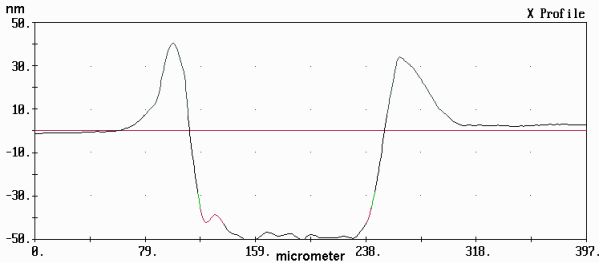

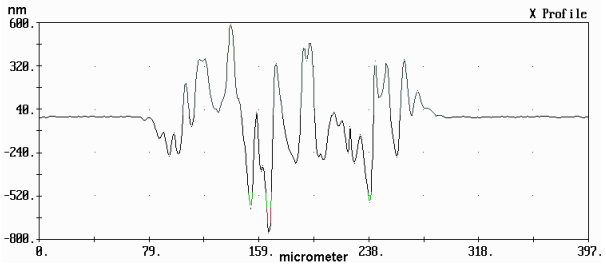

20 pulses

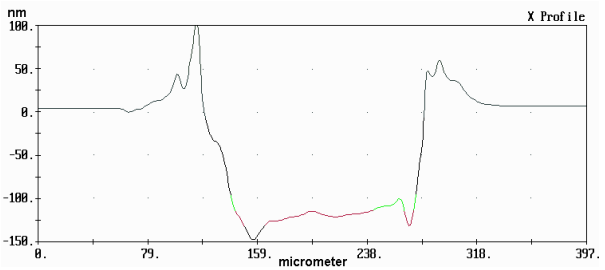

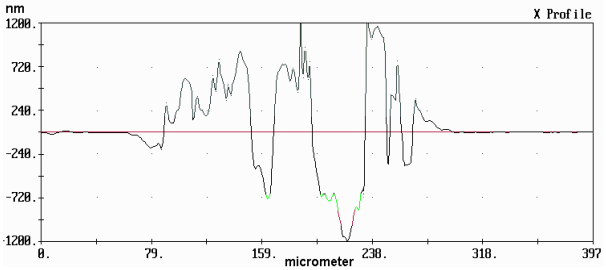

50 pulses

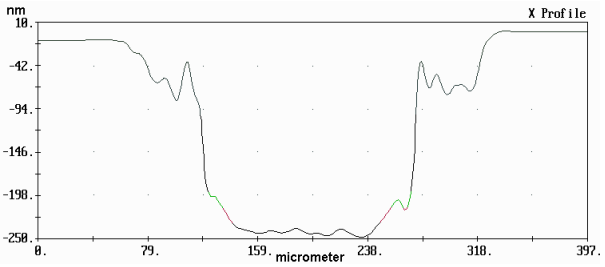

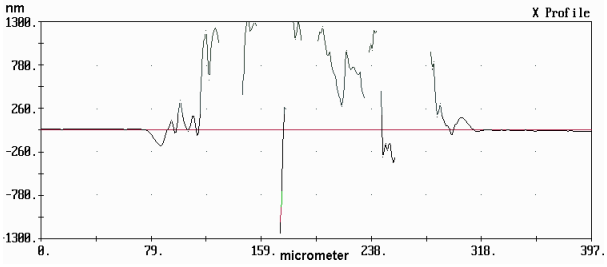

100 pulses

(a) In air (b) Under water

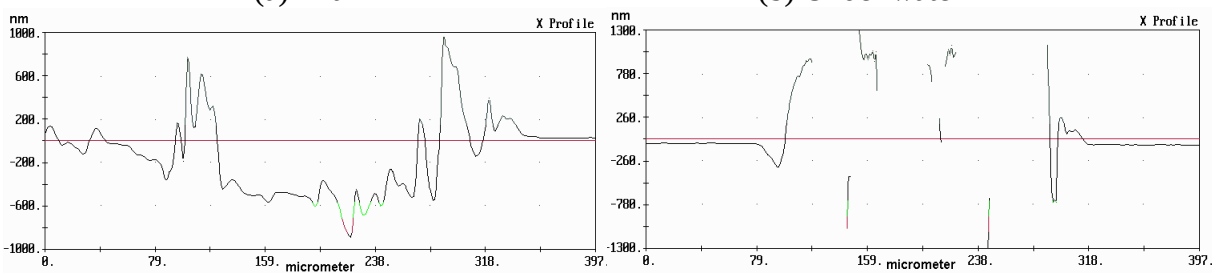

200 pulses

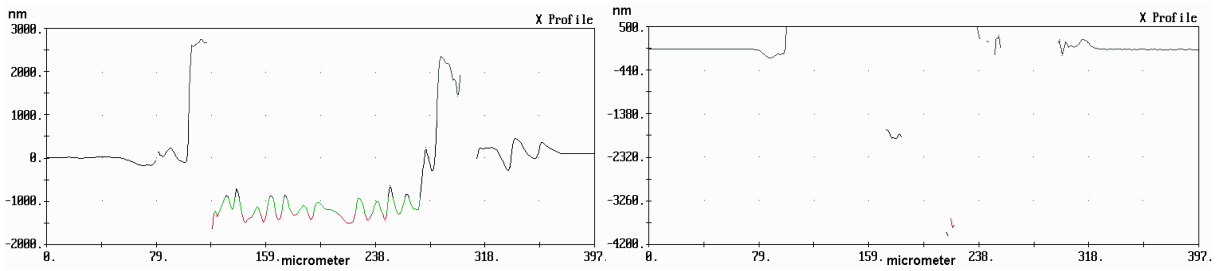

500 pulses

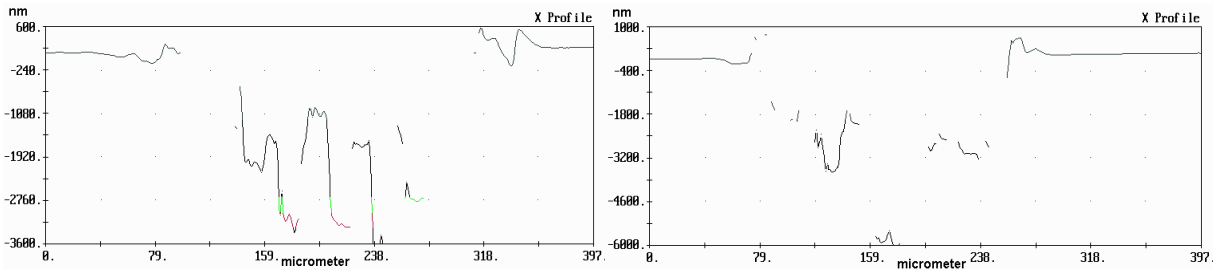

1000 pulses

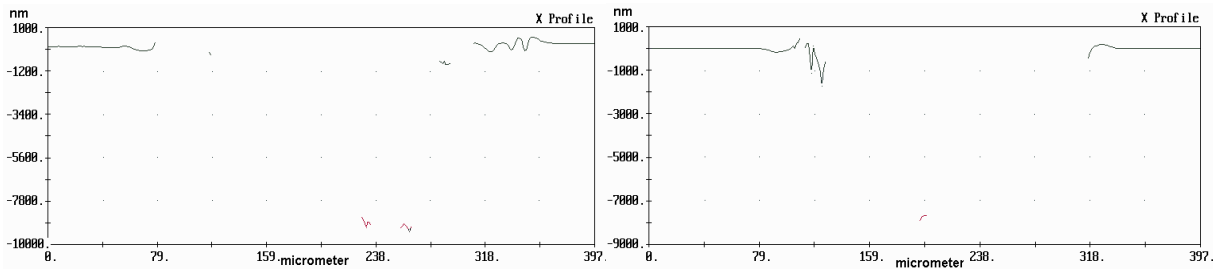

5000 pulses

Figure 8.5 Cross-sectional profiles obtained using MicroXAM laser interference microscope. (Note: surface height is in nanometers and the width of the hole (or cross section) is in micrometers)

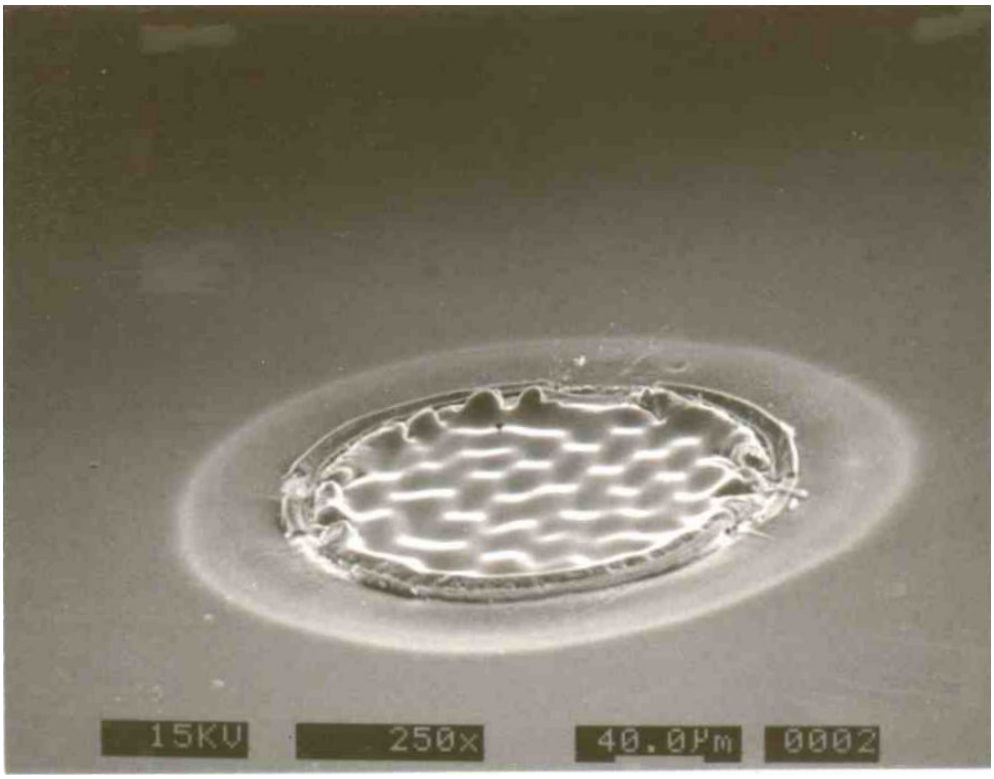

(a) In air

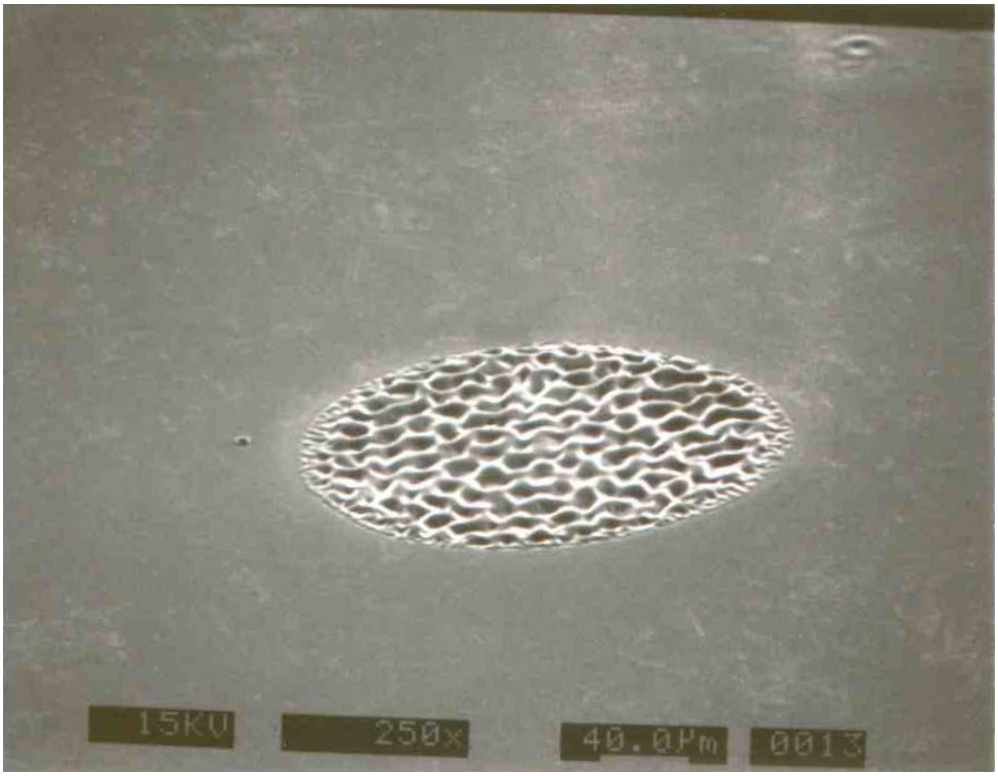

(b) Under water

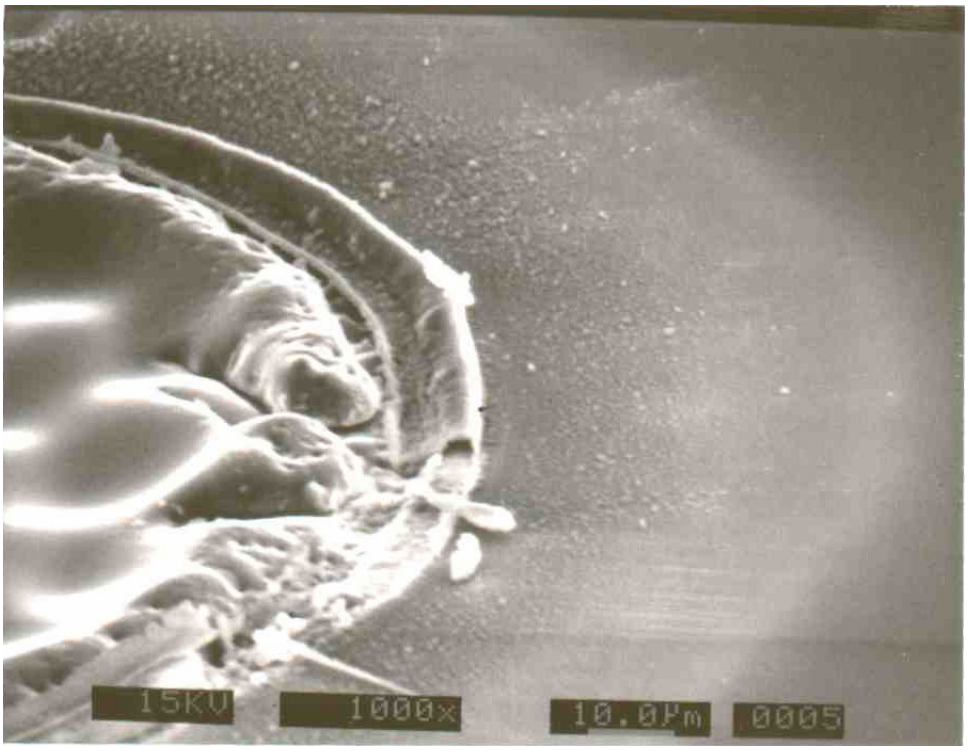

(a) In air

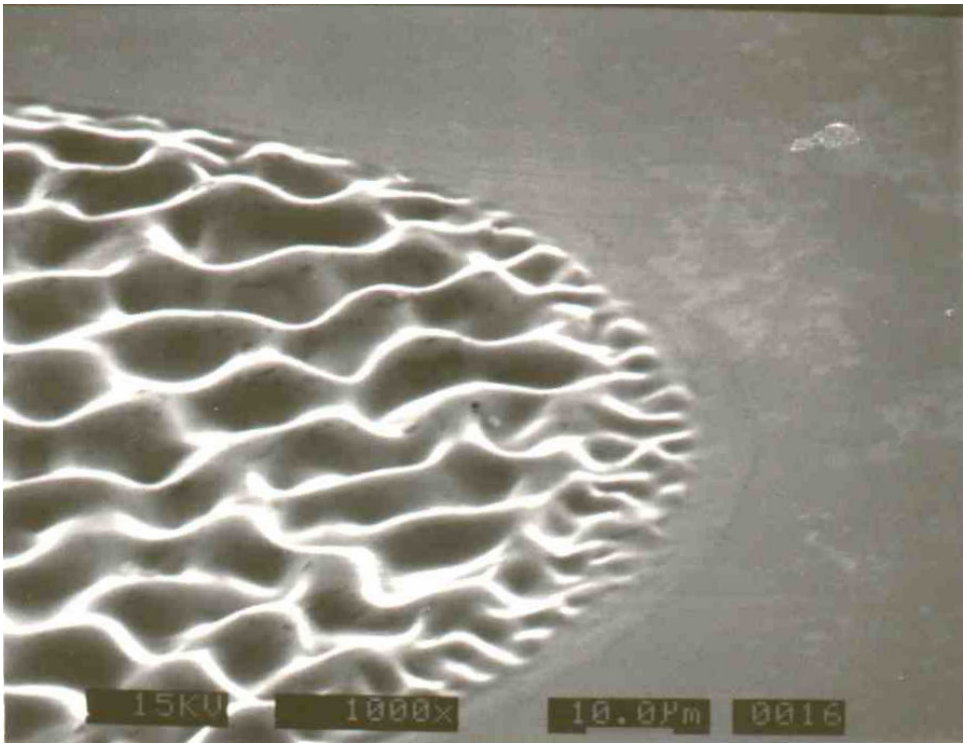

(b) Under water

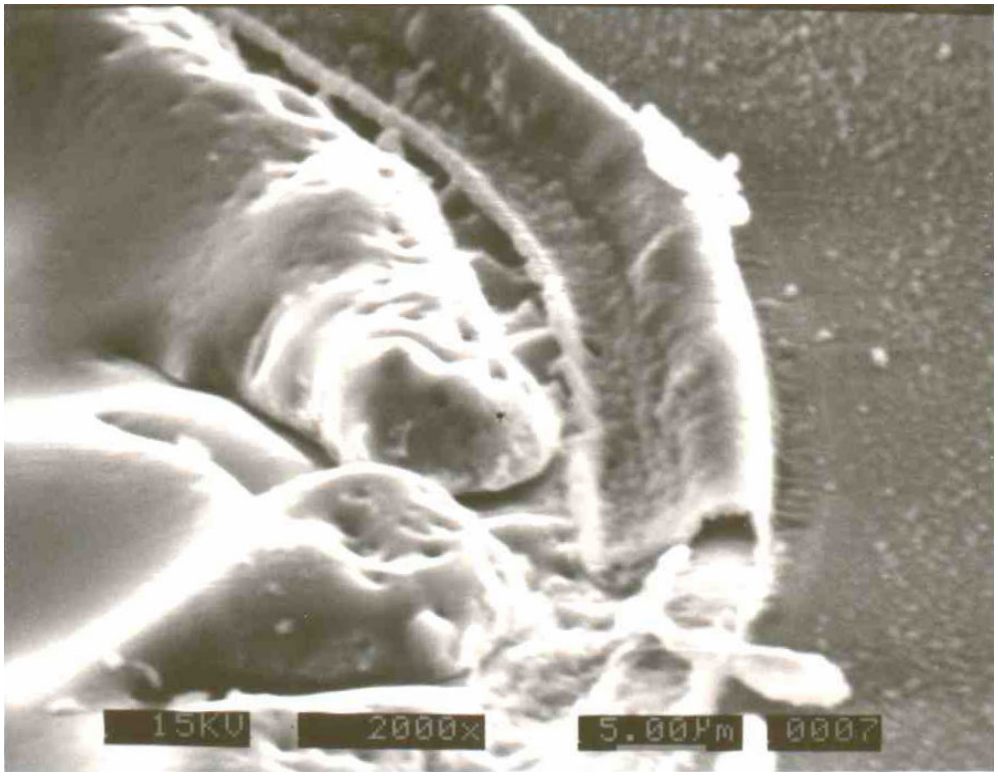

(a) In air

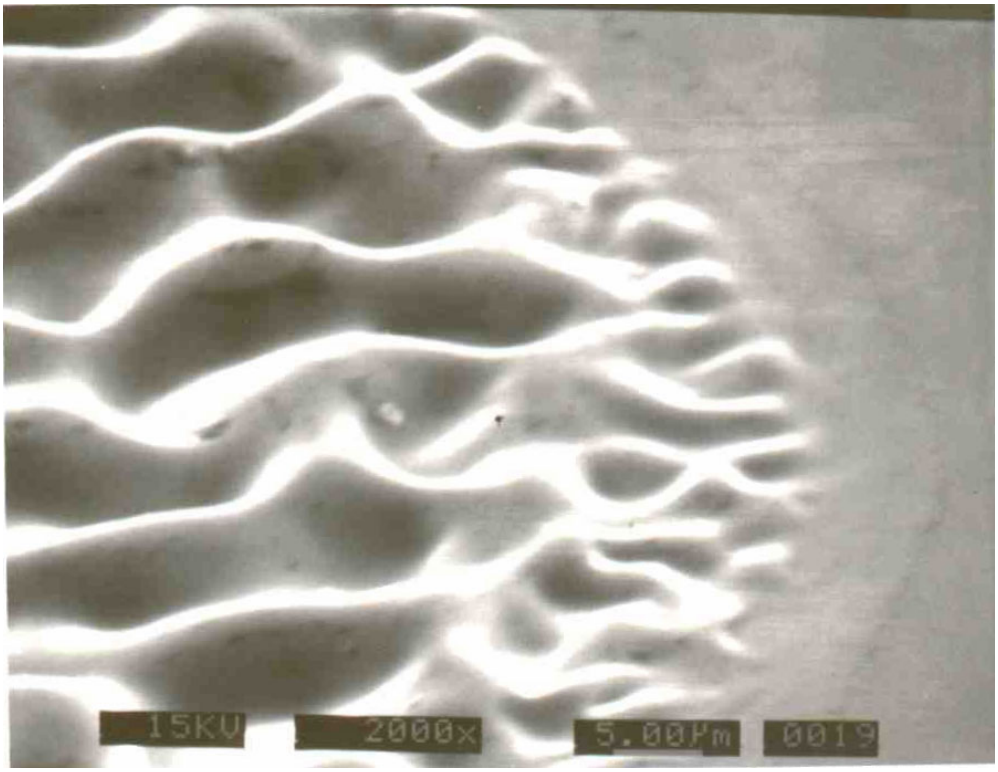

(b) Under water

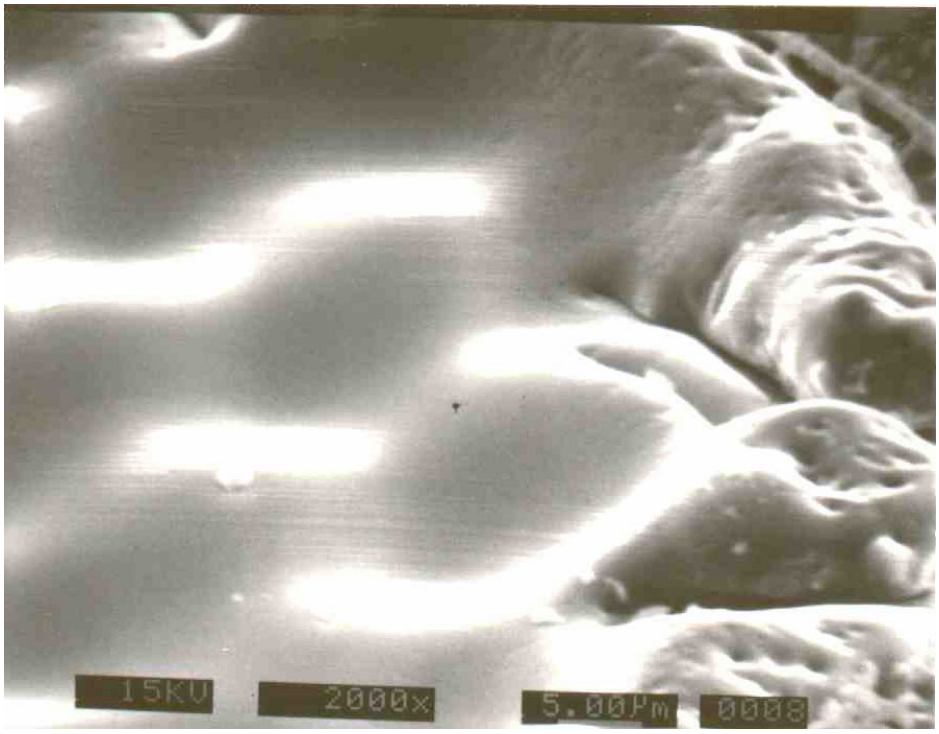

(a) In air

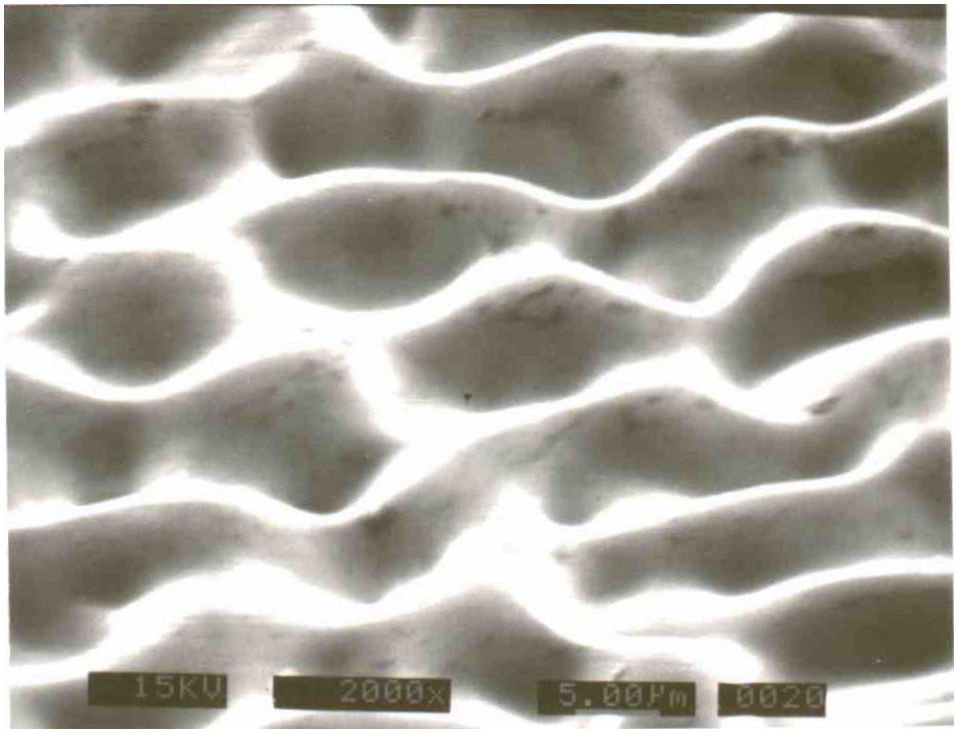

(b) Under water

Figure 8.6 SEM macrographs at various magnifications for silicon workpieces ablated with 1000 pulses at energy of 0.8 mJ in (a) air and (b) under water, respectively.

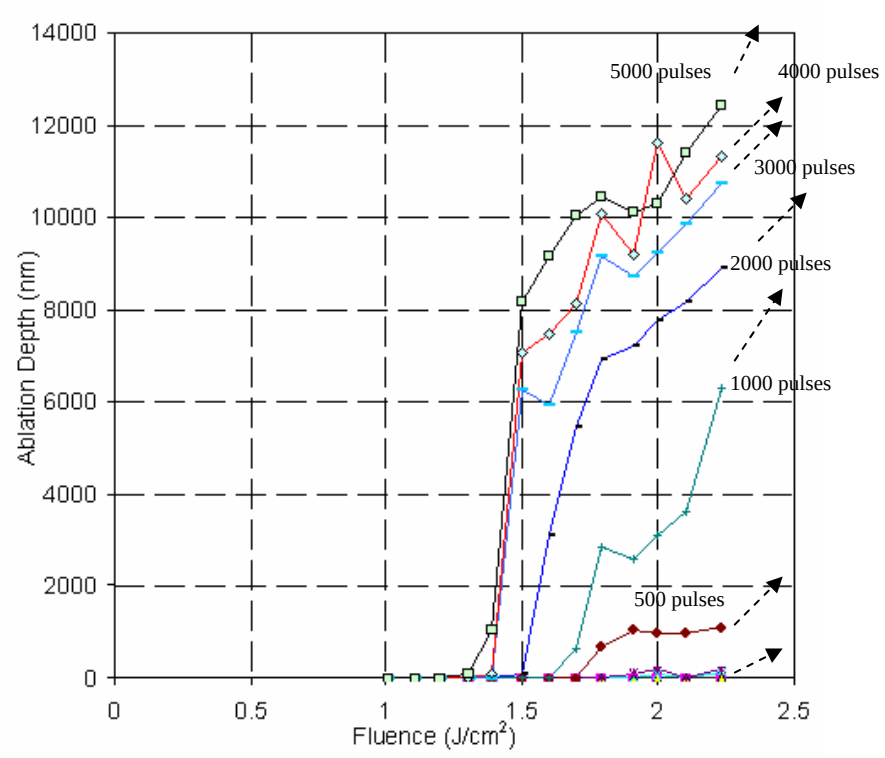

(a) In air

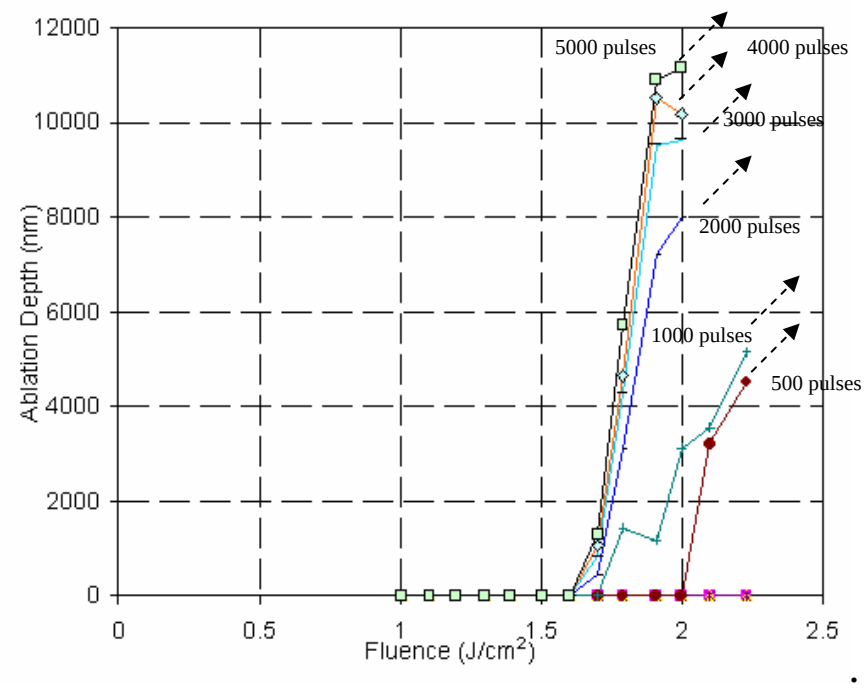

(b) Under water

Figure 8.7 Variation of ablation depth with laser fluence for different number of pulses (a) in air and (b) under water, respectively

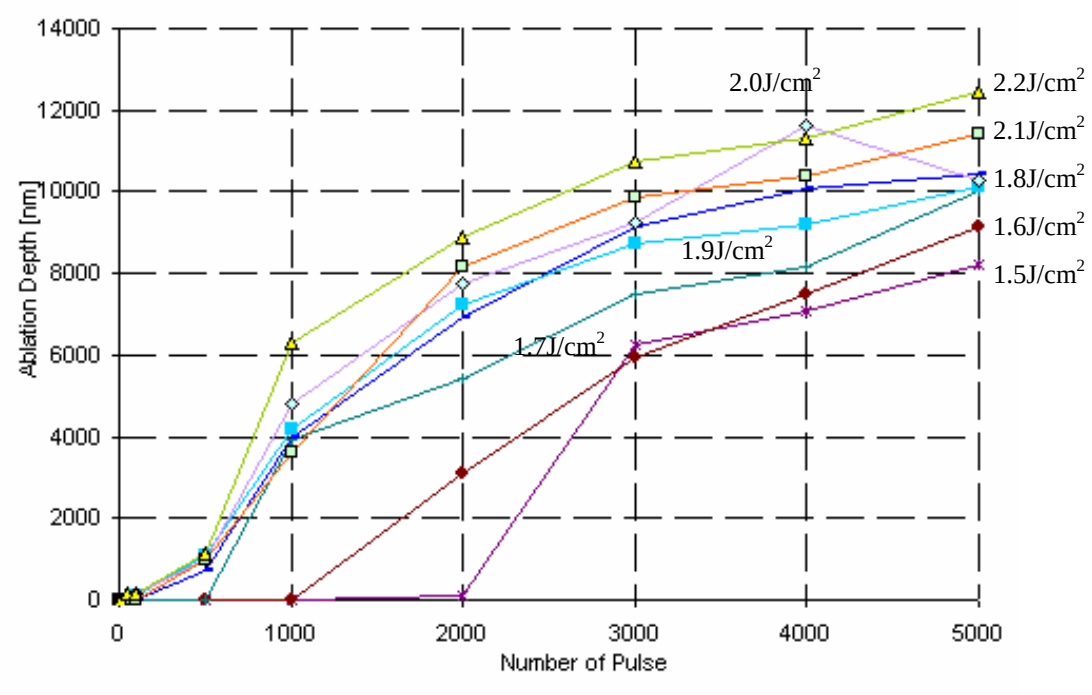

(a) In air

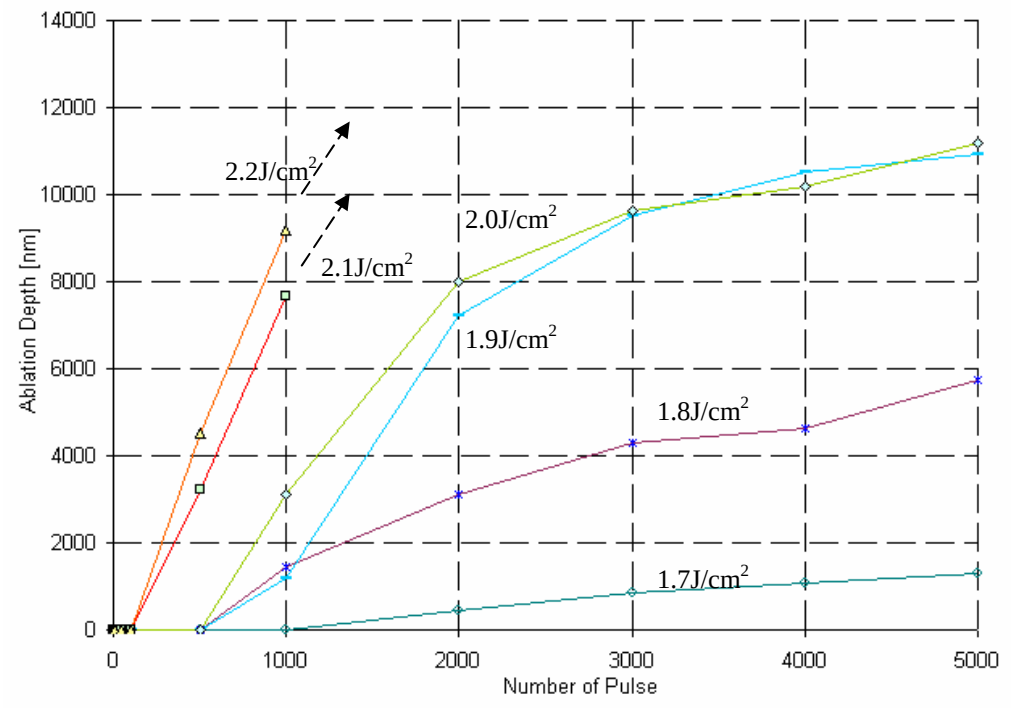

(b) Under water

Figure 8.8 Variation of ablation depth with the number of pulses for different laser fluence (a) in air and (b) under water, respectively

8.4 Alternate Method to Trap the Debris Generated in Laser Ablation

Underwater machining is one method to prevent the debris from redepositing on the finished surface. In this investigation, an alternate method is provided. This involves covering the surface of the silicon workmaterial to be ablated with a polymeric adhensive tape. Figure 8.9 (a) and (b) show macrographs of the holes generated by laser ablation before and after peeling-off of the tape, Figure 8.10 (a) and (b) are micrographs of the same area at higher magnification.

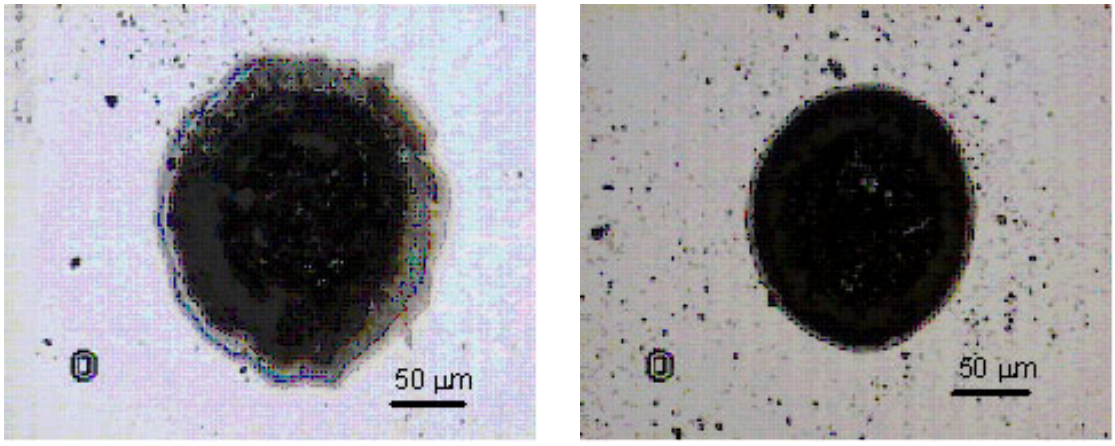

(a) Before (b) After

Figure 8.9 Macrographs of the holes before and after peeling off of the tape from the silicon workmaterial.

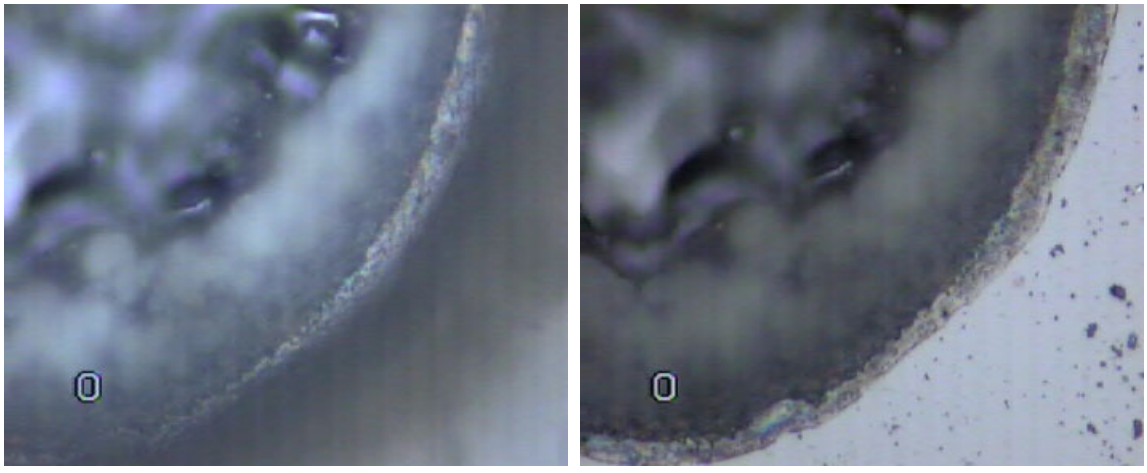

(a) (b)

Figure 8.10 Micrographs of the same area in Figure 8.9 at higher magnification.

Figure 8.11 shows optical macrograph of the tape that was peeled-off from the silicon surface showing redeposited molten and resolidified material from laser ablation. Two points are very clear from this test. One, the surface of silicon after the tape has been peeled-off shows minimal thermal damage and is similar to the macrograph of the hole ablated under water. The ablation depth with the tape, however, was found to be less than without the tape in under water ablation.

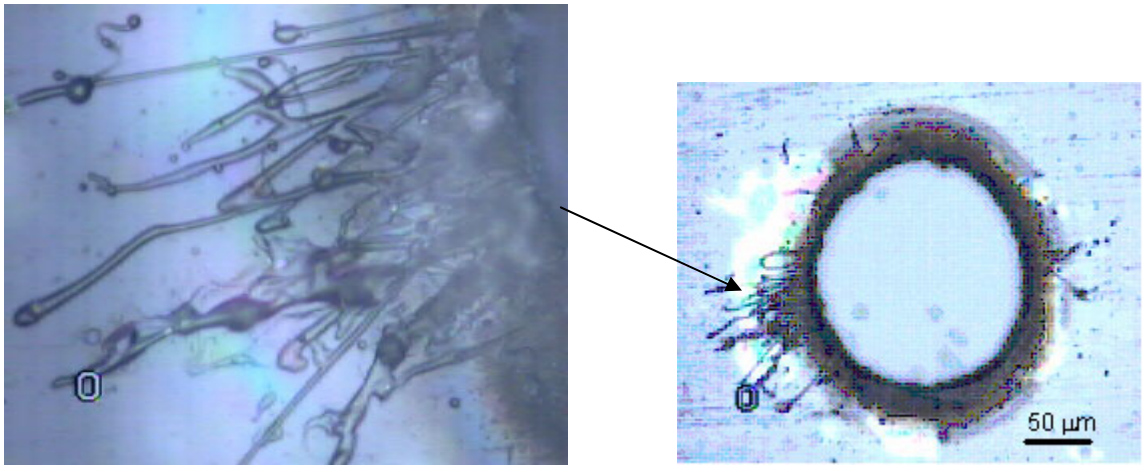

Figure 8.11 Optical macrograph of the debris on the tape peeled-off from the silicon surface showing redeposited molten and resolidified material from laser ablation.

CHAPTER 9

PULSED LASER MICRODRILLING OF BOROSILICATE GLASS

9.1 Introduction

When an intense pulsed laser light is irradiated on the surface of a workpiece, the following processes will occur. At the beginning of the laser pulse, the absorbed laser energy will heat up the substrate to the melting point and subsequently to the vaporization temperature. Depending on the fluence, vaporization can occur within a small fraction of the pulse duration. Evaporated material is pushed away due to recoil pressure. As the same time, the recoil pressure also exerts a force on the molten pool and expels it sideways. Material is removed both in vapor and liquid forms.

For a short and very intense pulse laser, laser induced shock will be generated. Shock wave could be generated by (1) recoil pressure due to rapid vaporization of material, (2) interaction of the laser and the plasma. The shock wave can impinge on the workpiece causing fracture. This damage is referred to as the mechanical damage.

9.2 Analysis

9.2.1 Behavior of Glass

In order to relieve internal stresses that may develop during glass formation, glass is annealed immediately after shaping. The transformation of a liquid to a glass actually

takes place over a range of temperatures at which glass shrinks (thermal contraction). Glass does not undergo a change from disordered liquid structure to ordered crystal structure as iron does at its transformation temperature. In glass, the transformation temperature is the temperature below which viscosity prevents any further configurational changes. Any contraction beyond the transformation temperature range is due only to the lower kinetic energy of the grouping.

The transformation temperature of a given glass composition depends on its constituents and upon the rate of cooling. Slow cooling results in a lower transformation range because the tetrahedral structure will have more time to rearrange. This results in tighter packing of the tetrahedral structure as the mass reaches its transformation range. When glass reaches room temperature, it volume will be smaller when cooled slowly than when cooled rapidly. Hence, slower cooling from the glass melt results in denser glass.

Glass is thermodynamically unstable at room temperature because configuration changes would result in a lower free energy configuration. However, the changes are so slow that they may be considered negligible (it requires eons of years).

As mentioned by Shiu *et al*. (1999) (refer to Figure 9.1) initially glass is considered to be a point *a*. CO_2 laser heating with microsecond pulse duration brings glass to the liquid state point *b* by following curve *1*. With a cooling rate of 10^6 ˚C/s, cooling is represented by the fast cooling curve with transition temperature T_g and eventually the molten glass reach point *c*. The difference in structure between point *a* and *c* results in a net volume increase.

Glass is a poor conductor of heat. Thus, hot common glass may crack when cold water is poured onto it because the surface exposed to the cold water will shrink while the dimensions of the interior remain unaffected.

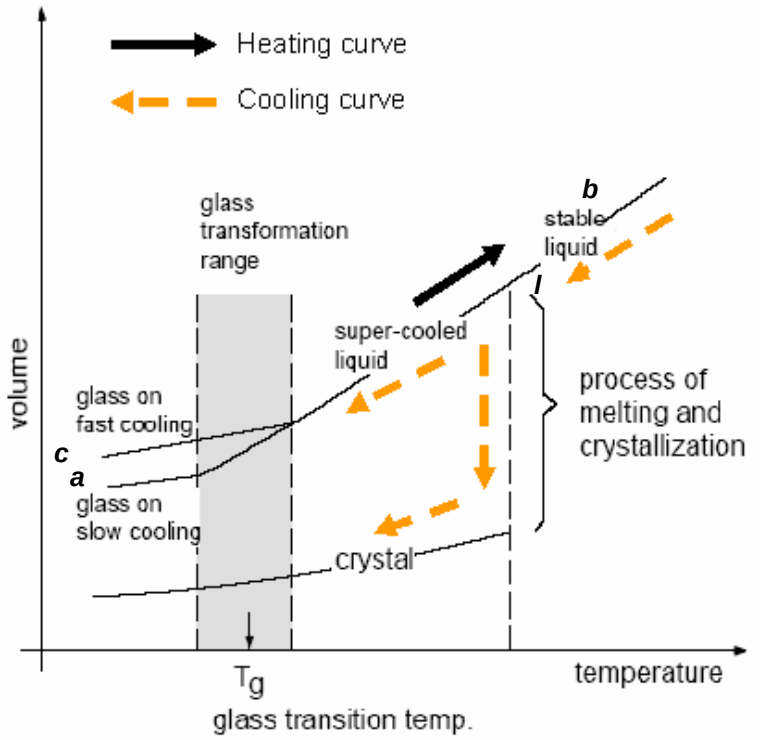

Figure 9.1 Volume changes associated with heating and cooling in systems susceptible to glass formation.

Glass has "no" crystal structure, and hence the phenomenon of slip cannot take place. Thus, together with the strong bonding between atoms, glass exhibits very high compressive strength and a theoretical tensile strength of about ~10^7 kN/m^2. Since glass has a "liquid structure" it may be considered as "saturated with dislocations." Hence, the molecular structure in the glass is unable to move. The presence of minute cracks or imperfections in glass permits stress concentrations to localize and exceed the bond strength between atoms – glass will crack.

9.2.2 Mechanism of Bump Formation

Normally, for most pure liquids, $\delta\sigma/\delta\tau < 0$, where σ is the surface tension. However, Kingery [85] found that $\delta\sigma/\delta\tau$ could be positive for certain liquids, such as $SiO_2B_2O_3$ melt due to dissociation with temperature. It is believed that surface tension of a liquid depends not only on the surface temperature but also on the surfactant concentration [86]. The temperature gradient drives the material towards the cooler region of higher surface tension, while the surfactant effect tends to move the material to lower surfactant concentration region [87]. Pulses following the first one would therefore be expected to drive less significant compositional capillarity, ultimately suppressing the central dome. Vaporization of absorbed oxygen and water was believed to be the main reason for generating gradients of surfactant composition.

For the case of laser-induced bump formation, pulsed heating creates a temperature gradient following the beam intensity profile along the radial direction. The temperature gradient induced thermocapilary flow, drives the material from the hot center to the cold periphery forming a bowl-shaped feature.

9.3 Experiment

The experimental setup used for silicon wafer studies (Chapter 8) was used. A borosilicate glass (Corning 0211 glass) was used as the workmaterial in this study. Table 9.1 lists some properties of the borosilicate glass.

TABLE 9.1

PROPERTIES FOR BOROSILICATE GLASS (CORNING 0211 GLASS)

General Properties	
Thickness	0.20mm
Density	2.53gm/cm^3
Coefficient of Expansion 0-300ºC	74x10^{-7}ºC
Annealing Temperature	550ºC
Softening Temperature	720ºC
Working Temperature	978ºC
Chemical Composition	
Silicon Dioxide	64%
Boron	9%
Zinc	7%
Potassium Oxide	7%
Sodium Oxide	7%
Titanium Oxide	3%
Aluminum Oxide	3%

9.4 Results and Discussion

Figures 9.2 show the variation of ablation depth with laser fluence for different number of pulses in air. The data is obtained using MicroXAM surface mapping profiler; it is obtained by choosing an area on the hole or irradiated area. It can be seen that there is a threshold value of laser fluence below which material removal by ablation does not take place. However, for the borosilicate glass workmaterial, a hump is observed.

The threshold value is determined by the onset of crater formation on the borosilicate glass workmaterial by laser ablation. This value is found to increase with decrease in the number of pulses. For low fluence at 1.07 J/cm^2, a hump with a height of 15nm is created with a single pulse laser, constantly increasing with increasing of number of pulses, to a maximum height of 25 nm at 1000 pulses

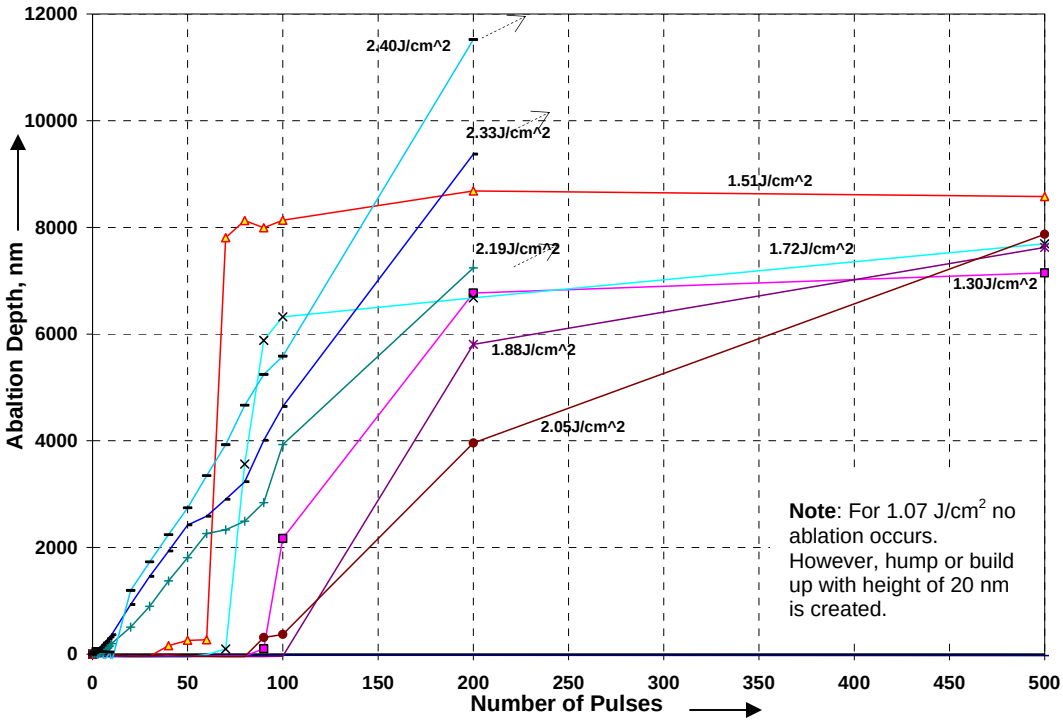

(a)

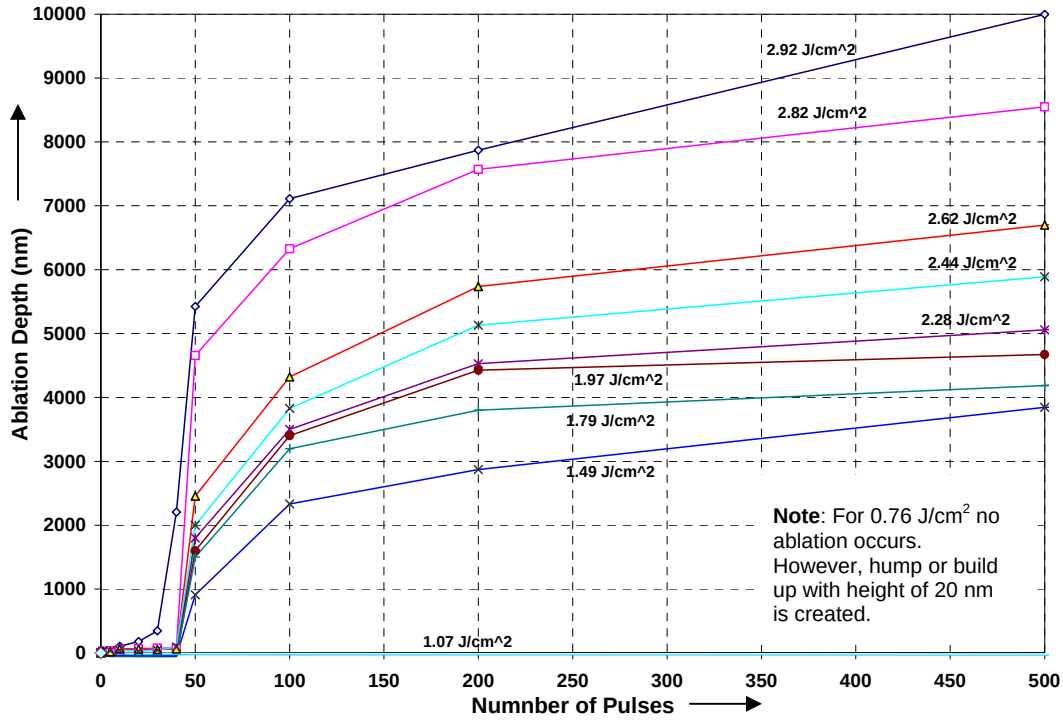

(b)

Figure 9.2 Variation of ablation depth with number of pulses at various laser fluences for machining borosilicate glass (a) in air and (b) under water, respectively.

For fluence of 1.30 J/cm^2, 1.51 J/cm^2, 1.72 J/cm^2 and 1.88 J/cm^2 a hump is created at low number of pulses, with a maximum height of ~50nm before being removed after 90, 40, 60 and 100 pulses, respectively. More pulses are needed for fluences between 1.51 and 2.0 J/cm^2 because of plasma shielding (referred to Figure 9.4 (a)). For fluence at 2.05 J/cm^2, creation and removal of hump is on and off for the first 80 pulses and ablation begin after 80 pulses. For fluence between 2.19 and 2.40 J/cm^2, ablation starts at the first pulse and constantly increases with increase in the number of pulses.

Figure 9.3 shows the variation of ablation depth with laser fluence for the first 20 pulses in air. It shows that a hump is created for fluences equivalent to or lower than 2.05 J/cm^2. From fluence equivalent to or greater than 2.19 J/cm^2, ablation begins from the first pulse. In the case of 2.40 J/cm^2, a different phenomenon is observed. Creation of a hump and ablation is on and off. The height of the hump can reach up to a maximum of 150 nm after irradiating with 2 pulses.

Figure 9.4 shows the variation of ablation depth with laser fluence for different number of pulses in air. It can be seen that there are two ablation regions. The first region, at fluence between 1.30 and 2.05 J/cm^2, thermal ablation takes place. In this region, energy is not enough to break the bond energy between atoms or molecules. However, the energy is enough to cause thermal boiling and thermal explosion and evaporation for the borosilicate glass workmaterial. And the ablation is max at 1.5 J/cm^2 and it drops after this critical point. It is believed that plasma shielding phenomena will occurr after this point. Energy is sufficient to create a plasma with the evaporated material that is caused by the thermal ablation. This plasma cloud absorbs most of the energy. The final energy or UV light reaching the surface material is much reduced. This

causes the ablation to decrease. At a fluence of 2.19 J/cm^2, ablation is regained at this point.

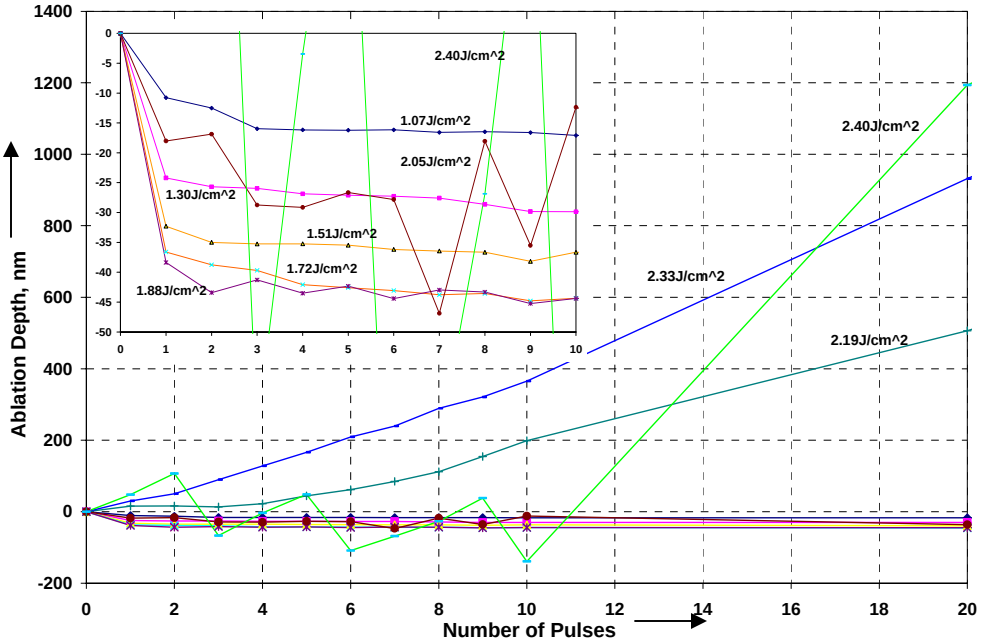

(a)

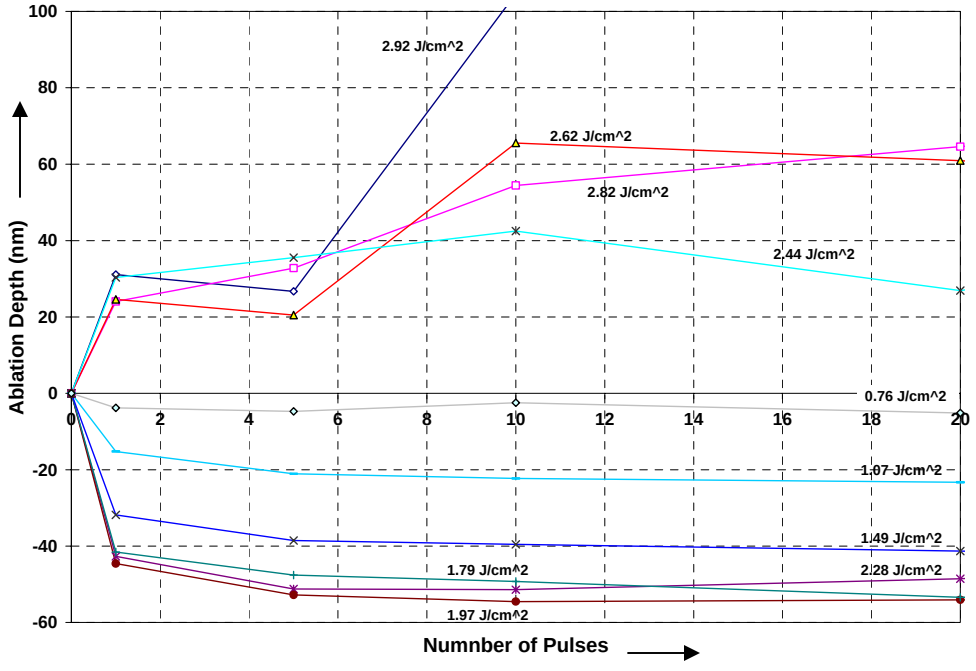

(b)

Figure 9.3 Variation of ablation depth with number of pulses at various laser fluences for machining borosilicate glass (a) in air and (b) under water, respectively.

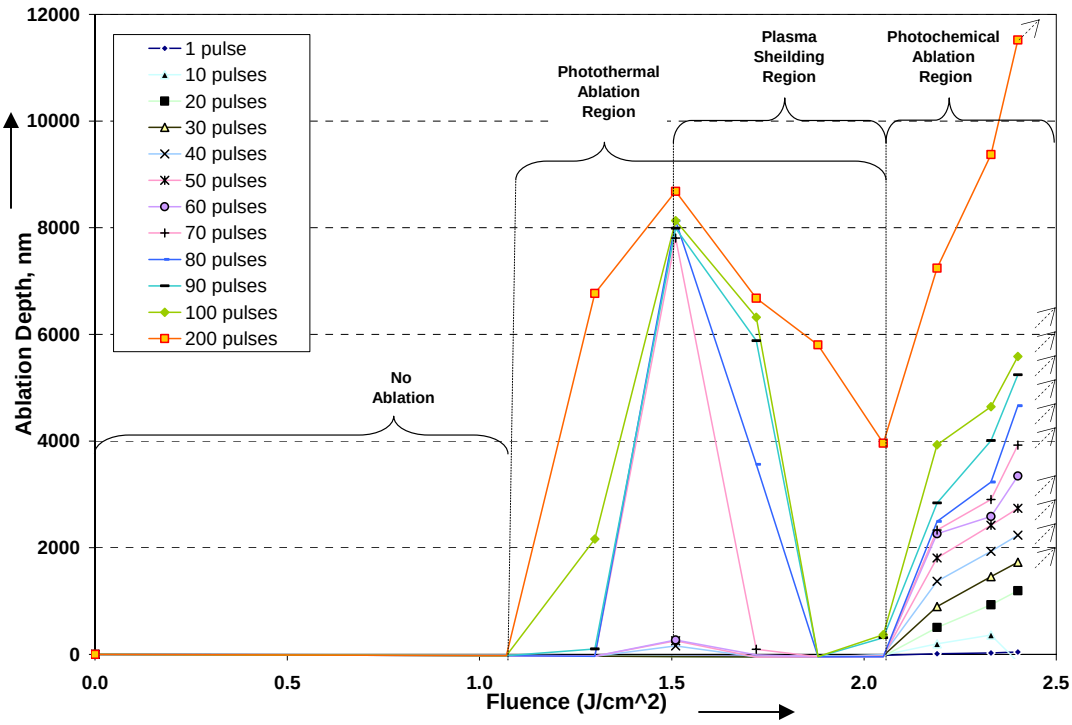

(a)

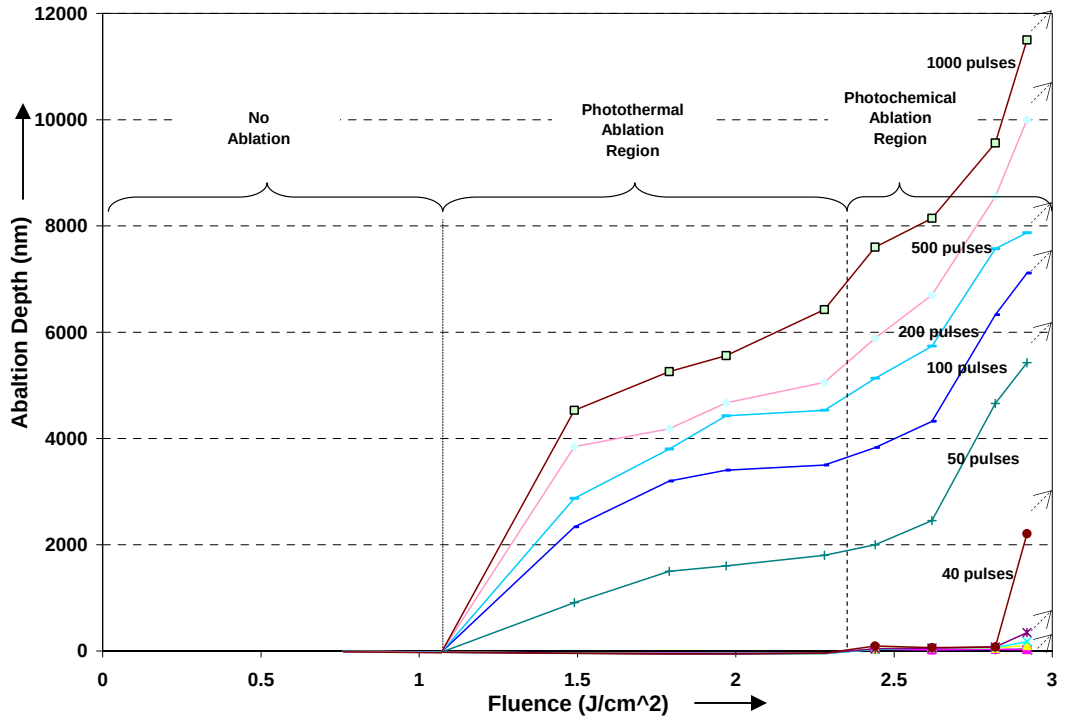

(b)

Figure 9.4 Variation of ablation depth with laser fluence for different number of pulses (a) in air and (b) underwater, respectively.

On comparing Figures 9.3 and 9.4, it can be seen that at 2.19 J/cm^2 ablation takes place at the first laser pulse, this evidenced that photochemical ablation took place. This fluence is named as threshold fluence, at which energy is enough to break the bonding energy between atoms or molecules. After this threshold fluence, the ablation depth appears to be depending of number of pulses.

Figure 9.5 shows the cross-section profiles obtained using MicroXAM surface mapping profiler. They are obtained by measuring the cross sectional profiles at a given line on the diameter of the hole. Figure 9.5 (a) to (h) clearly show evidence that a hump is created at low fluence (< 2.05 J/cm^2). The increment of volume could be due to the glass behavior as mentioned in Section 9.2.1.

Figure 9.6 shows a lot of air bubbles trapped in the irradiated area. Theses air bubbles only can be seen inside the laser irradiated area by using optical microscopy. The creation of bubbles that trapped in borosilicate glass workpiece can be cause by the scission of the bonding that release gases, such as O_2, O_3, which has been proved of releasing of gases (CO_2 and CO) in polymer by Brandon *et al.* [31] and Estler *et al*. [42]. And, this may also caused the increment of volume in the laser irradiated region.

The hump could only reach to a maximum height of 50 nm. When there is a crack initialed by the laser pulses, a significant increase in ablation is observed, as show in Figure 9.2 for fluence 1.5 and 1.7 J/cm^2 at 60 pulses.

Formation of bump is clearly seen in Figures 9.5 (g) to (i) and 9.10 (b). Mechanism of bump formation has been mentioned in Section 9.2.2.

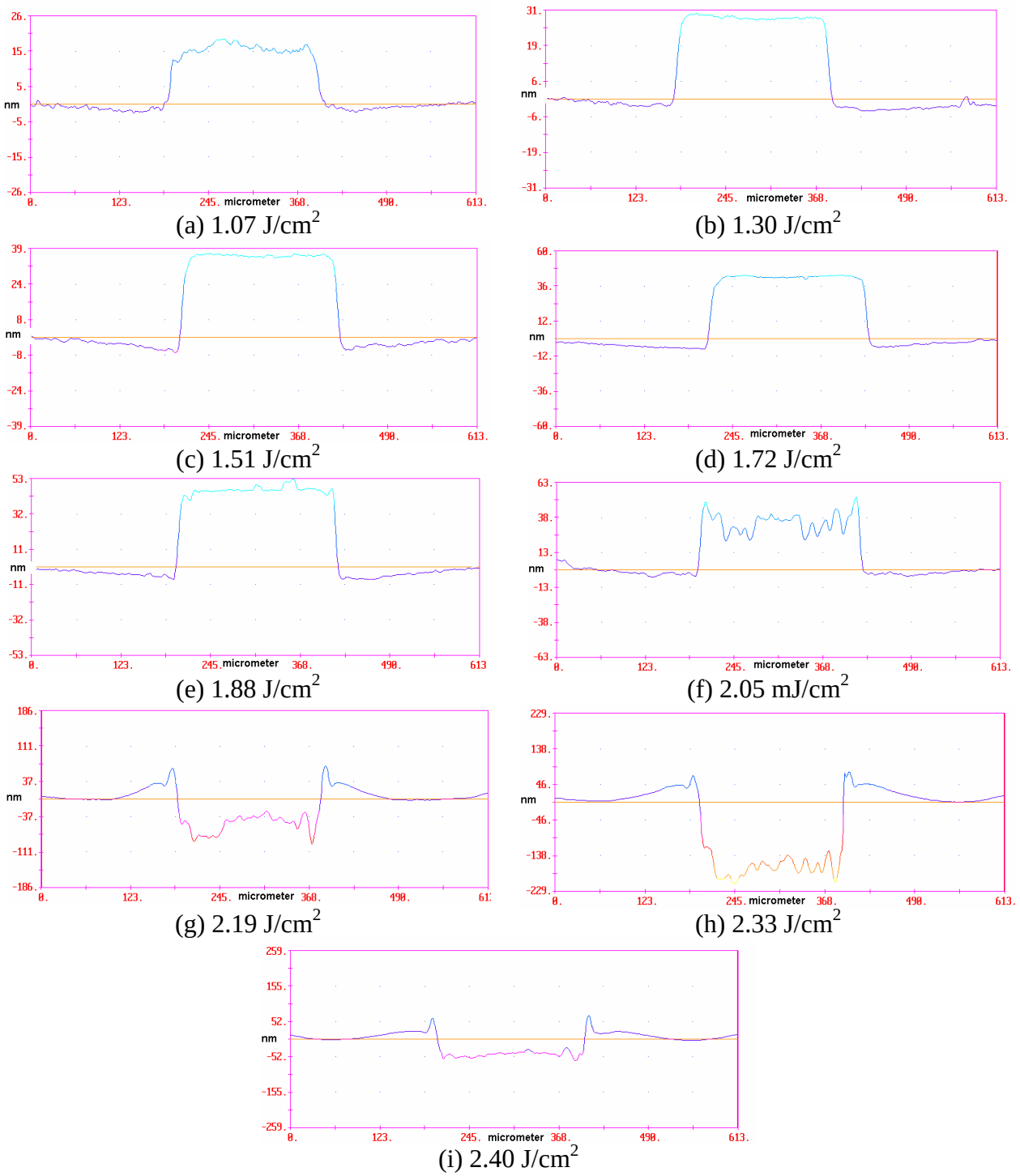

Figure 9.5 Cross-section profiles of borosilicate glass exposed to 5 laser pulses in air from 1.07 J/cm^2 to 2.4 J/cm^2 obtained using MicroXAM surface mapping microscope.

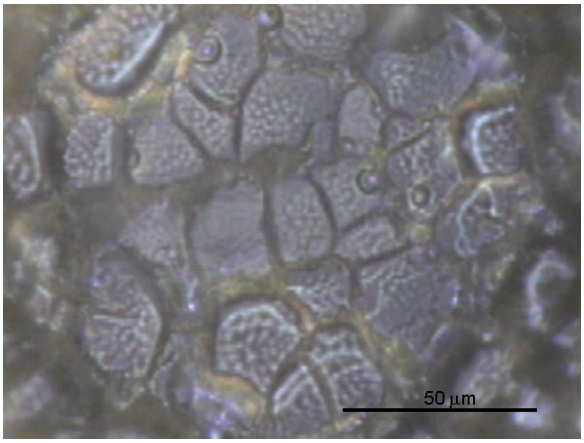

Figure 9.6 Optical micrographs of the top view of borosilicate glass workpieces ablated at 1.30 J/cm^2 for 1000 pulses under water.

Figures 9.7 (a) and (b) show optical micrographs of the top view of borosilicate glass workpieces ablated at a fluence of 2.55 J/cm^2 and at different number of pulses from 10 to 5000 in air and under water. Two important differences between machining in air and under water can be seen. The first one is the absence of thermal damage in the case of underwater machining from 10 pulses to all the way up to 5000 pulses while significant thermal damage is present in the case of machining in air as shown in Figure 9.7. It is for this very reason that underwater machining is preferred. The second one is the nature of the material removal in the two cases. While ablated surface showed less cracking in the case of machining in air, and more cracking in the case of underwater machining. It is believed that high pressures and high temperatures associated with laser driven intense shockwaves are initially responsible for cracking. In the case of underwater machining, water immerged through the cracks and thermal expansion causes more cracking. It is interesting to note that the crack do no proceed beyond the laser irradiated area in both underwater and in air machining.

(a) In air (b) Under water

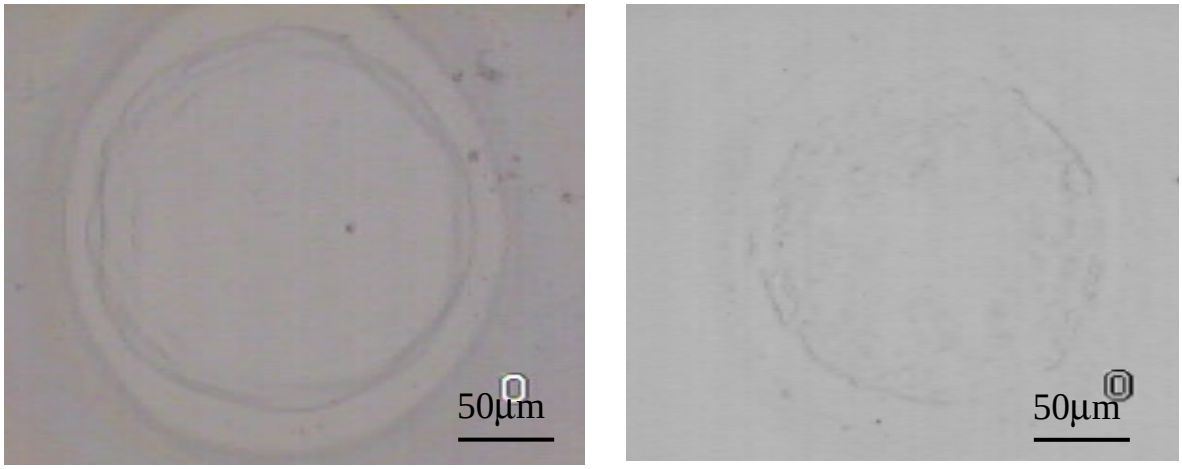

10 pulses

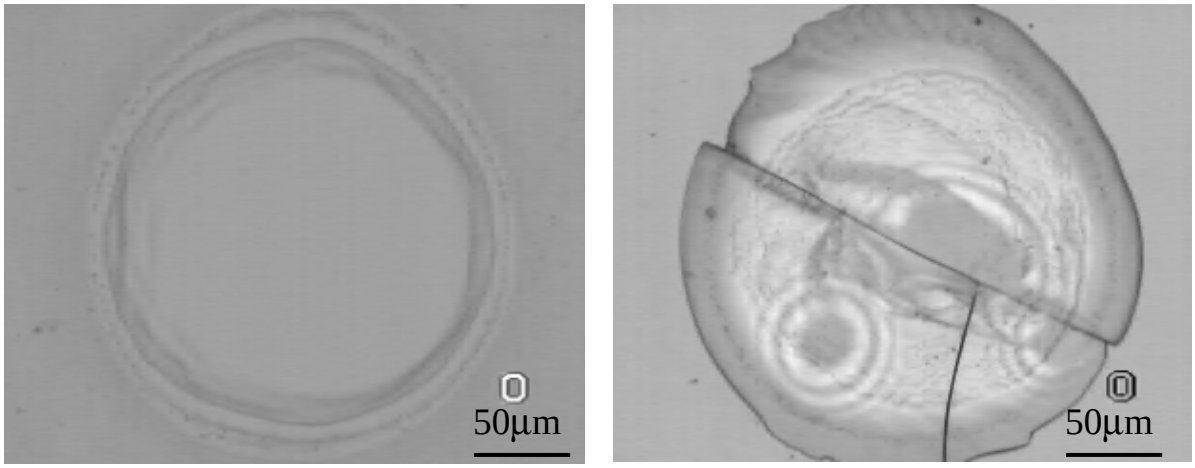

20 pulses

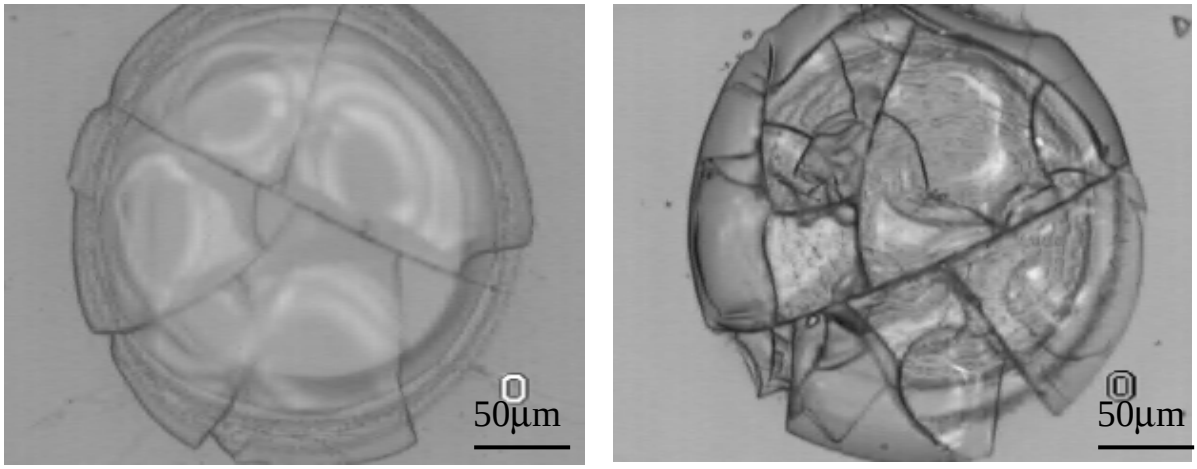

50 pulses

(a) In air (b) Under water

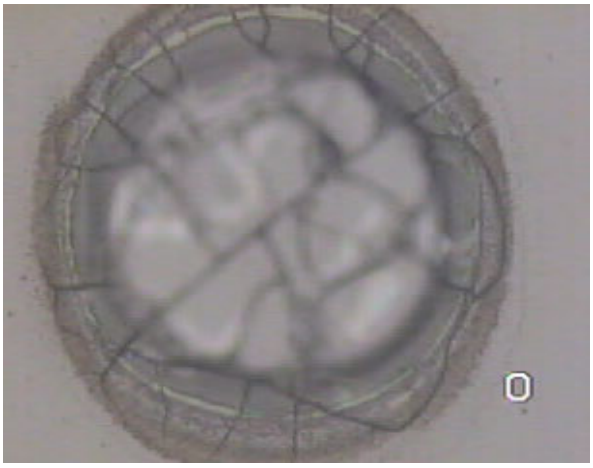
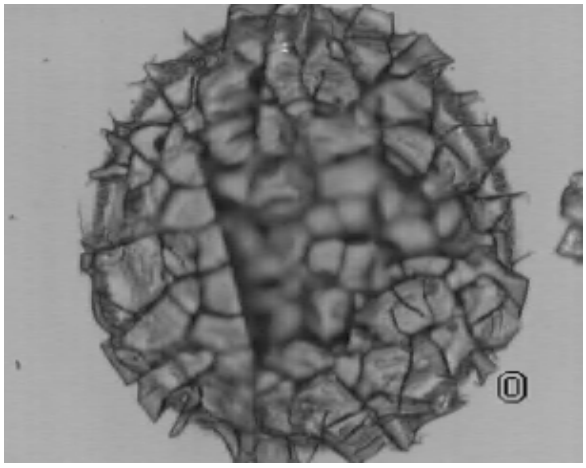

100 pulses

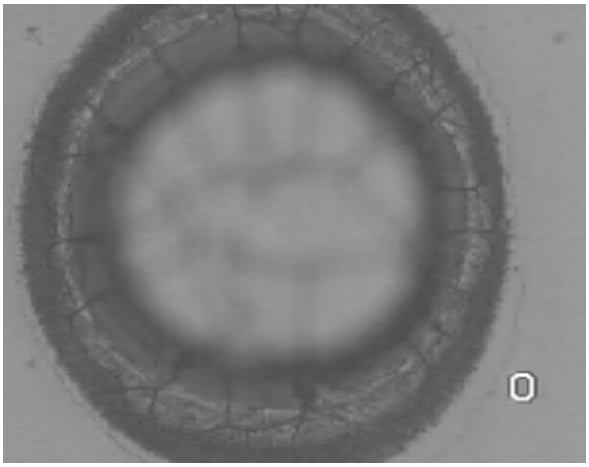
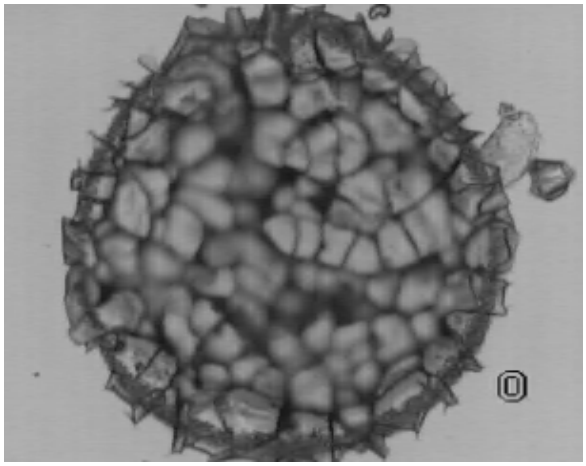

200 pulses

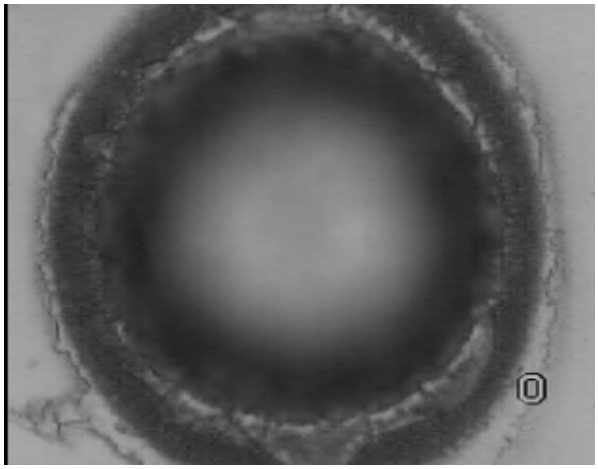
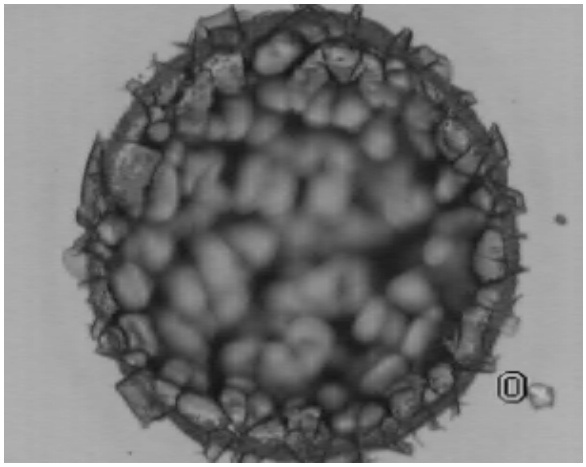

500 pulses

(a) In air (b) Under water

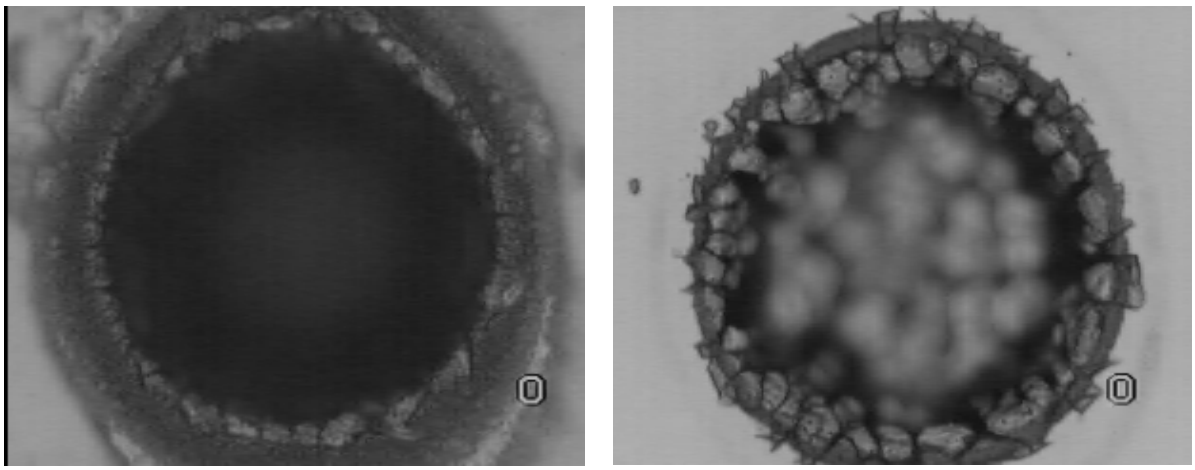

1000 pulses

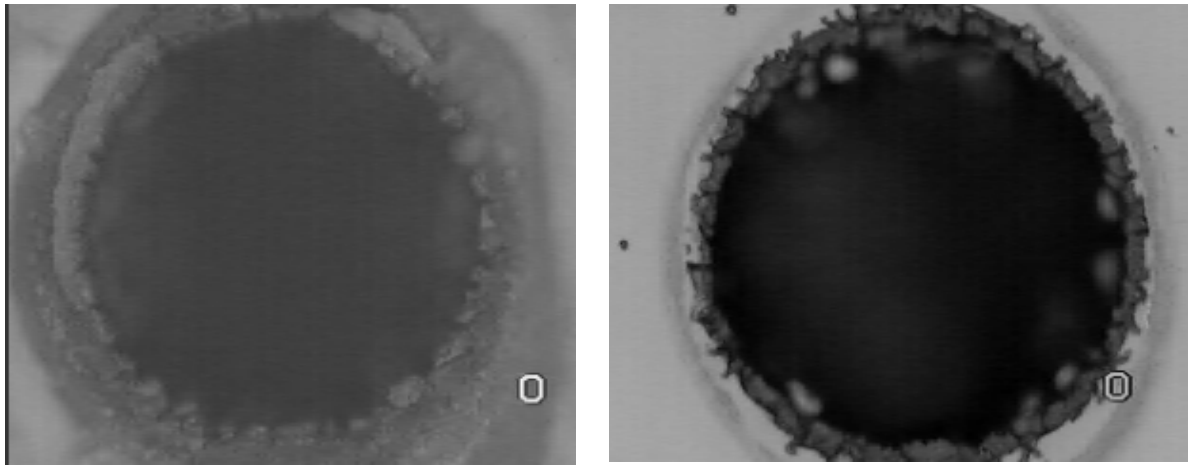

5000 pulses

Figure 9.7 Optical micrographs of the top view of borosilicate glass workpieces ablated at pulse energy of 2.55 J/cm^2 and at different number of pulses from 10 to 5000 pulses (a) in air and (b) under water, respectively.

Figures 9.8 (a) and (b) show SEM micrographs of borosilicate glass ablated in air and under water with a fluence of 0.28 J/cm^2. Redeposition of debris is observed for ablation in air. Debris is ejected out as far as 150 μm from the boundary of the hole as shown in Figures 9.8 (a) and 9.9.

(a) In air (b) Under water

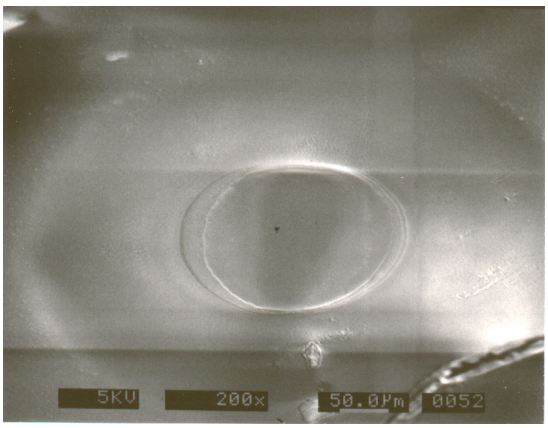

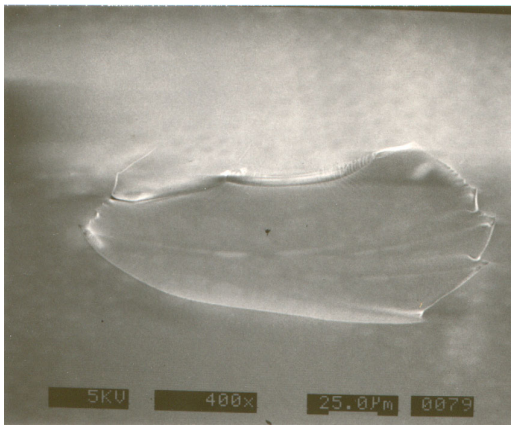

50 pulses

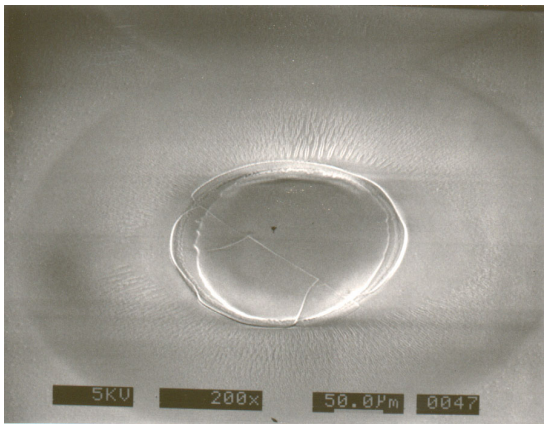

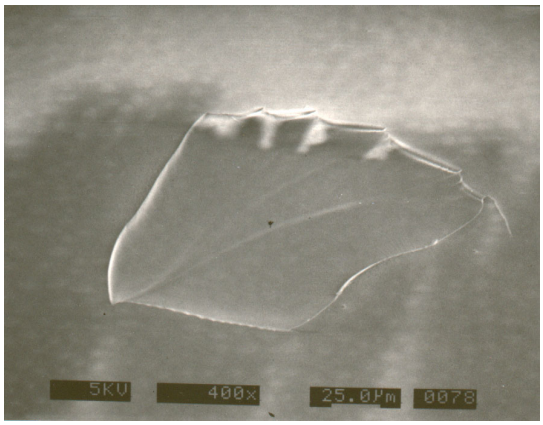

100 pulses

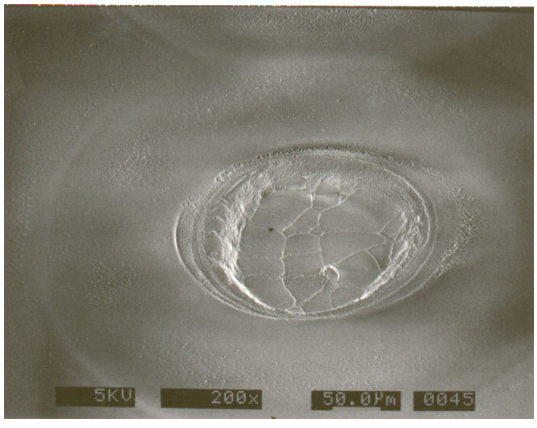

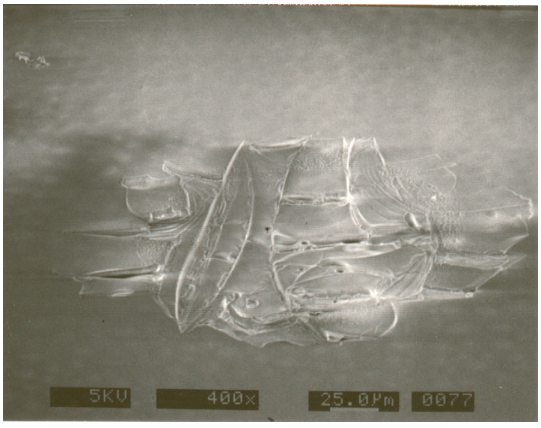

500 pulses

(a) In air (b) Under water

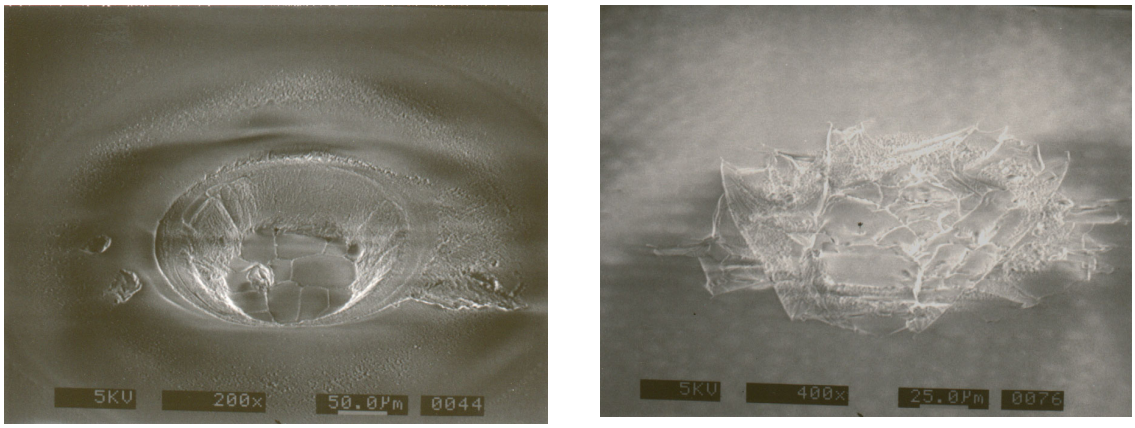

1000 pulses

Figure 9.8 SEM micrographs of borosilicate glass irradiated with a fluence of 0.28 J/cm^2 in air and under water respectively. Note: the scale in air is 50 µm and under water is 25 µm.

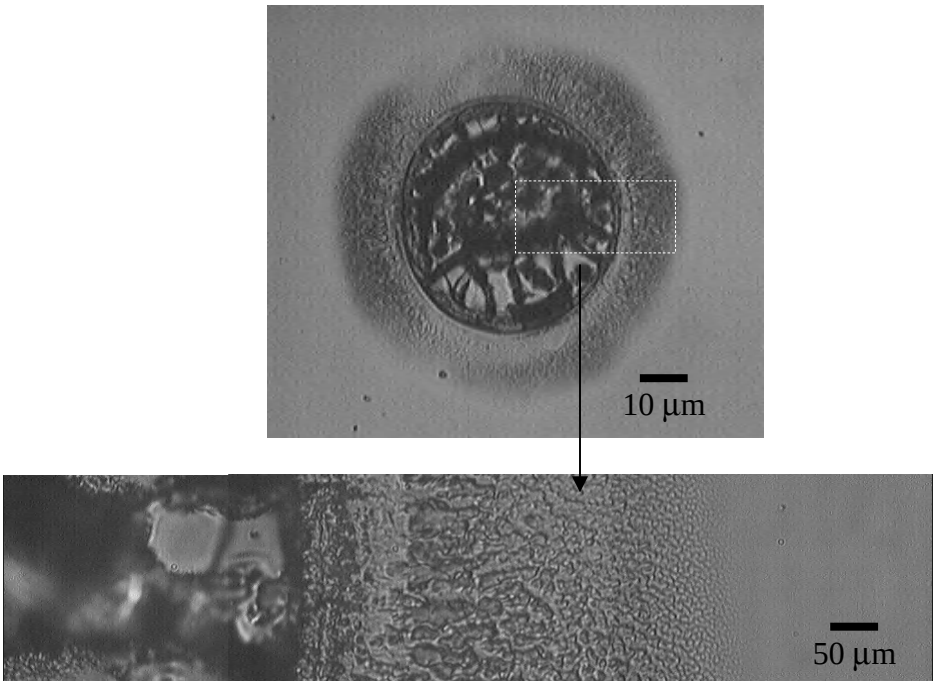

Figure 9.9 Optical micrographs of the top view of borosilicate glass workpiece ablated at 2.42 J/cm^2 for 1000 pulses in air.

For under water ablation, some of the platelets have become detached from the surface. This may be due to the initial pulse, which is not enough to photochemically ablate the borosilicate glass, heating up the irradiated volume followed by rapid cooling by water and resulting in initial cracking. These rapid heating and cooling cycles also cause thermal shock and crack growth initiated after a few tens of pulses. Shock front of the laser pulse also causes blast off of the platelets and produce 'blow holes'. Figure 9.8 (b) shows cracking and formation of platelets in ablation under water. The size of the fractured platelets is reduced with increasing number of pulses and fluence.

The structure of the periphery for ablation in air and under water is totally different. Figure 9.10 (a) show the periphery for ablation in air. Cracking are all over the irradiated area inside the diameter of the beam can be seen. Figure 9.10 (b), (c) and (d) show thesurface features at the periphery, center and boundary of the hole ablated in air. At the center of the hole, cracking of material could be observed. This is due to thermally induced cracking by the laser beam. The periphery evidences laser-induced bump formation. Pulsed heating creates a temperature gradient following the beam intensity profile along the radial direction. The temperature gradient induces thermocapilary flow, driving the material from the hot center to the cold periphery and forming a bowl-shaped feature.

Recoil pressure causes the debris or molten material to splash out. The resolidified material causes a bowl-shape feature as shown in Figure 9.11 (a) and (b). For 100 pulses of irradiation, molten material begins to eject out and the pattern of ejection can be seen in Figures 9.11 (a) and (b). As number of pulses increase, the accumulation of resolidified molten material form in the shape of a bowl.

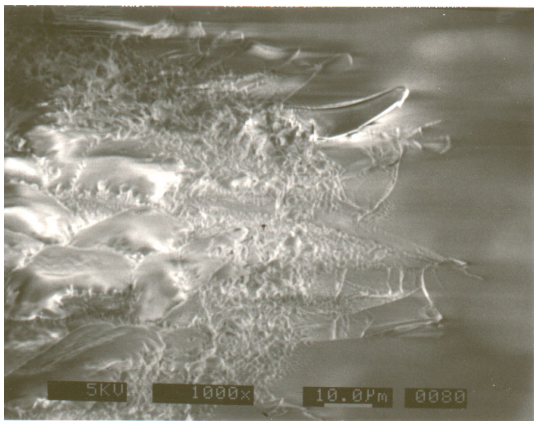

(a) Under water

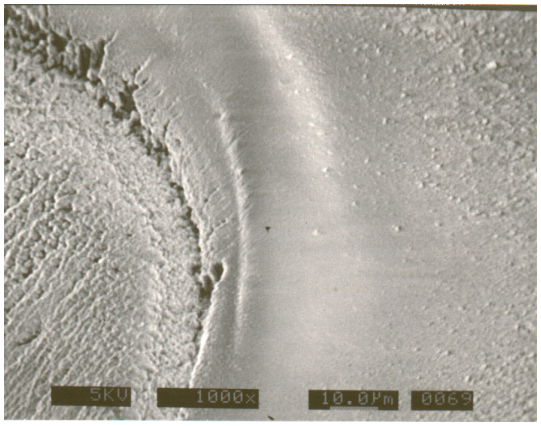

(b) In air(periphery)

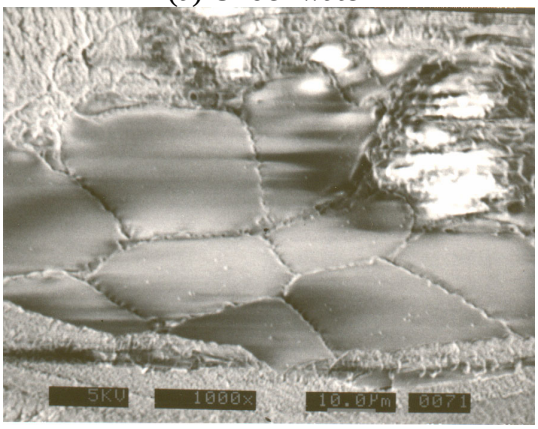

(c) In air (center)

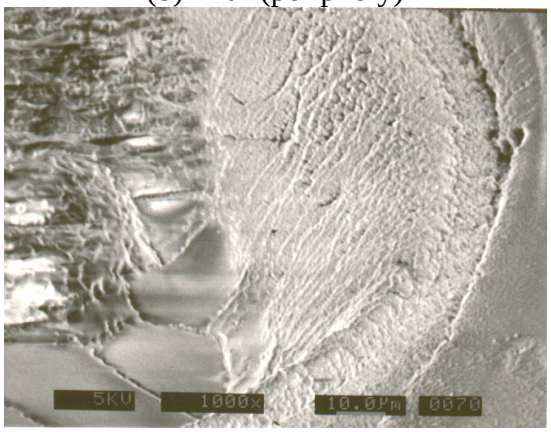

(d) In air (boundary)

Figure 9.10 SEM micrograph of the surface topology of various sections for borosilicate glass irradiated with an excimer laser at a fluence of 0.28 J/cm^2.

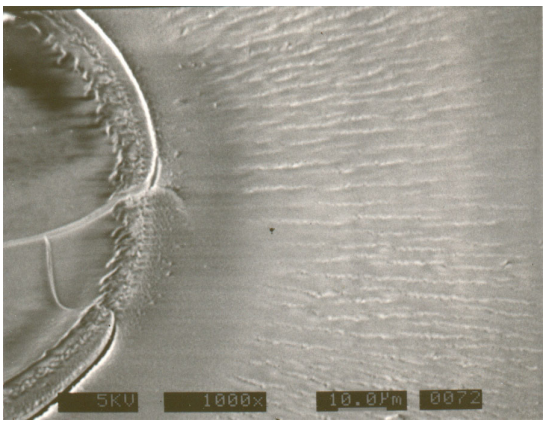

(a) 100 pulses

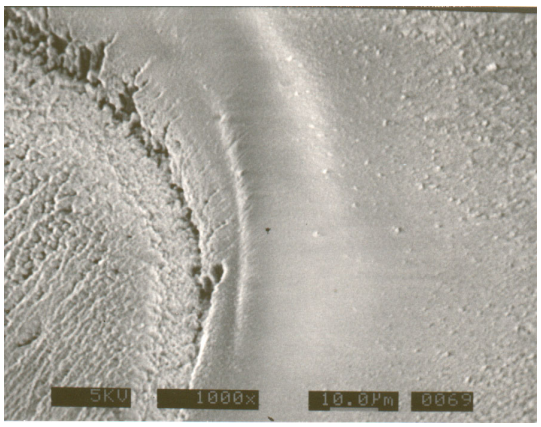

1000 pulses

Figure 9.11 SEM micrographs showing ejection of molten material at 100 and 1000 pulses irradiated with a fluence of 0.28 J/cm^2 in air.

9.5 Alternate Method to Trap the Debris Generated in Laser Ablation

Under water machining is one method to prevent the debris from redepositing on the furnished surface. In this investigation, an alternate method is proposed. This involves covering the surface of the borosilicate glass workmaterial to be ablated with a polymeric adhesive tape. Figure 9.12 (a) and (b) show macrographs of hole generated by laser ablation without and with (after peeling off) the tape. Figures 9.13 show optical micrograph of the tape that was peeled-off from the borosilicate surface. Redeposited molten and resolidified materials from laser ablation are attached on the tape. Two points are very clear from test. One, the surface of borosilicate glass after the tape has been removed shows minimal thermal damage and is similar to the macrograph of the hole ablated under water. The ablation depth with the tape, however, was found to be less in air than without the tape in under water ablation.

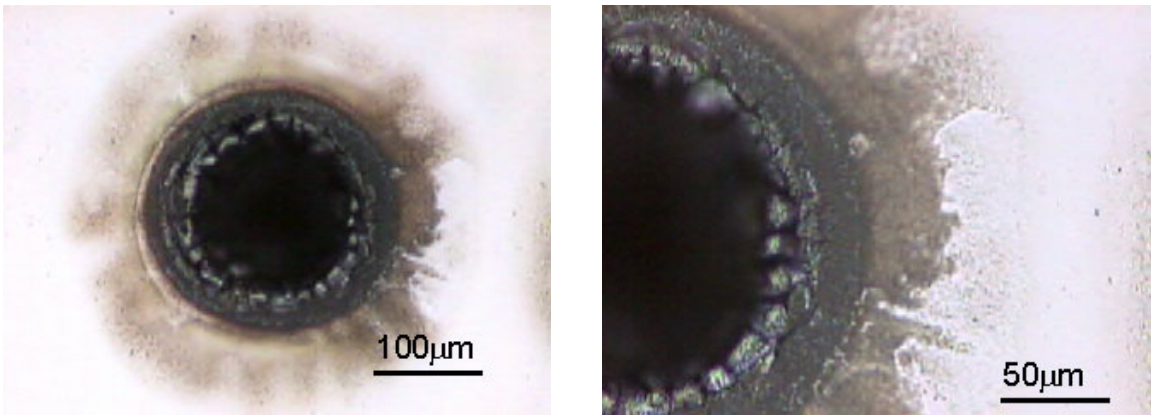

(a)

continue/-

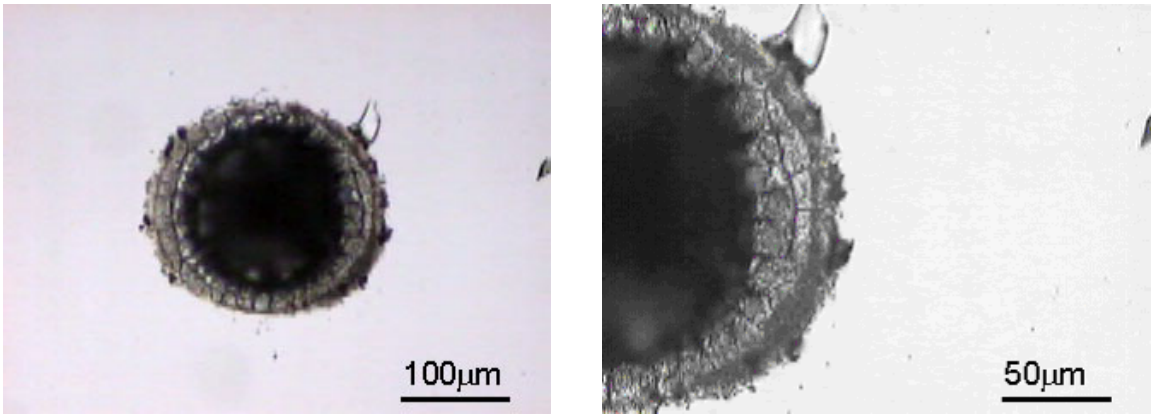

(b)

Figure 9.12 Optical micrograph of holes without and with (after peeling-off) Scotch tape from the borosilicate glass workmaterial.

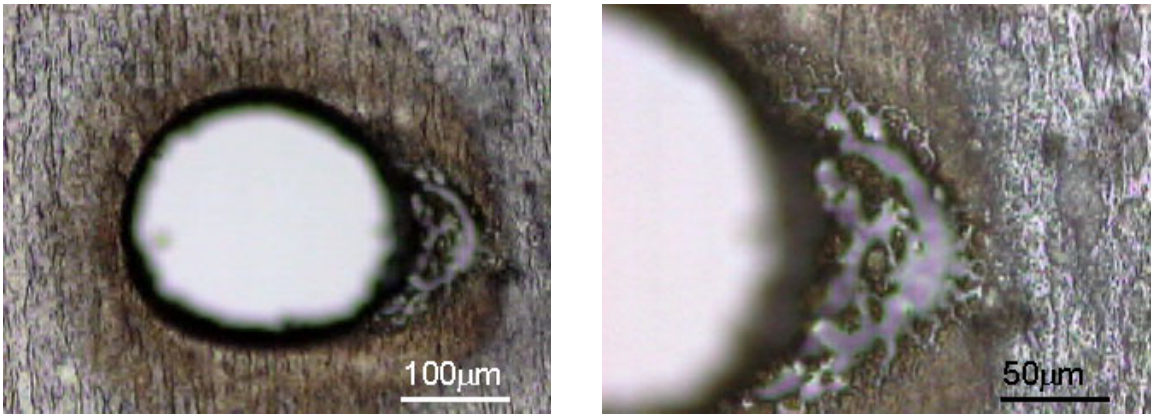

Figure 9.13 Optical micrograph of debris on the tape peeled off from the borosilicate glass surface showing redeposied molten material and resolidifed material from laser ablation.

CHAPTER 10

PULSED LASER MICROMACHINING

10.1 Introduction

As mention in Chapter 2, pulsed laser micromachining is complex and involved a lot of parameter, such as reflectivity, absorption and conduction of material to the laser wavelength. After determine the focus point, fluences and frequency in previous, in this chapter 3-D machining is performed.

10.2 Experiment

Different programs (mainly PSO code and G code) are written to command the movement of the translation stages and firing the laser pulses. Meanwhile, different CIMCAD is used to draw and convert CAD drawing into PSO and G code as well. Substrate such as PMMA, Polyurethane, silicon wafer and borosilicate glass are used as workpiece. Circular beam obtained by masking technique is used to perform 3-D machining. Different diameters of holes are used.

Continue/-

10.3 Results and Discussion

Figure 10.1 show the MicroXAM 3D micrograph of borosilicate glass irradiated with 5 laser pulses at fluence of 1.88 J/cm^2. A 3D hump (rise-up) is clearly reflecting the uniformity of the laser beam profile that is used for the investigation.

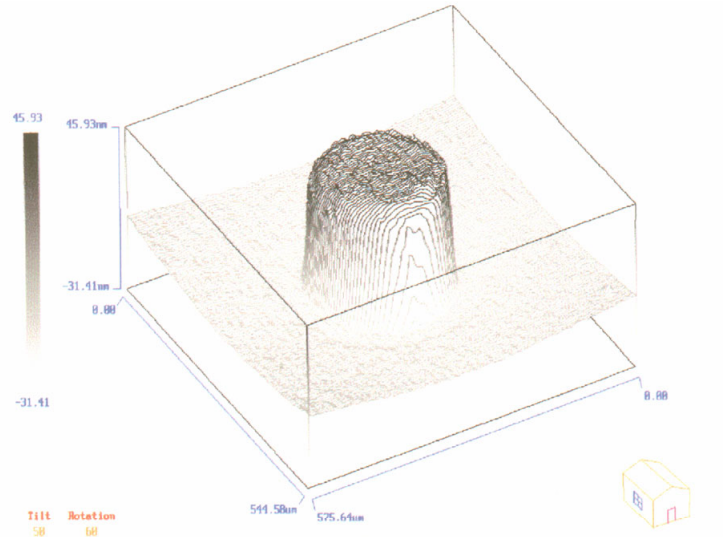

Figure 10.1 MicroXAM 3D micrograph of borosilicate glass irradiated with 5 laser pulses at fluence of 1.88 J/cm^2

Figure 10.2 shows the cross section of the mechanism of line machining. Laser beam is moving forward with different increments of distance.

Figure 10.2 Mechanism of line machining

10.3.1 Effect of Energy

Figures 10.3 (a) to (f) show the 3-D and cross sectional view of a line machined with various laser energies. For energies ≤ 125 mJ, a wall (rise-up) is obtained. This is due to the properties of glass as discussed in Chapter 8. For energies ≥ 175mJ, clean cuts are obtained.

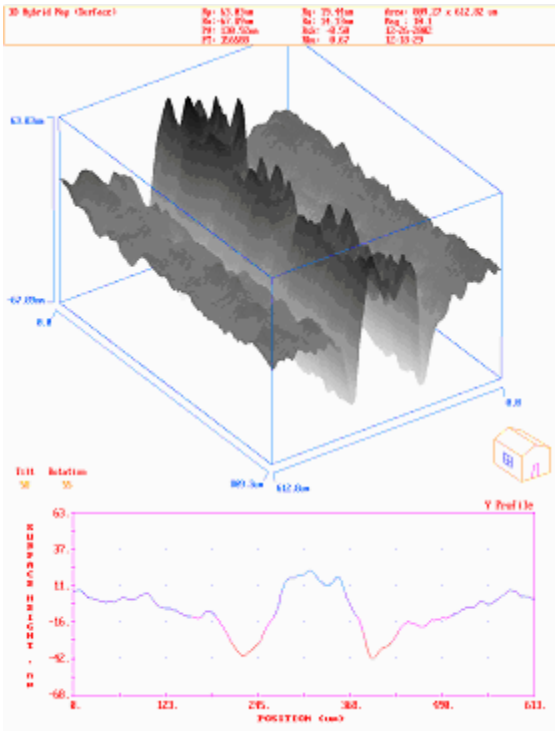

(a) 100 mJ

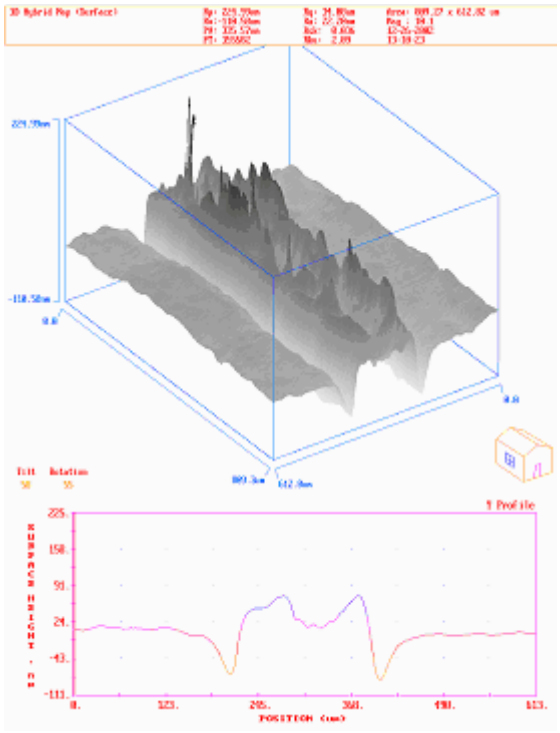

(b) 125 mJ

Continue/-

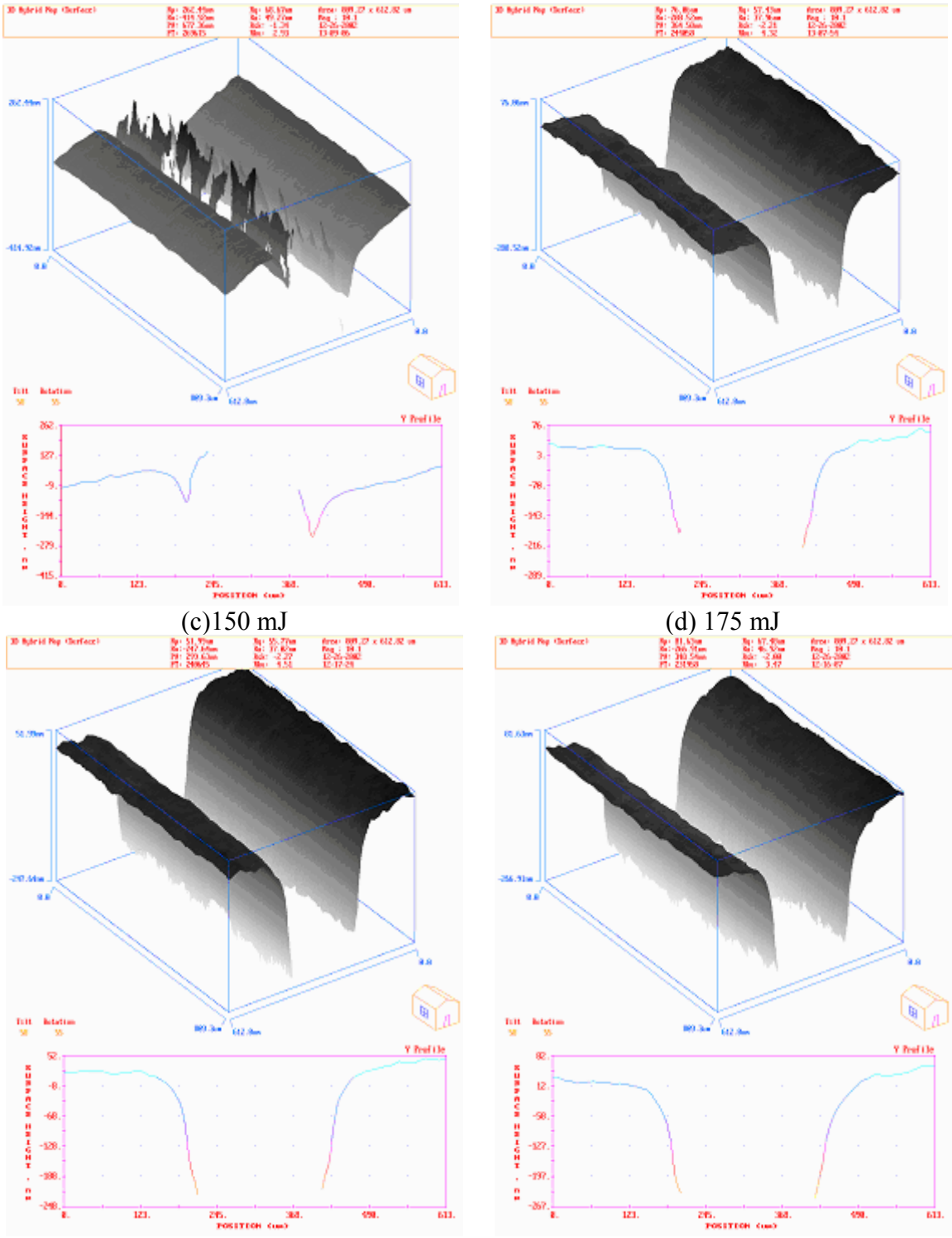

(c)150 mJ (d) 175 mJ

(e) 200 mJ (f) 300mJ

Figure 10.3 MicroXAM micrographs of borosilicate glass machined with various energies.

10.3.2 Effect of Feed Rates

A laser beam of 70 µm diameter is used to machine a line on a borosilicate glass. Different feedrates from 1 to100 µm/pulse are used. Figures 10.4 show the MicroXAM micrographs for the finishing. Detailed cross sections for each feed rate is shown. For feedrates ≥ 40 µm/pulse, the effect is the same as in microdrilling. For feedrate of 20 µm/pulse, the ablation region is covered up by the resolidified molten material. For the feedrates ≤ 5µm/pulse, the width of the line is increased. This may have been caused by the heat from the ejected molten material (or debris), and diffraction of the beam energy (Fresnel effect) after passing through the mask.

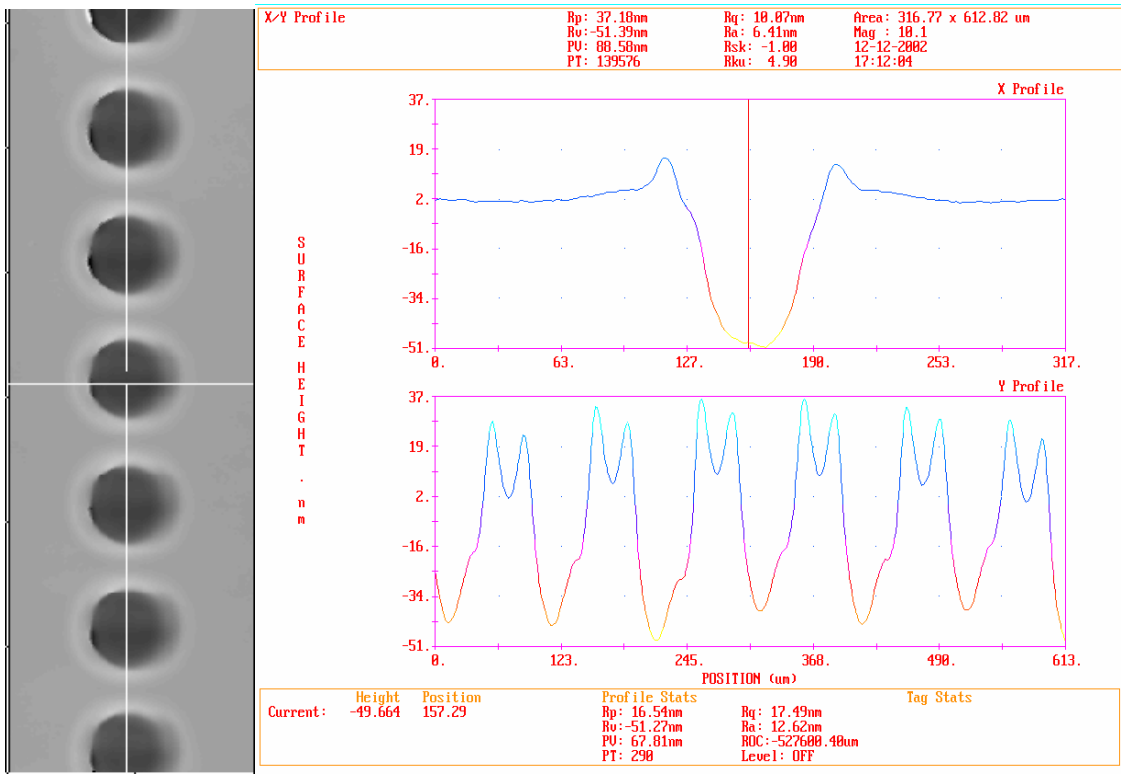

(a) f = 100 µm/pulse

Continue/-

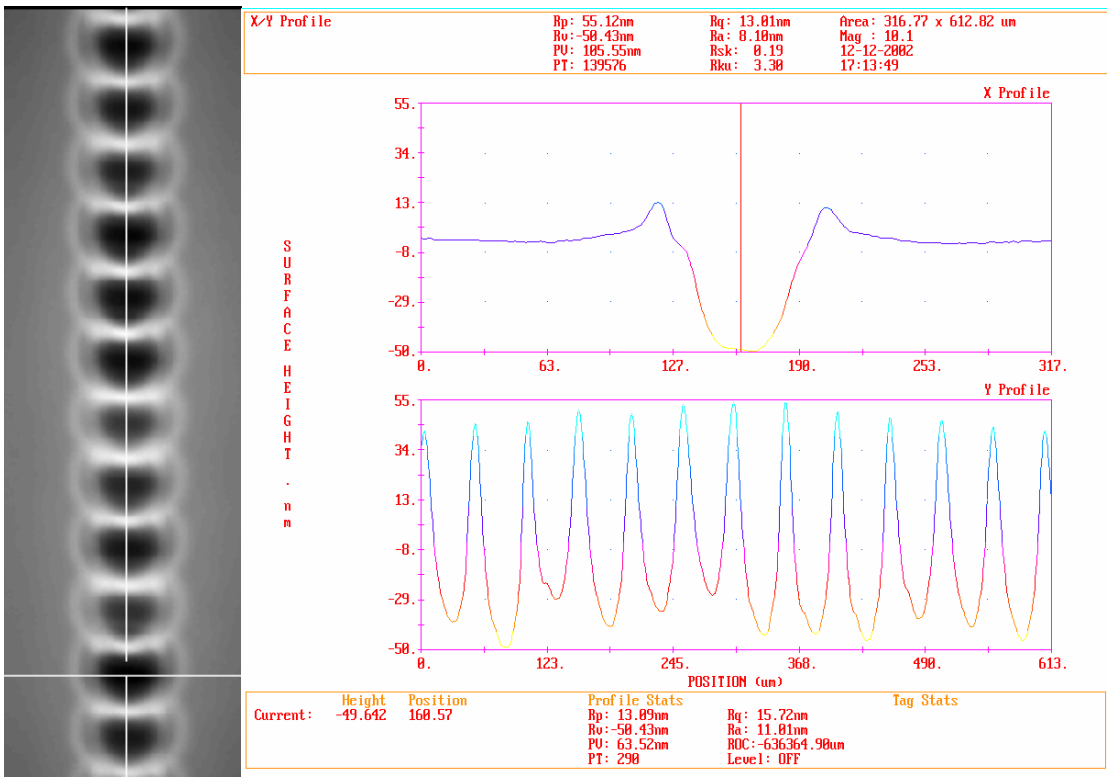

(b) f = 50 µm/pulse.

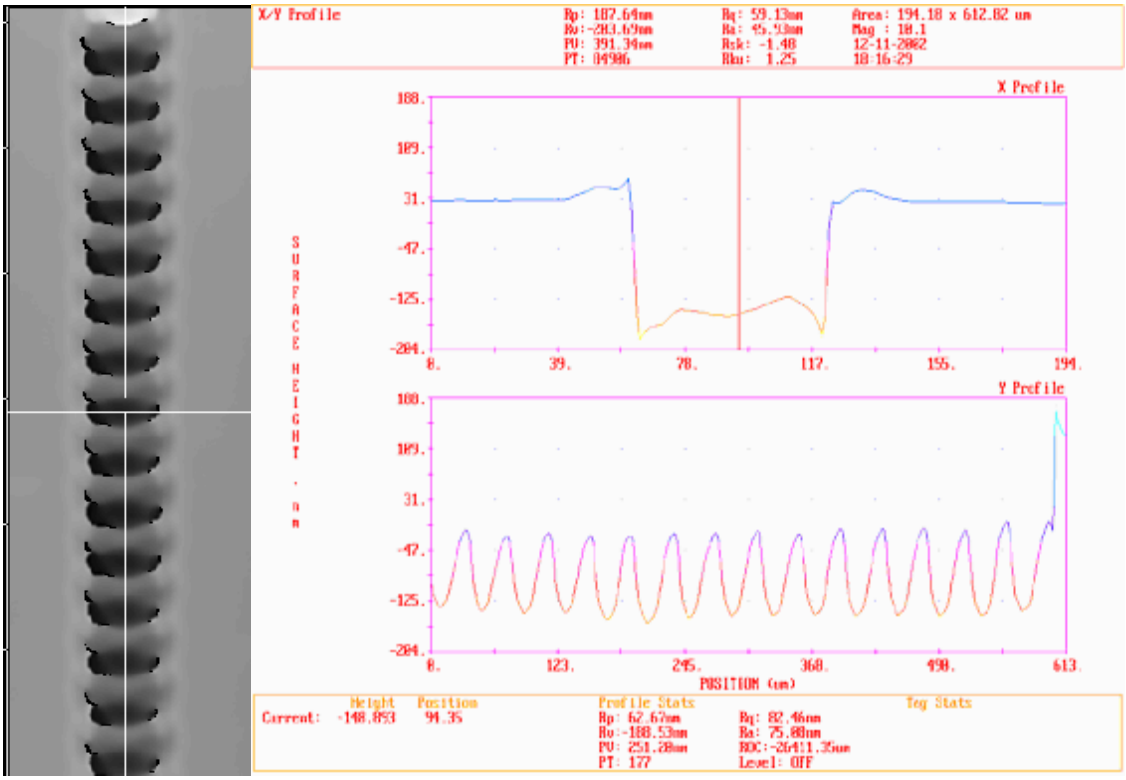

(c) f = 40 µm/pulse.

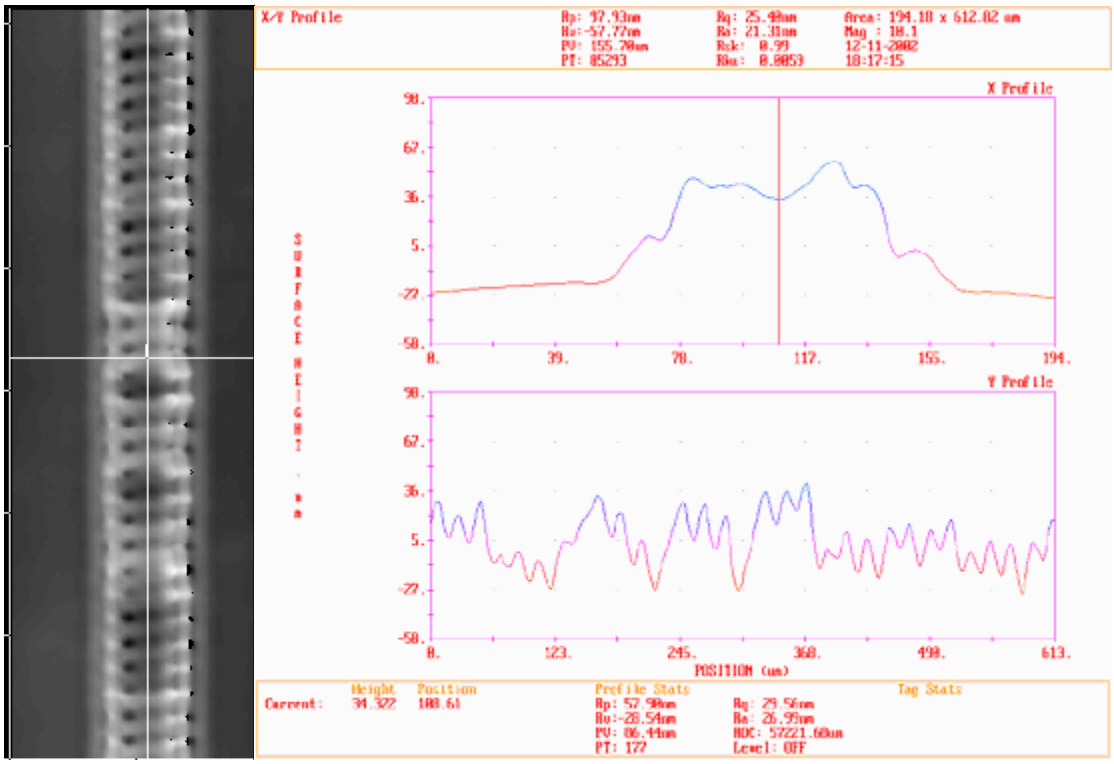

(d) f = 20 µm/pulse

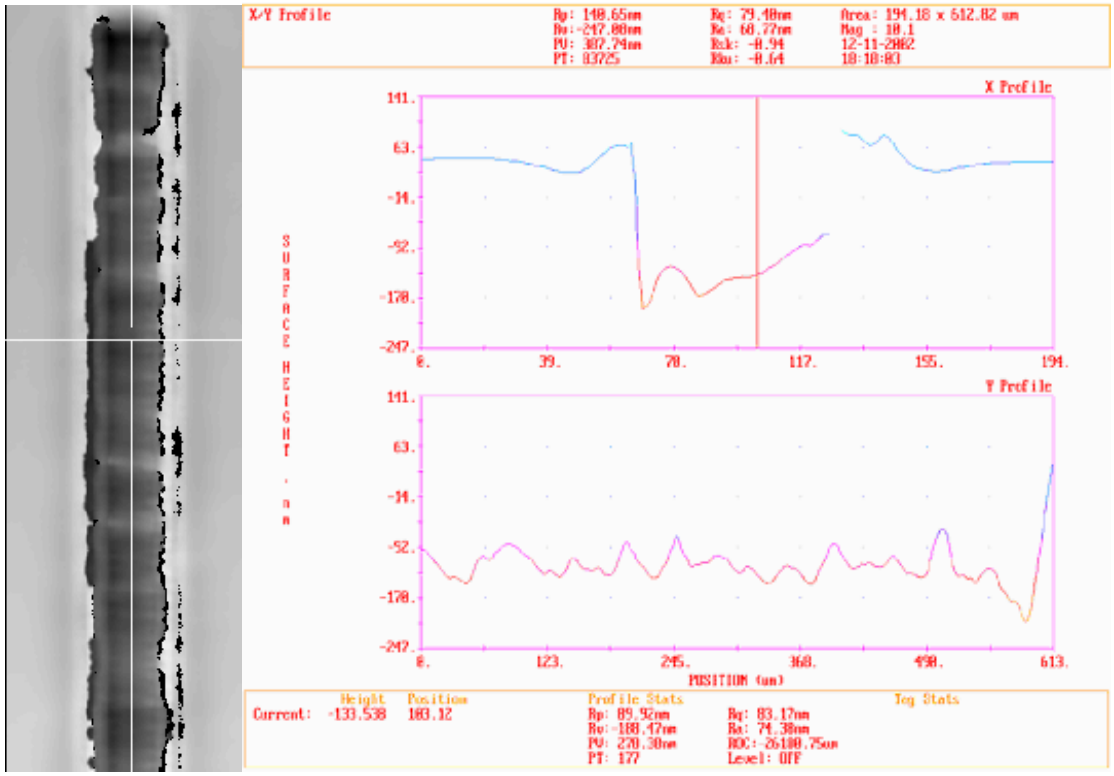

(e) f = 10 µm/pulse.

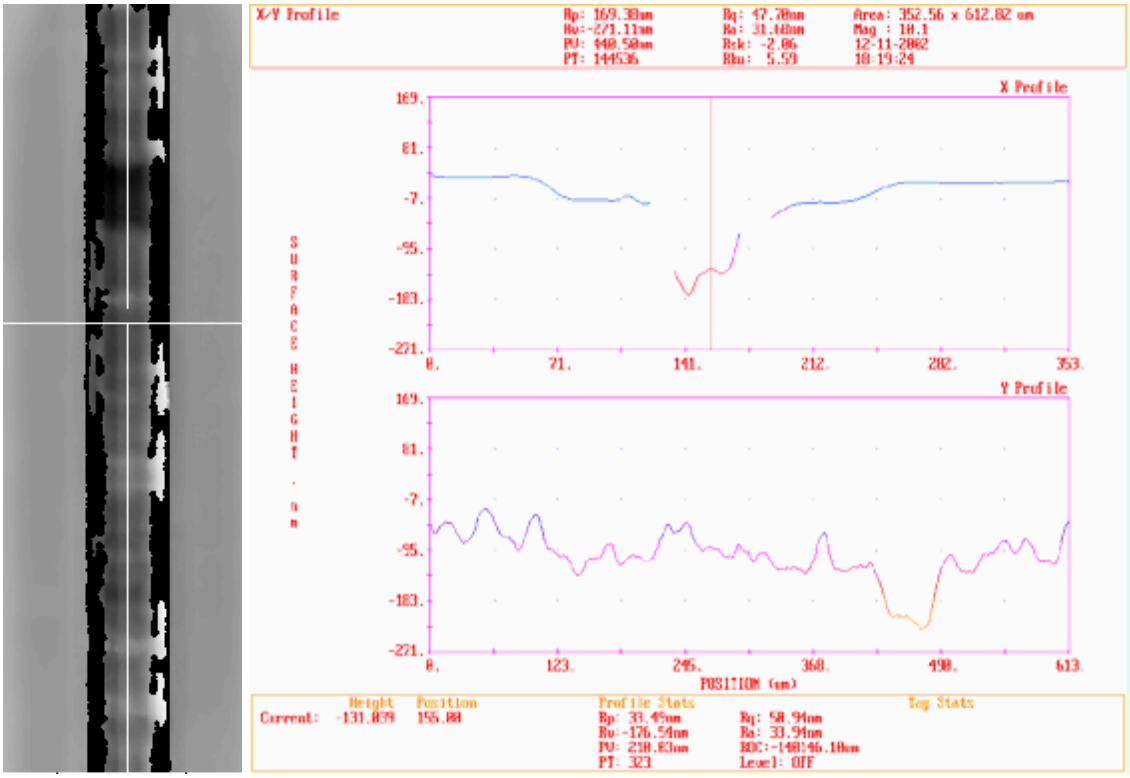

(f) f = 5 µm/pulse

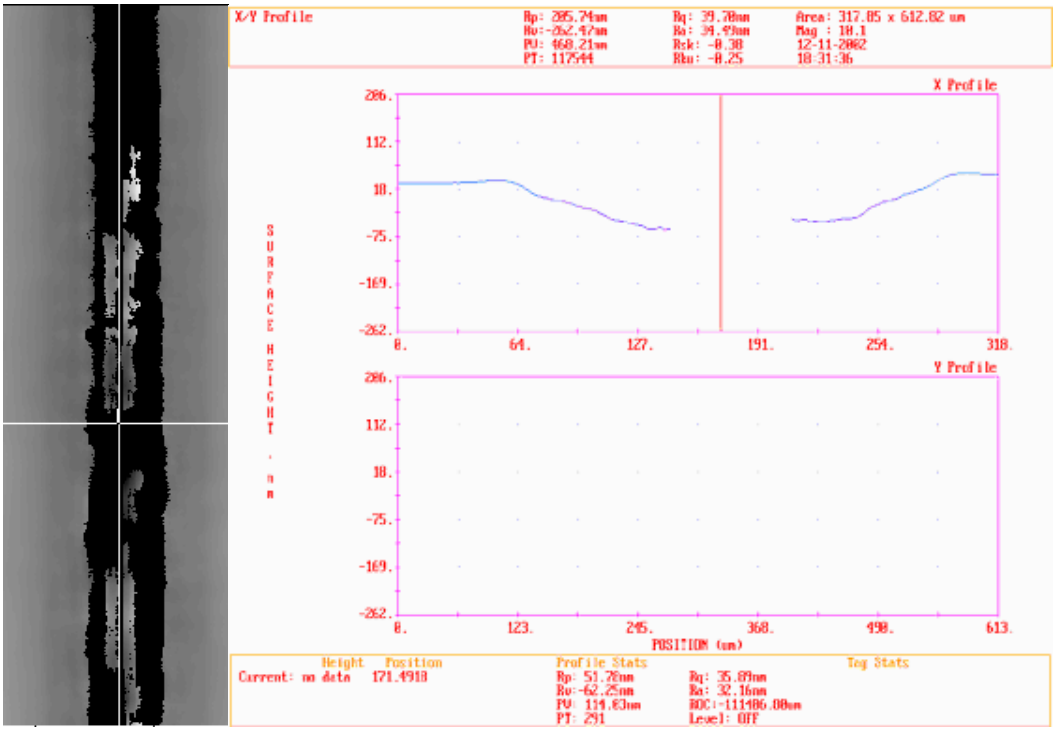

(g) f = 2 µm/pulse

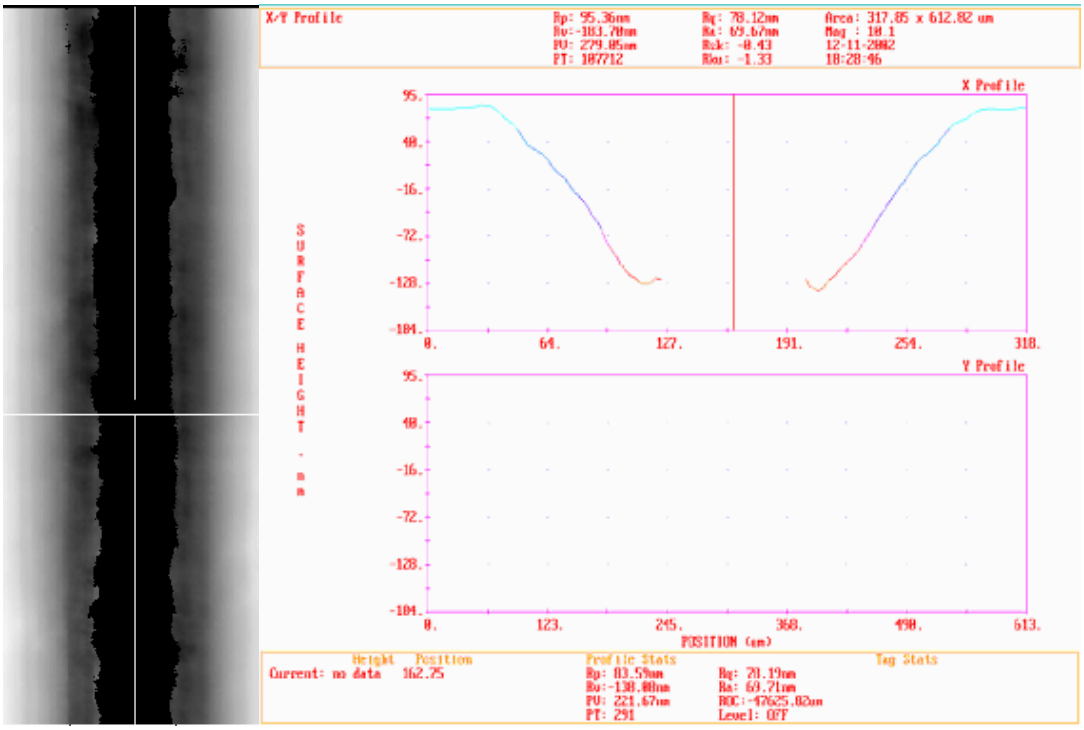

(h) f = 1 μm/pulse

Figure 10.4 MiroXAM micrographs for a borosilicate glass machined with a laser beam (diameter ~ 70 μm) at various feedrates.

10.3.3 Effect of Medium

Figures 10.5 (a) and (b) show optical micrographs of a line machined on borosilicate glass at different number of passes. Much finer cracks are observed in under water machining than in air. For both cases, the cracks do not extend beyond the non-irradiated area. The width of both under water and in air machining remains the same. However, for machining in air, the edge is smooth with a bump created same as in microdrilling.

Figure 10.6 shows a microcircuit machined on borosilicate glass. The microcircuit is created by using 2.14 J/cm^2 with a beam diameter of 60 μm. Feedrate of 1 mm/pulse is used, and laser irradiated area rise up and a pattern of microcircuit appear with a uniform height of ~ 20 nm. The final product could use as a micromold to create microstructure by pouring molten polymer.

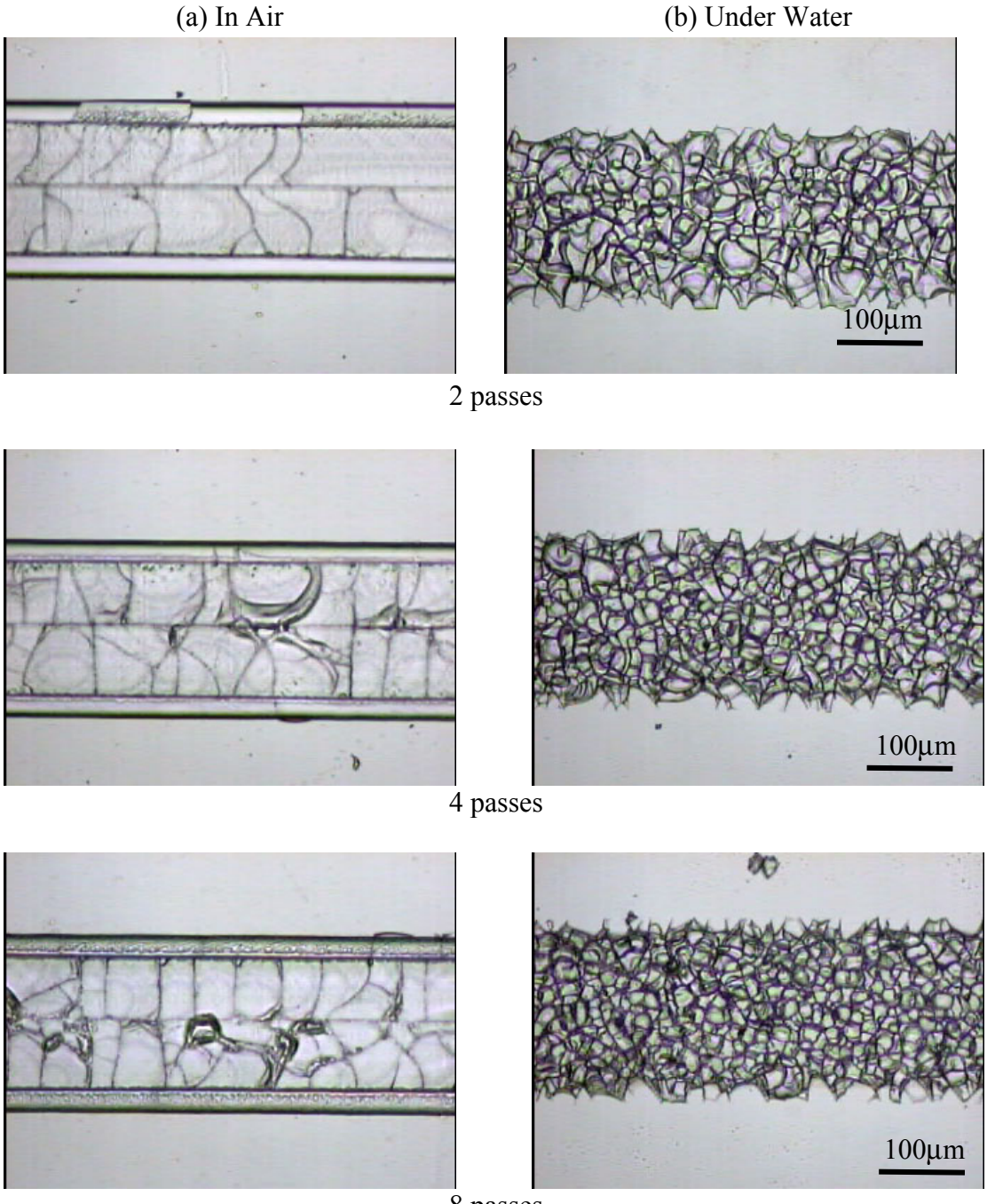

Figure 10.5 Optical micrographs of borosilicate glass machining with 1.38 J/cm^2 with various passes (a) in air and (b) under water, respectively.

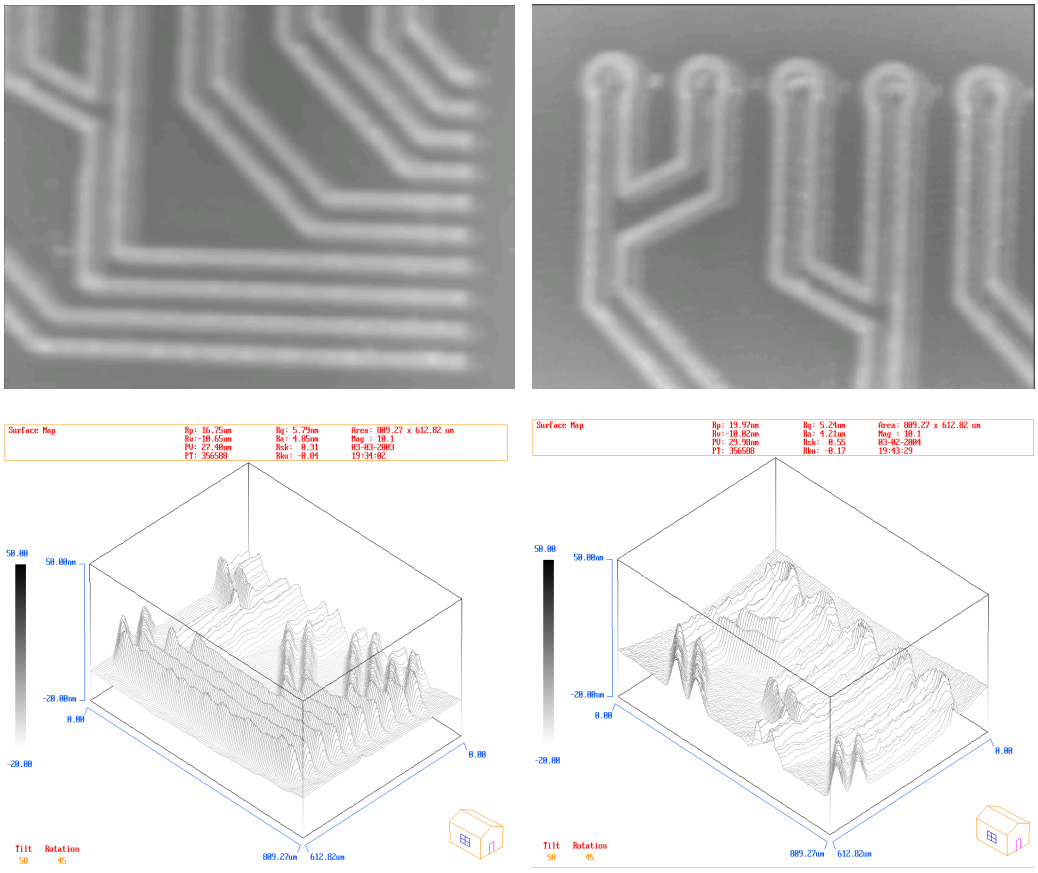

Figure 10.6 MicroXAM 3D view of a microcircuit machined on borosilicate glass.

10.4 Sample of 3-D Structures

Due to the limitation of the laser energy, 3-D microstructures were only generated by micromachining of polymer. In this investigation, PMMA and polyurethane are used as workpieces. Figures 10.8 show a gear is cut out form a piece of PMMA. A laser beam with a diameter of 10 μm was used. The depths of cut are ~ 750 and 2500 nm for 1 and 3 loops, respectively.

Figures 10.8 show a microgear machined on polyurethane. Figure 10.8 (d) shows one of the teeth of the gear, the tip is sharp but covered with debris. Ultrasonic bath with alcohol solution was used to clean away the debris.

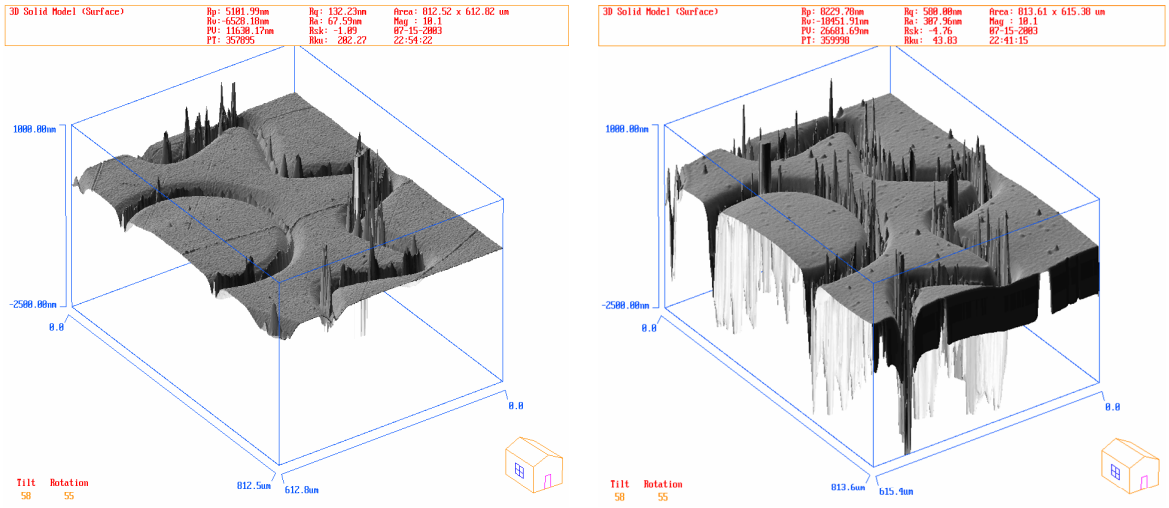

(a) Single loop (b) 3 loops

Figure 10.7 MicroXAM 3D view of a microgear machined with an excimer laser on PMMA with (a) single loop and, (b) 3 loops of machining steps.

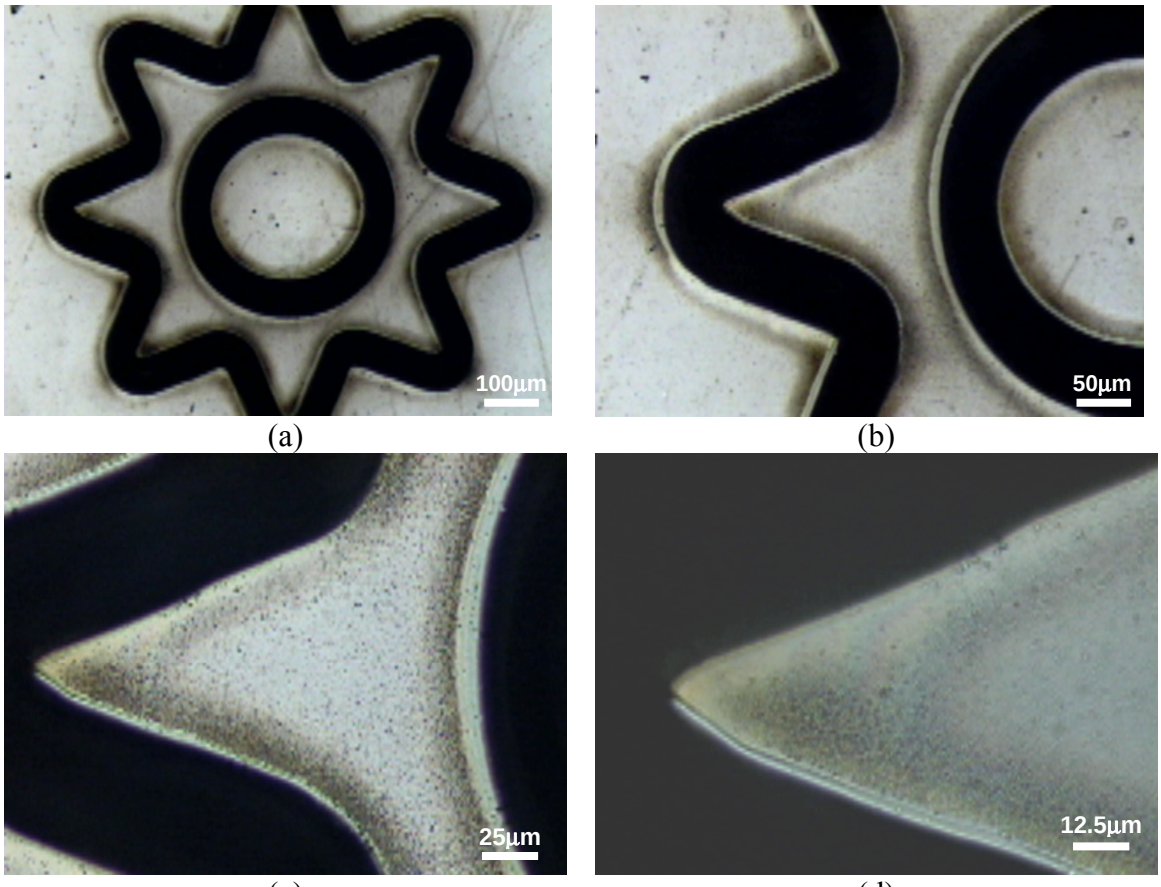

(a) (b)

(c) (d)

Figure 10.8 Optical micrographs of a microgear machined with an excimer laser on polyurethane.

CHAPTER 11

SUMMARY AND CONCLUSIONS

11.1 PMMA

Photochemical ablation is the main mechanism in the case of excimer laser machining for wavelength of 248 nm or less. The finishing features of the hole are influenced by the focal point. When the focal point falls above the surface of the substrate, a large oval shape hole is obtained; at focal point, a prefect round hole is obtained (same as the mask used). Focus point of the laser facility setup is obtained by observing the depth of ablation, which is around ± 0.05 mm.

Ablation rate reduces with increase in the number of pulses due to wall effect, and redeposited material that cause Fresnel effect.

The large production of droplets during the ablation process can be best explained by the capillary wave instability of the molten material. The instability itself seems to be generated or enhanced by the irregular energy distribution within the focal spot. A rapidly expanding plume generated by most intense part of the laser beam was identified as the source for this force.

A secondary region, called ‘incubation’ region is also observed, which is due to laser induced modification of the material. Both incubation region and redeposited material can be easily removed by placing the sample in an ultrasonic isopropyl alcohol bath.

11.2 Microdrilling

Laser microdrilling of silicon and borosilicate glass workmaterial were carried out in air and under water using a short pulse (25 ns), KrF (λ = 248 nm) excimer laser at various laser energies from 100 mJ to 480 mJ and at different number of pulses from 1 to 5000. The variation of ablation depth with laser fluence and number of pulses in air and under water were determined. Figure 11.1 shows flow carts of phenomena for excimer laser micromachining in air. Phenomena of excimer laser micromachining in air can be summarized in the following steps:

STEP 1:

When pulsed laser is applied on a substrate, the laser could penetrate into the substrate for a certain depth (d) which follows the equation:

$$d = \ln(\frac{f}{f_t}) * \frac{1}{\alpha}$$

where

d is depth in μm

f is laser fluence in J/cm^2

f_t is threshold fluence in J/cm^2

α is absorption coefficient of substrate in μm^{-1}

Once the molecules of the workpiece in the irradiated area receive extra energy, they start to vibrate. If the energy is equivalent or greater than the ablation fluence, it follow STEP 2A; otherwise STEP 2B.

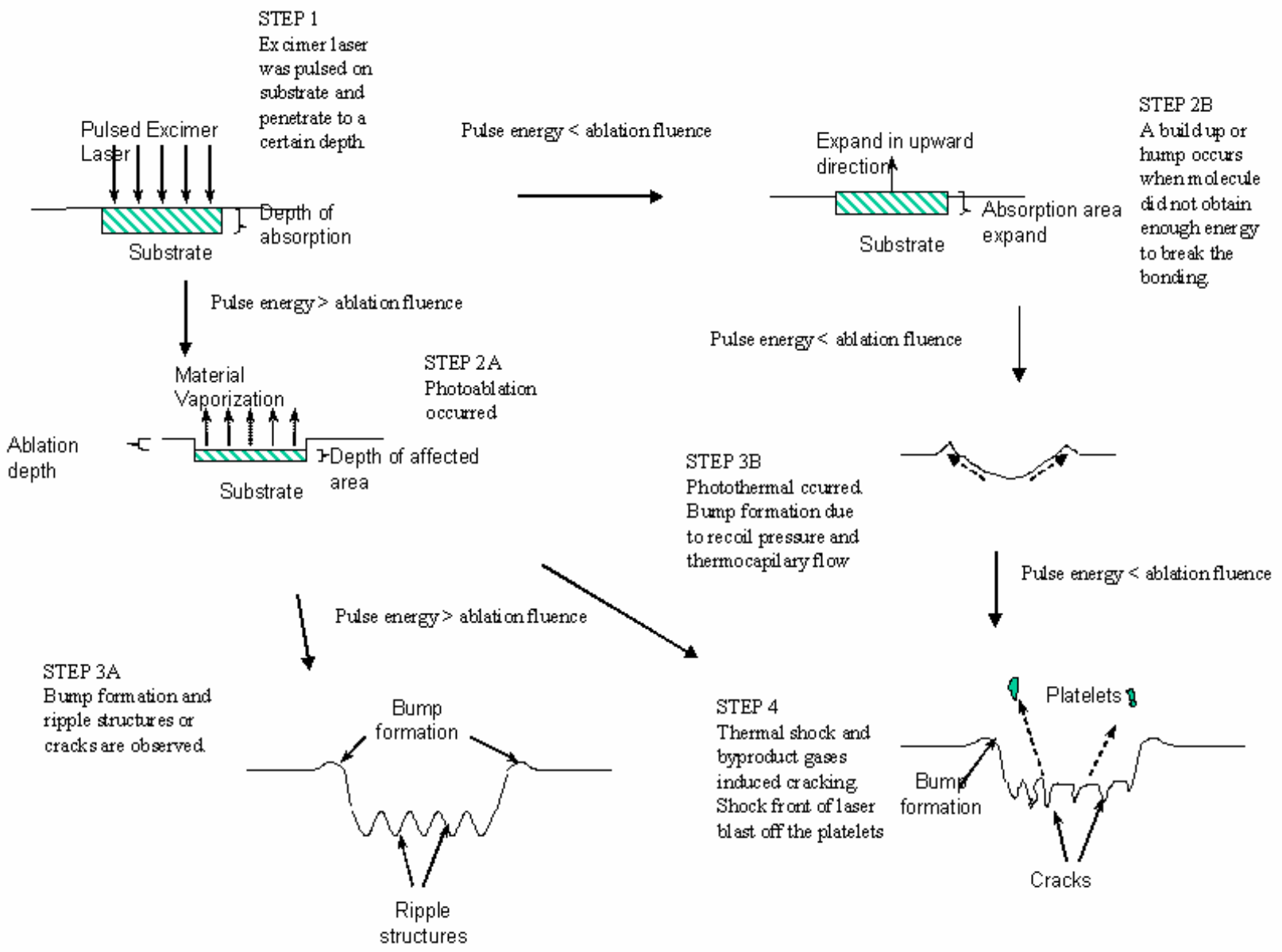

Figure 11.1 Flow carts of phenomena for excimer laser micromachining in air.

STEP 2 A:

The molecules in the irradiated area obtain enough energy to break the bonding, vaporization occurs and an ablation depth is observed. The ablation depth is depended on (1) laser fluence, (2) laser absorption coefficient of the workpiece, and (3) surface roughness of the workpiece.

STEP 2 B:

If the affected area did not obtain enough energy to break down energy bonding, incubation happens. Properties of material will be changed. For example, a build up or hump can be observed in borosilicate glass and incubation show in PMMA. The following pulses are irradaiated on the incubation region and less energy is needed. The ablation will took place as stated in STEP 2A.

STEP 3A:

After the laser impact, ejected materials (or debris) with extremely high temperature redeposited back onto the surface of the workpiece. Most of the heat of the debris was conducted into the workpiece and caused thermal damage. Most reposited materials (or debris) could be seen around the periphery of the ablated area. The travel distance for the ablated material is highly depending on the laser fluence. The smallest the chromophores created from the chain scissions (degradation) process, the lighter the weight it becomes and can travels further. Accumulation of the resolidified molten material (or debris) at the periphery form in a shape of a bowl.

At the very bottom of the laser and material interaction boundary, a melting pool is created due to insufficient energy are given to break the bonding. The molten pool is

quenched from very high temperature to room temperature, Formation of ripple like structures are found. The interval between the peaks of the ripple structures reduced with increase of laser fluence. In the case of under water machining, the interval between of the ripples is far shorter than in air machining because water rapidly cool down the molten pool. It has been reported that the formation of ripple is cause by residual stress of the melting pool.

STEP 3B:

Pulsed heating creates a temperature gradient following the beam intensity profile along the radial direction. The temperature gradient induces thermocapilary flow, driving the material from the center to the cold periphery and forming a bowl-shaped feature. Recoil pressure also causes the molten material to splash out and formed a bowl-shaped feature.

Step 4

For borosilicate glass, cracking is observed due to the rapid cooling and heating cycles cause thermal shock and the releasing of byproduct gases. Shock front of laser pulse also cause blast off of the platelets and produce 'blow hole.' Cracks are only seen inside the irradiated area.

Based on those studies, the following conclusions are reached.

Silicone Wafer

1. Significant differences in the nature of ablation and thermal damage were observed between laser ablation in air and under water. They include absence of thermal damage in the case of machining under water while significant thermal damage in the case of machining in air. This thermal damage is found to increase with the number of pulses in

the case of machining in air. It is for this reason that underwater machining is preferred. In addition, the nature of the material removal in the two cases are different. For example, while the ablated surface is smooth in the case of machining in air, it is somewhat rough in the case of underwater machining. The surface in the case of machining under water shows the result of molten silicon rapidly solidified with a dendritic structure.

2. Once the laser fluence exceeds a certain threshold value (1.4 to 1.7 J/cm^2) depending on the number of pulses, the ablation depth was found to increase rapidly with laser fluence with the variation being nonlinear. The influence of laser fluence on the ablation depth is much more significant in the case of underwater machining than in air. At lower fluence, the ablation depth is more in the case of machining in air than under water. This difference is much less at higher laser fluences.

3. The presence of a liquid layer (in the present case water) on top of the silicon workmaterial plays an important role in the mechanism of ablation. Water acts as a cooling media and carries away the debris and eliminates the redeposition of molten materials.

Borosilicate Glass

1. Significant differences in the nature of ablation and thermal damage were observed between laser ablation in air and under water. They include absence of thermal damage in the case of machining under water while significant thermal damage in the case of machining in air. This thermal damage is found to increase with the number of pulses in the case of machining in air. It is for this very reason that underwater machining is preferred. In addition, the nature of the material removal in the two cases is different. For

example, while the ablated surface has longer cracks in the case of machining in air, there were much more cracks in the case of underwater machining.

2. There are two ablation regions, photothermal and photochemical. In the photothermal region, material is ablated by the accumulation of thermal energy causing explosive boiling or evaporation. In between the transition to photochemical ablation, plasma shielding phenomena is observed. UV irradiation is reduced and mainly absorbed by the plasma cloud. In photochemical ablation region, ablation is mainly happen by bond breaking between atoms or molecules. The critical point where photochemical ablation starts it is called the ablation threshold fluence. This value is around 2.19 J/cm^2.

3. The presence of a liquid layer (in the present case water) on top of the borosilicate glass workmaterial plays an important role in the mechanism of ablation. Water acts as a cooling media and carries away the debris and eliminates the redeposition of molten material.

A simple, alternate method of collecting the debris generated in laser ablation and prevention from material redepositing on the finished surface was considered. It involves covering the surface of the workmaterial to be ablated with an adhesive polymer tape. Results of the holes ablated before and after peeling off of the tape show, minimal thermal damage similar to the hole ablated by excimer laser under water and absence of redeposited molten and resolidified material from laser ablation. This material, in fact, shows up on the tape film which can be discarded.

11.3 3-D Structuring

3-D structure is machined using a single laser (direct writing), the phenomena in both air and under water are the same as microdrilling. Due to the limitation of pulse energy, cut off of microstructuring only can be performed on polymers. Microstructures with sharp edge up to 10 μm were manufactured.

Due to the properties of borosilicate glass, hump (rise up) structure is obtained with low fluences. Microstructures with a uniform build up in nanometer scale are obtained. This structure could be used as a micromold.

11.4 The Main Effects Limiting Quality of Laser Machining

In every real laser machining process, significant fraction of liquid phase remains at the irradiated zone after the end of the laser pulse. Formation of a large amount of liquid and its incomplete removal from the surface are adverse and hard-to-control phenomena which cause a considerable decrease of efficiency and quality of laser micromachining.

The redistribution of the liquid prior to crystallization plays a decisive role in a final shape formation. As a result of the redistribution, the surface shape to the end of solidification can differ substantially from that determined by the beam geometry, the vaporization kinetics, and the hydrodynamic rejection of part of the liquid-phase material at the end of the laser pulse.

11.4.1 Main Reasons for Liquid Phase Increase

1. The decrease of the light flux density due to the gradual beam defocusing with the hole-depth growth;
2. The slow power decrease at the pulse trailing edge contributes to the increase of the volume of liquid-phase residue at the surface after the pulse;
3. Extra duration of action time: the longest is the action time, the greater is the melted volume and, therefore, the greater is the hole size and cut width scatter. In addition, a long action time cause the development of a zone of considerable size where oxidation and structural changes occur, as well as the appearance of defects on the cut surface as a result of the increase of the depth of heat-affected layer (incubation region).

CHAPTER 12

FURTURE RECOMENDATIONS

In this investigation, the KrF excimer laser was installed and used in drilling and some 3-D machining of PMMA, polyurethane, silicon wafer and borosilicate glass. Due to the high energy limitation, a higher demagnification lens should be installed to obtain smaller beam without wasting energy (masking technique is used). With this upgrade, ceramics and metals with high ablation fluence could be machined and testing could be conducted.

Different shape of masks could be used, for example, a triangle shape can use to obtain a 'V' glove valley while machining a line. The same experiment could be repeated and compared with using CO_2 and Nd:YAG laser which are available in Dr. Komanduri's Research Laboratory.

Thermal modeling and MD simulation of laser drilling process can be conducted and compared with the experimental results.

An ultrahigh-speed camera, could be installed to capture the image where material-laser interactions take place, and it would contributed toward further understanding of the laser-material interaction.

Etchant KOH and IPA could be used on the silicon wafer to observe the change of surface finishing. It was proposed by Nilson *et al*. [81] that 3M KOH + 2 M IPA at 60˚C for 6 minutes will reduce the (110) etch rate and surface roughness.

REFERENCES

1. Einstein, A., "Zur Quantentheorie der Strahlung" Physikalische Gesellschaft Zürich Mitteilungen Nr. 16 (18) (1916) 47-62; an English translation appears in B.L. van der Waerden, ed., “Sources of Quantum Mechanics,” North Holland, Amsterdam (1967).
2. Arthur L. Schawlow and Charles H. Townes, “Infrared and Optical Masers,” Physical Review 112 (1958) 1940
3. Winburn, D.C., “What Every Engineer Should Know About Lasers,” Marcel Dekker, Inc., New York (1987).
4. Hecht, J. and D. Teresi, “Laser, Supertool of the 1980’s,” Ticknor and Field, New York (1982).
5. Hecht, J., “Understanding Laser,” Howard W. Sam & Company Hayden Books, California (1990).
6. Chryssolouris, G.,“Laser Machining: Theory and Practice,” Springer –Verlag, New York (1991).
7. Ready, J. F., “Lasers in Modern Industry,” Society of Manufacturing Engineering, Dearborn, Michigan, (1979).
8. McGeough, J. A., “Advanced Methods of Machining,” Chapman and Hall, London and New York (1988).
9. Waver, L. A., “Machining and Welding Applications,” Laser Applications Vol. 1, Academic Press, New York and London (1971) 579-602.

10. Carlaw, H. S., and J. C. Jaeger, "Conduction of Heat in Solids," 2nd edition, Oxford University Press, Oxford (1959).
11. Ready, J. F. and D. F. Farson, "LIA Handbook of Laser Material Processing," 1st edition, Laser Institute of American (2001).
12. Philippe, B., C., William and Ali S., "Introduction to Micromachining Handbook," Version 2.2, Clark-MXR, Inc. (2001).
13. "The UNIDEX® 500 Motion Controller and Windows Sofftware Operation & Technical Manual," Version 1.2, Aerotech, Inc.
14. "The ATS 100 Series Position Stages Instruction Manual," Version 1.0, Aerotech, Inc.
15. Philipp, H. R., Cole, H. S., Liu, Y. S., and T. A. Sitnik, "Optical Absorption of Some Polymers in the Region 240-170nm," Appl. Phys. Lett. 48 (2) (1986) 192-194.
16. Srinivasan, R., and V. Mayne-Banton, "Self-Developing Photoetchining of Poly(ethyleneterephthalate) Films by Far-Ultraviolet Excimer Laser Radiation," Appl. Phys. Letts. 41 (1982) 576-578.
17. Garrison, B. J and R. Srinivasan," Laser Ablation of Organic Polymers: Microscopic Models for Photochemical and Thermal Processes," J. Appl. Phys. 57, (1985) 2909-2914.
18. Srinivasan, R., and W. J. Leigh, "Ablative Photodecomposition: Action of Far-Ultraviolet (193nm) Laser Radiation on Poly (ethylene terephathalate) Films," J. Am. Chem. Soc. 104 (1982) 6784-6785.

19. Srinivasan, R., Braren, B., Casey, K. G., and M. Yeh, "Ultrafast Imaging of Ultraviolet Laser Ablation and Etching of Polymethylmethacrylate," Appl. Phys. Lett. 55 (1989) 2790-2791.
20. Lauren, P., Sadrs, B., Decobert, F., Arefi, F., and J. Amouroux, "Modifications of Polyether-Etherketone Surface after 193 nm and 248 nm Excimer Laser Radiation," Appl. Surf. Sci, 138-139 (1999) 93-96.
21. Feng, Y., Liu, Z. Q., and X.-S. Yi, "Co-occurrence of Photochemical and Thermal Effects during Laser Polymer Ablation via a 248-nm Excimer Laser," Appl. Surf. Sci. 156 (2000) 177-182.
22. Chen, Y. H., Zheng, H. Y., Wong, K. S., and S. C. Tam, "Excimer Laser Drilling of Polymers," Proceeding of SPIE – The International Society of Optical Engineering 3184 (1997) 202-210.
23. Dyer, P. E., and D. M. Karnakis, "High Quality ArF Laser Ablation of Photoincubated Polymer," Appl. Phys. Lett. 64 (1994) 1344-1346.
24. Braun, A., Zimmer, K., and F. Bigl, "The Influence of Ambient Temperature on KrF Laser Ablation of Polyimide in Air," Appl. Surf. Sci., 154-155 (2000) 73-77.
25. Srinivasan, R. and B. Braren, "Influence of Pulse Width on Ultraviolet Laser Ablation of Poly(Methylmethacrylate)," Appl. Phys. Lett. 53 (1998) 1233-1235.
26. Dijkkamp, D., Gozdz, A. S., Venkatesan, T., and X. D. Wu, "Evidence for the Thermal Natural of Laser-Induced Polymer Ablation," Phys. Lett. 58 (1987) 2142-2145.
27. Dyer, P. E., and J. Sidhu, "Excimer Laser Ablation and Thermal Coupling Efficiency to Polymer Films," J. Appl. Phys. 57 (1985) 1420-1422.

28. Gorodetsky, G., Kazyaka, T. G., Melcher, R. l., and R. Srinivasan, “Calorimetric and Acoustic Study of ultraviolet Laser Ablation of Polymers,” Appl. Phys. Lett. 46 (1985) 828-830.

29. Daneilzik, B., Fabricius, N., Rowekamp, M. and D. von der Linde, “Velocity Distribution of Molecular Fragments from Polymethylmethacrylate Irradiated with UV Laser Pulses,” Appl. Phys. Lett. 48 (3) (1986) 212-214.

30. Srinivasan, R., Smrtic, M. A. and S. V. Babu, “Excimer Laser Etching of Polymers,” J. Appl. Phys. 59 (11) (1986) 3861-3867.

31. Brannon, J. H., Lankard, J. R., Baise, A. I., Burns, F., and J. Kaufman, “Excimer Laser Etching of Polyimide,” J. Appl. Phys. 58 (5) (1985) 2036-2043.

32. Srinivasan, R., Braren, B., and R. W. Dreyfus, “Ultraviolet Laser Ablation of Polyimide Films,” J. Appl. Phys. 61 (1) (1987) 372-376.

33. Dyer, P. E. and R. Srinivasan, “Nanosecond Photoacoustic Studies on Ultraviolet Laser Ablation of Organic Polymers,” Appl. Phys. Lett. 48 (6) (1986) 445-447.

34. Dyer, P. E. and Karnakis, D. M., and G. A. Oldershaw, “Analysis and Experimental Study of One-Photon Incubated Absorption in Polymers,” Appl. Surf. Sci. 86 (1995) 1-6.

35. Dyer, P. E., Karnakis, D. M., Key, P. H., and P. Monk, “Excimer Laser Ablation for Micro-Machining: Geometric Effects,” Appl. Surf. Sci. 96-98 (1996) 415-419.

36. Sirivasan, R., Casey, K. G., Braren, B., and M. Yeh, “The Significance of a Fluence Threshold for Ultraviolet Laser Ablation and Etching of Polymers,” J. Appl. Phys. 67 (3) (1990) 1604-1606.

37. Sutcliffe, E, and R. Sirivasan, “Dynamic of UV laser Ablation of Organic Polymer Surfaces,” J. Appl. Phys. 60 (9) (1986) 3315-3322.

38. Sirivasan, R., Braren, B. and K. G. Casey, “Mature of “Incubation Pulses” in the Ultraviolet Laser Ablation of Polymethyl Methacrylate,” J. Appl. Phys. 68 (4) (1990) 1842-1847.

39. Kueper, S., and M. Stuke, “Femtosecond UV Excimer Laser Ablation,” Appl. Phys. B. 44 (4) (1987) 199-204.

40. Davis, G. M., and M. C. Gower, “Time Resolved Transmission Studies of Poly(Methyl Methacrylate) Films During Ultraviolet Laser Ablative Photodecomposition,” J. Appl.Phys. 61 (5) (1987) 2090-2092.

41. Srinivasan, R., Braren, B., Seeger, D. e., and R. W. Dreyfus, “Photochemical Cleavage of a Polymeric Solid: Details of the Ultraviolet Laser Ablation of Poly(Methyl Methacrylate) at 193 and 248nm,” Macromoleclues, 19 (1986) 916-921.

42. Estler, R. C., and N. G. Nogar, “Mass Spectroscopic Indentification of Wavelength dependent UV Laser Photoablation Fragments from Polymethylmethacrylate,” Appl. Phys. Lett. 49 (18) (1896) 1175-1177.

43. Dyer, P. E., Karnakis, D. M., Key, P. H., and J. P. Tait, “Excimer Laser Ablation of Low and High Absorption Index Polymers,” Appl. Surface Sci. 96-98 (1996) 596-600.

44. Kelly, R., and J. E. Rothenberg, “Laser Sputtering Part III. The Mechanism of the Sputtering of Metals low energy densities,” Nucl. Instr. Meth. Phys. Res. B7/8 (1985) 755-765.

45. Roth, S. and M. Gieger, ”Novel technique for High Quality Microstructuring with Excimer Lasers,” Proc. SPIE 3933 (2000) 338-346

46. Kruusing, A, "Underwater and Water-assisted Laser Processing: Part 1 - General Features, Stream Cleaning, and Shock Processing," Optics and Lasers in Engineering 41 (2004) 307-327.

47. Kruusing, A, "Underwater and Water-assisted Laser Processing: Part 2 - Etching, Cutting, and Rarely Used Methods," Optics and Lasers in Engineering 41 (2004) 329-532.

48. Davis, G. M., Thomas, D. W., and M. C. Gower, “Excimer Laser Direct Etching of GaAs,” J. Phys. D: Appl. Phys. 21 (1988) 683-687.

49. Dupont, A., Caminat, P., Bournot, and J. P. Gauchon, "Enhancement of Material Ablation Using 248, 308,532, 1064 nm Laser Pulse with a Water Film on the Treated Surface," J. Appl. Physics 78 (3) (1995) 2022-2028

50. Park, H. K., Kim, D., Grigoropoulos, C. P., and A. C. Tan, ”Pressure Generation and Measurement in the Rapid Vaporization of Water on a Pulsed Laser Heated Surface,” J Appl. Phys. 80 (7) (1996) 4072-4081

51. Sano, Y., Mukai, N., Okazaki, K., and M. Obata, "Residual Stress Improvement in Metal Surface by Underwater Laser Irradiation," Nuclear Instruments and Methods in Physical Research B 121 (1977) 432-436

52. Kim, D and C. P. Grigoropoulos, "Phase-Change Phenomenon and Acoustic Transient Generation in the pulsed laser Induced Ablation of Absorbing Liquids," Applied Surface Science 127-129 (1998) 53-58

53. Kim, D., Ye, M., and C. P. Gregoropoulos, "Pulsed Laser-induced Ablation of Absorbing Liquids and Acoustic-transient Generation," Applied Physics A: Materials Science and Processing A 67(2) (1998) 169-181

54. Ho, J. R., Grigoropoulos, C. P., and J. A. C. Humphrey, "Computational Study of Heat Transfer and Gas Dynamics in the Pulsed Laser Evaporation of Metals," J of Applied Physics 78 (7) (1995) 4696-4709

55. Geiger, M., Roth, S., and W. Becker, "Microstructing and Surface Modification by Excimer Laser Machining Under Thin Liquid Films," Proc. SPIE, 3407 (1998) 200-208.

56. Andriac, Z., Henc-Bartolic, V., Gracin, D., and M. Stubicar, ”Droplet Formation During Laser Sputtering of Silicon,” App. Surface Science 136 (1998) 73-80.

57. Feng, Y., Liu, Z. Q., and X. S. Yi, “Co-occurrence of Photochemical and Thermal Effects During Laser Polymer Ablation via a 248-nm Excimer Laser,” Applied Surface Science 156 (2000) 177–182

58. Jeong, S.H., Grief, R., and R. E. Russo, “Shock Wave and Material Vapor Plume Propagation during Excimer Laser Ablation of Aluminum Samples”, J. Phys. D: Appl. Phys. 32 (1999) 2578-2585.

59. Yoo, J.H., Jeong, S. H., Grief, R., and R. E. Russo, “Explosive Change in Crater Properties During High Power Nanosecond laser,” J of Applied Physics 88 (3) (2000) 1638-1649

60. Zhu, S., Lu, Y. F., Hong, M. J., and X. Y. Chen, "Laser Ablation of Solid Substrates in Water and Ambient Air," J of App. Physics 89 (4) (2001) 2400-2403

61. Jeschke, H. O., Garcia, M. E., Lenzer, M., Bonse, J., Kruger, J., and W. Kautek, "Laser Ablation Thresholds of Silicon for Different Pulse Durations: Theory and Experiment" Applied Surface Science 197-198 (2002) 839-844

62. Craciun, V., Bassim, N., Singh, R. K., Craciun, D., Hermann, and C. Boulmer-Leborgne, "Laser Induced Explosive Boiling During Nanosecond Laser Ablation of Silicon" Appl. Surface Science 186 (2002) 288-292

63. Amer, M., L. Dosser, S. LeClair, and J. F. Maguire, "Induced Stresses and Structural Changes in Silicon Wafers as a Result of Laser Micro-machining," App. Surface Science 187 (2002) 291-296

64. Kawaguchi, Y., Narazaki, A., Sato, T., Niino, H., Yabe, A., Langford, S.C. and J.T. Dickinson, "The Onset of Optical Breakdown in KrF-Laser-Irradiated Silica Glass Surfaces," Appl. Surf. Sci. 197–198 (2002) 50–55

65. Ihlemann, J., "Excimer Laser Ablation of Fused Silica," Appl. Surf. Sci. 54 (1992) 193-200

66. Omori, N. and M. Inoue, "Excimer Laser Ablation of Inorganic Materials," Appl. Surf. Sci. 54 (1992) 232-236

67. Kruger, J. and W. Kautek, "Femtosecond-Pulse Visible Laser Processing of Transparent Materials," Appl .Surf. Sci. 96-98 (1996) 430-438

68. Sokolowski-Tinten, K, Bialkowski, J., Cavalleri, A., and D. Von Der Linde, "Observation of A Transient Insulating Phase of Metals and Semiconductors during Short-Pulse Laser Ablation," Appl. Surf. Sci. 127–129 (1998) 755–760

69. Buerhop, C., Blumenthal, B., Weissmann, R., Lutz, N. and S. Biermann, "Glass Surface Treatment with Excimer and CO_2 Laser," Appl. Surf. Sci. 46 (1990) 430-434.

70. Buerhop, C., Weissmann, R. and N. Lutz, “Ablation of Silicate Glasses by Laser Irradiation: Modeling and Experimental Results,” Appl. Surf. Sci. 54 (1992) 187-192.

71. Jackson, S. R., Metheringham, W. J. and P. E. Dyer, “Excimer Laser Ablation of ND:YAG and Nd:Glass,” Appl. Surf. Sci. 86 (1995) 223-227.

72. Dyer, P. E., Farley, R. J., Giedl, R. and D. M. Karnakis, “Excimer Laser Ablation of Polymers and Glasses for Grating Fabrication,” Appl. Surface Sci. 96-98 (1996) 537-549.

73. Keiper, B., Exner, H., Loschner, U. and T. Kuntze, “Drilling of Glass by Excimer Laser Mask Projection Technique,” ICALEO M110 (1999) 1-7

74. Konovalov, I. A. and P. R. Herman, “Ablation-Induced Stresses in Fused Silica by 157-nm F2-Laser Irradiation,” Mat. Res. Soc. Symp. 617 (2000) J3.3.1-J3.3.7.

75. Allcock, G., Dyer, P. E., Elliner, G. and H. V. Snelling, “Experimental Observations and Analysis of CO_2 Laser-Induced Microcracking of Glass” J. Appl. Phys. 78 (1995) 7295-7303.

76. Zhang, W. and Y. L Yao, “Micro Scale Laser Shock Processing of Metallic Components,” J. Manufac. Sci. Eng., 124 (2002) 369-378.

77. Peyre, P., Fabbro, R., Merien, P. and H. P. Lieurade, “Laser Shock Processing of Aluminum Alloys. Application to High Cycle Fatigue Behavior,” Mat. Sci Eng. A A210 (1996) 102-113.

78. Peyre, P., Berthe, L., Scherpereel, X., Fabbro, R. and E. Bartnicki, “Experimental Study of Laser-Driven Shcok Waves in Stainless Steel,” J. Appl. Phys. 84 (1998) 5985-5992.

79. Berthe, L., Fabbro, R., Peyre, P., Tollier, L. and E. Bartnicki, “Shock Waves from a Water-Confined Laser-Generated Plasma,” J. Appl. Phys. 82 (1997) 2826-2831.

80. Jeong, J. H. Grief, R. and R. E. Russo, “Shock Wave and Material VApour Plume Propagateion during Exciemr Laser Ablation of Aluminum Samples,” J. Phys. D: Appl. Phys. 32 (1999) 2578-2585.

81. Nilsson, D., Jensen, S. and Menon, “Fabrication of Silicon Molds for Polymer Optics,” J. Micromech. Microeng, submitted.

82. Choo, K. L, Ogawa, Y., Kanbargi, G., Raff, L. M., and R. Komanduri, “Micromachining of Silicon by Short Pulse Laser Ablation in Air and Under Water”, Proceedings of NSF Workshop on Research Needs in Thermal Aspects of Material Removal Processes (2003) 346-365. Also, in print Material Science B (2004).

83. Fox, J. A., “Effect of Water and Paint Coating on Laser-Irradiated Target,” Appl. Phys. Lett. 24 (10) (1974) 461-464.

84. Herzberg, G., “Spectra of Diatomic Molecules,” New York: D. Van Nostrand Company, Inc. (1950).

85. Kingery, W. D., “Surface Tension of Some Liquid Oxides and Their Temperature Coefficients,” J. Am. Ceram. Soc, 42 (1959) 6-10.

86. Guthrie, R. I. L., and T. Iida, “Thermodynamic Properties of Liquid Metals,” Mater. Sci. Eng. A A178 (1994) 35-41.

87. Balandin, Yu, V., Otte, D., and O. Bostanjoglo, “Thermocapillary Flow Excited by Focused Nanosecond Laser Pulses in Contaminated Thin Liquid Iron Films,” J. Appl. Phys. 78 (1995) 2037-2044.

APPENDIX A: SYSTEM OPERATOIN INSTRUCTIONS

Turn On Procedure

1) Wear safety goggles that block 248 nm laser radiation.
2) Remove bracelets, rings, watch, or other reflective jewelry.
3) Before turning the laser on, make sure the safety window is close.
4) Turn key switch to ON
5) Turn main switch to ON
6) The laser will operate in the self-testing mode.
    a. first the internal data link is checked
    b. at the same time, the controller watchdog and the communication between the terminal and laser is checked.
7) The laser is now in warm up mode for 8 min.
8) While waiting for the laser to warn up, turn on the exhaust vent and the cooling water supply.
9) Turn on the power supply for the attenuator; it should be ~24 VDC.
10) Switch on the computer and DR500 Drive Chassis.

Operating Procedure

1) After the warm up, the laser is ready for normal operation.
2) Push key <<TRIGGER INT/EXT>>, second line on the display shows the current mode. Use the arrow key to choose the external trigger and then push key <<ENTER>>.

3) Push key <<HV>>, then punch in the desired voltage between 18.0 to 27.0 follow by pushing key <<ENTER>>. The chosen value will pop up on the display.
4) Push key <<RUN/STOP>> on the control terminal. The message 'RUN LASER' will pop up on the display.
5) Press <<EXE>> on the control terminal. Control LED at key <<RUN/STOP>> will light up.
6) Load the U500 software in the computer. A window of U500 will pop up.
7) Reset all the X, Y, Z, and U axes by dragging the mouse to the RESET icon or press F9.
8) Load the program written for specific application into the U500 software. For details on the command please refer to the instruction manual. Basically the program contains G codes and PSO codes, where G code commands the table movement and the PSO code commands the firing of the laser.
9) After loading the program, make sure nothing is blocking in front of all the optical components.
10) Dust off all the optical components with compress air.
11) Open the safety window.
12) Now, start laser machining by pressing the icon, RUN or F6.

Shutdown Procedure

Long term Shutdown

1) Push key <<RUN/STOP>> on the terminal control. This will stop the laser to fire.
2) Turn main switch and key switch to the OFF position. This will disable the high voltage.
3) Close the safety window.
4) Turn off the DR500 Chassis.
5) Close the U500 window and turn off the computer.
6) Turn off the power supply for the attenuator.

Emergency Shutdown

1) Press ABORT icon on the U500 window, or
2) Push key <<RUN/STOP>> on the terminal control, or
3) Turn the main switch, OFF, or
4) Turn switch key to OFF.

VITA

Choo Kok Leong

Candidate for the Degree of

Master of Science

Thesis: MICROMACHINING USING AN EXCIMER (248 nm) LASER

Major Field: Mechanical Engineering

Biographical:

Personal Data: Born in Ipoh, Perak, Malaysia, on October 14, 1974, the youngest son of Mr. Choo Si Pei and Madam Ng Yoke Lan.

Education: Received Bachelor of Science in Mechanical Engineering from Oklahoma State University, Stillwater, in May 1999. Completed the requirements for the Master of Science degree with a major in Mechanical Engineering from Oklahoma State University, Stillwater, in May 2004.

Experience: Worked as a Teaching Assistant in Mechanical and Aerospace Engineering Department, Oklahoma State University, Stillwater, Oklahoma, August 1999 – December 2000. Graduate Research Assistant in Mechanical and Aerospace Engineering Department, Oklahoma State University, Stillwater, Oklahoma, August 2000 – Present.

Professional Membership: The American Society of Mechanical Engineers.